NUMERICAL MODELING OF EDREMIT GEOTHERMAL FIELD

A THESIS SUBMITTED TO
THE GRADUATE SCHOOL OF NATURAL AND APPLIED SCIENCES
OF
MIDDLE EAST TECHNICAL UNIVERSITY

BY

EMRE GÜNAY

IN PARTIAL FULFILLMENT OF THE REQUIREMENTS
FOR
THE DEGREE OF MASTER OF SCIENCE
IN
GEOLOGICAL ENGINEERING

SEPTEMBER 2012

Approval of the thesis:

NUMERICAL MODELING OF EDREMIT GEOTHERMAL FIELD

submitted by **EMRE GÜNAY** in partial fulfillment of the requirements for the degree of **Master of Science in Geological Engineering Department, Middle East Technical University** by,

Prof. Dr. Canan ÖZGEN _____
Dean, Graduate School of **Natural and Applied Sciences**

Prof. Dr. Erdin BOZKURT _____
Head of Department, **Geological Engineering**

Prof. Dr. Nurkan KARAHANOĞLU _____
Supervisor, **Geological Engineering Dept., METU**

Examining Committee Members:

Prof. Dr. Mahmut PARLAKTUNA _____
Petroleum and Natural Gas Engineering Dept., METU

Prof. Dr. Nurkan KARAHANOĞLU _____
Geological Engineering Dept., METU

Prof. Dr. Nilgün GÜLEÇ _____
Geological Engineering Dept., METU

Prof. Dr. Erdin BOZKURT _____
Geological Engineering Dept., METU

Assist. Prof. Dr. Koray K. YILMAZ _____
Geological Engineering Dept., METU

Date: 28.09.2012

I hereby declare that all information in this document has been obtained and presented in accordance with academic rules and ethical conduct. I also declare that, as required by these rules and conduct, I have fully cited and referenced all material and results that are not original to this work.

Name, Last name: Emre GÜNAY

Signature :

ABSTRACT

NUMERICAL MODELING OF EDREMIT GEOTHERMAL FIELD

Günay, Emre
M.Sc., Department of Geological Engineering
Supervisor: Prof. Dr. Nurkan Karahanoğlu

September 2012, 97 pages

The purpose of this study is to examine the geothermal potential, sustainability, and reinjection possibility of Edremit geothermal field. In order to investigate this, a numerical model consisting of a hot and cold water aquifer system is established. A two dimensional cross sectional model is set to simulate this geothermal system. Different pressure and temperature values are applied to the nodes at the boundaries to perform a steady state calibration which minimizes the computed results and observed values obtained from the near well logs. After the calibration, three alternative scenarios are proposed and the response of the pressure and temperature to these conditions is evaluated. At first the water is pumped from the wells of Yağcı, Derman, Entur and ED-3 seperately at a mass rate of 5 kg/s and energy rate of 4.182×10^5 J/s. Then, in scenario 2 the water is pumped at the same rate from all the wells mentioned in the first scenario together. For the third scenario another well is opened to the geothermal system and 80% of the pumped water (temperature being 20^0C) is injected to the system from the wells while all the wells mentioned are working. The results of these scenarios are utilized to evaluate the reservoir in terms of its response to different production and re-injection conditions. Interpretation of the reservoir response in view of the

pressure and temperature declines emphasize that such a simulation study can be applied to assess potential and sustainability of the geothermal systems.

Keywords: Edremit Geothermal Field, two dimensional cross sectional model, geothermal system, steady state calibration, simulation, reinjection possibility

ÖZ

EDREMİT JEOTERMAL SAHASININ SAYISAL MODELLEMESİ

Günay, Emre
Yüksek Lisans, Jeoloji Mühendisliği Bölümü
Tez Yöneticisi: Prof. Dr. Nurkan Karahanoğlu

Eylül 2012, 97 sayfa

Bu çalışmanın amacı Edremit jeotermal sahasının jeotermal potansiyelini, sürdürülebilirliğini ve reenjeksiyon olasıklarını araştırmaktır. Bunu yapmak için bir sıcak ve soğuk su akiferinden oluşan sayısal bir model kurulmuştur. Bu jeotermal sistemi simule etmek için iki boyutlu enine kesitsel bir model kurulmuştur. Hesaplanmış ve yakındaki kuyu loglarından elde edilen gözlemlenen değerler arasındaki farkı en aza indirgeyen olağan hal kalibrasyon yapımını sağlamak için sınırdaki noktalara değişik basınç ve sıcaklık değerleri uygulanmıştır. Kalibrasyondan sonra üç alternatif senaryo önerilmiş ve sıcaklık ve basıncın bu şartlara verdikleri tepkiler değerlendirilmiştir..İlk önce Yağcı, Derman, Entur ve ED-3 kuyularından ayrı ayrı 5 kg/s kütle oranında ve 4.182 x 10^5 J/s enerji oranında su çekilmiştir.. İkinci senaryoda ise ilk senaryoda belirtilen kuyuların hepsinden aynı anda aynı oranda birlikte çekim yapılmıştır. Üçüncü senaryo içinse jeotermal sisteme yeni bir kuyu açılmış ve ikinci senaryodaki kuyuların hepsi çalışırken pompalanmış suyun %80'i (20^0C sıcaklığında) sisteme geri basılmıştır. Bu senaryoların sonuçları rezervuarı farklı üretim ve reenjeksiyon şartlarına cevapları açısından değerlendirmek üzere kullanılmıştır. Rezervuarın sıcaklık ve basınç düşümlerine verdiği cevabın yorumlanması böyle bir

simülasyon çalışmasının jeotermal sistemin potansiyel ve sürdürülebilirliğini değerlendirmede uygulanabileceğini vurgulamaktadır.

Anahtar kelimeler: Edremit Jeotermal Sahası, iki boyutlu enine kesitsel model, jeotermal sistem, olağan hal kalibrasyon, simulasyon, reenjeksiyon olasılığı

To my family

ACKNOWLEDGEMENTS

I would like to thank Prof. Dr. Nurkan Karahanoğlu for his support, guidance, advice and patience during the period of this thesis.

I would like to thank examining committee members Prof. Dr. Mahmut Parlaktuna, Prof. Dr. Nilgün Güleç, Prof. Dr. Erdin Bozkurt, and Assist. Prof Dr. Koray Yılmaz for their contributions.

I would also like to thank Dr. Müfit Şefik Doğdu and Lütfi Gür Köksal for their contribution to this thesis.

Thanks to Işıl Ömeroğlu, Arif Mert Eker, Selim Cambazoğlu, Mustafa Kaplan for their support during this thesis.

Finally, I would like to thank my family, my mother Birsen Günay, my father Mehmet Turhan Günay and my brother Mehmet Selim Günay for their invaluable love, support and encouragement throughout my entire life.

TABLE OF CONTENTS

LIST OF TABLES

TABLES

LIST OF FIGURES

FIGURES

CHAPTER 1

INTRODUCTION

1.1 Purpose and Scope

Turkey is an energy dependent country. It imports almost 60% of its energy from the rest of the world since it has limited number of fossil fuels like petroleum and natural gas. In order to decrease its demand to the other countries, she needs to use some clean, domestic, and renewable energy resources. Geothermal energy, the part of the Earth's heat that can be used by man, is one of them. Situated in the middle of Alpine-Himalayan orogeny and is highly affected by volcanism, fumarole hydrothermal alterations and more than 600 hot springs, some of which is above 100^{o}C, Turkey has one of the highest geothermal energy potential in the world.

Geothermal energy is mainly used for space heating and electricity production purposes. If the temperature of the hot water is quite hot (above 120^{o}C), electricity is produced from that energy. If the water is not extremely hot, it is generally used for space heating. Edremit is one of the important geothermal energy fields for district heating purposes. The water there is about 60^{o}C which is relatively low for those kinds of geothermal resources.

The purpose of this thesis is to investigate the geothermal potential, sustainability and reinjection possibility of the Edremit Geothermal Field. For this purpose, a model that comprises a hot and a cold water aquifer system is constructed. In order to do so; some wells penetrates the confined aquifer and the others, the unconfined aquifers, are taken into consideration.

1.2 Previous Studies

The report of the Hydraulic State Works (Devlet Su İşleri in Turkish abbreviated as DSİ) in 1977 can be considered as the very beginning hydrogeological studies in the region. This report gives information about the hydrogeological features of the area and the data from 99 wells (11 exploration wells, 77 exploitation wells and 11 boreholes for drinking purposes of the municipalities) with depths between 45 and 300 meters around that zone. However, that report is based only on the upper cold aquifer. The lower hot aquifer is not mentioned in this report at all.

Ural (1978) utilized the report written by General Directorate of Hydraulic State Works and made a digital model using a relatively new method in those days known as "finite difference method" to model the Edremit valley aquifer. Here, he found that there exists an artesian aquifer in the west part of Edremit plain close to the shoreline. He used transmissivity values ranging 1400-5400 m^2/day and storage coefficient between 10^{-3} and 10^{-2} for the artesian aquifer. He calculated the transmissivity value of the water table aquifer as well. He assumed the average thickness of the confined and unconfined aquifers around 100 m and 60 m, respectively.

Sarp et al. (1998) completed a study in Edremit Geothermal Field. Four geothermal gradient and exploration wells were drilled and a conceptual model was proposed; it states that the water becomes hotter and hotter and rises to the surface using faults .They predicted the reservoir temperature as nearly as 90^{o}C. They also mapped a new East-West-striking normal fault near Derman.

Three new wells were drilled in the area in 2001 by the General Directorate of Mineral Research and Exploration (Maden Tetkik ve Arama Genel Müdürlüğü abbreviated as MTA in Turkish). The depths of these wells range between 195 and 495 meters (MTA, 2001). Six new wells were then drilled with depths between

216 and 300 meters by General Directorate of Bank of Provinces (İller Bankası abbreviated as İB in Turkish).

Demirel et al. (2004) performed a study about the occurrence of geothermal systems in the tectonically compressive regions in Derman geothermal field which is located in the Biga Peninsula close to our study area. They reported hot springs with temperatures ranging between 30 and 100^{o}C. They stated that faults and fractures are the routes for flow of water. Furthermore, they claimed heat sources are affected by the volcanism, granitic intrusion and tectonic activities. Additionally they mentioned that hot waters reach the surface along tensional fractures associated with strike slip faulting. They made a geological model and proposed that meteoric water flows through these tensional fractures and water is heated by conduction and convection. They have concluded that tectonic activities and volcanism are the main cause for geothermal systems to develop.

Coşkun et al. (2009) used four new parameters to evaluate daily, monthly and annual geothermal energy data for the applied to the Edremit Geothermal District Heating System (abbreviated as GDHS). These parameters are energetic renewability ratio, exergetic renewability ratio, energetic reinjection use, and exergetic reinjection use; these terms are defined as "the ratio of useful renewable energy obtained from the system to the total energy input", "the ratio of useful renewable exergy obtained from the system to the total exergy input", "the ratio of renewable energy discharged to the environment or reinjected to the well from the system to the to the total geothermal energy supplied to the system", and "the ratio of renewable exergy discharged to the environment or reinjected to the well from the system to the total geothermal exergy supplied to the system", respectively (Coşkun et al., 2009). They mention that this study is made during two seasons: (i) summer (warm) season during which domestic hot water production is significant and (ii) the cold (heating) season during which heating purposes are the major factor and domestic hot water production is added as a secondary purpose. They calculated the energetic renewability and exergetic ratio between 0.32 and 0.33 and 0.25 and 0.35 in the summer, respectively. These parameters are between 0.33

and 0.34 and 0.53 and 0.63 for the cold season. It is observed that both two parameters decrease as the temperature decreases in heating season and increases in warm season. The energetic and exergetic reinjection ratios range between 0.59 and 0.62 and 0.10 and 0.20 during the hot season, respectively, while they range between 0.65 and 0.66 and 0.30 and 0.43 in the heating season, respectively. It is therefore concluded that both parameters increase as the temperature declines in cold season and rises in summer time.

Avşar (2011) studied Edremit geothermal field and made a hydrogeochemical model of this field by considering hydraulic, geophysical and chemical parameters. He then added 3rd dimension to draw the 3D block diagram of the region. He divided the wells into five types according to the depth of penetration of the wells into the aquifer (cold, warm and hot) and the position of the wells near major faults. After this modeling study, the geothermal potential assessment of the study area is evaluated. He calculated the accessible resource base and recoverable heat energy as 34,500 TJ and 9.1 MW_t respectively, with the probability of 0.90.

1.3 Layout of the Thesis

This thesis is comprises five chapters.

Chapter 1 is mainly about the purpose and scope of this study and summarizes the results of the previous works that have been made.

Chapter 2 focuses on the geographical and geological setting of the Western Anatolia and geology of the Edremit geothermal field.

Chapter 3 discusses how the numerical model is performed.

Chapter 4 proposes numerical applications and future predictions in the numerical model.

Final Chapter, Chapter 5, gives a brief summary of what has been done in this study and makes recommendations.

CHAPTER 2

REGIONAL AND LOCAL GEOLOGY

2.1 Geographical Setting

The study area is located in Edremit Plain in the northwest Anatolia, Aegean Region in Balıkesir, Turkey (Figure 2.1). It lies between Edremit Bay in the south and Kazdağları in the north. The latitude and longitude of the region are 39^{o} 35' N and 27^{o} 2' E, respectively. It is bounded by high mountains like Kazdağları, Eybek Mountain and Gürgen Mountain. The elevation of the highest point in the region lies at the peak of Kazdağları with the altitude of 1767 meters whereas the lowest elevation of the area is situated in Edremit Plain with the altitude of 20 meters (T.C. Edremit Kaymakamlığı, 2012).

The region has a typical Mediterranean climate where the summers are hot and dry while winters are cool and rainy. The annual mean temperature is 20^{o}C. The highest extreme temperature is 42^{o}C. -19^{o}C ,on the other hand, is the lowest extreme temperature observed in the region. The average yearly precipication is estimated as 707 mm. The mean moisture content is measured as 65%. The typical flora of the region is olive trees which cover the area from the sea level to 500 meters. The pine trees begin from this height and continue up to the mountain peaks (Devlet Meteoroloji İşleri Genel Müdürlüğü, 2012). The average and extreme values of Balıkesir is given in Table 2.1.

Table 2.1 Official statistics about the climate of Balıkesir (MGM, 2012)

	Jan	Feb	Mar	Apr	May	Jun	Jul	Aug	Sep	Oct	Nov	Dec
avg. temp (^{o}C)	4.8	5.8	8.3	13.1	17.8	22.7	24.9	24.5	20.7	15.6	10.0	6.4
avg. highest temp (^{o}C)	9.0	10.4	13.9	19.3	24.5	29.3	31.2	30.9	27.6	21.8	15.3	10.3
avg. lowest temp (^{o}C)	1.1	1.7	3.4	7.0	10.9	15.0	17.8	18.0	14.1	10.2	5.4	2.8
avg. sunshine time (hours)	3.0	3.4	4.7	6.1	8.7	10.8	11.9	10.5	8.3	5.8	3.7	2.3
number of avg. rainy days	12.7	11.5	10.6	9.3	7.0	4.2	1.6	1.4	3.7	7.3	9.4	12.9
mean monthly total rain amount (kg/m^2)	67.3	64.9	65.8	50.4	41.3	19.3	9.5	16.6	38.1	46.4	80.9	95.8

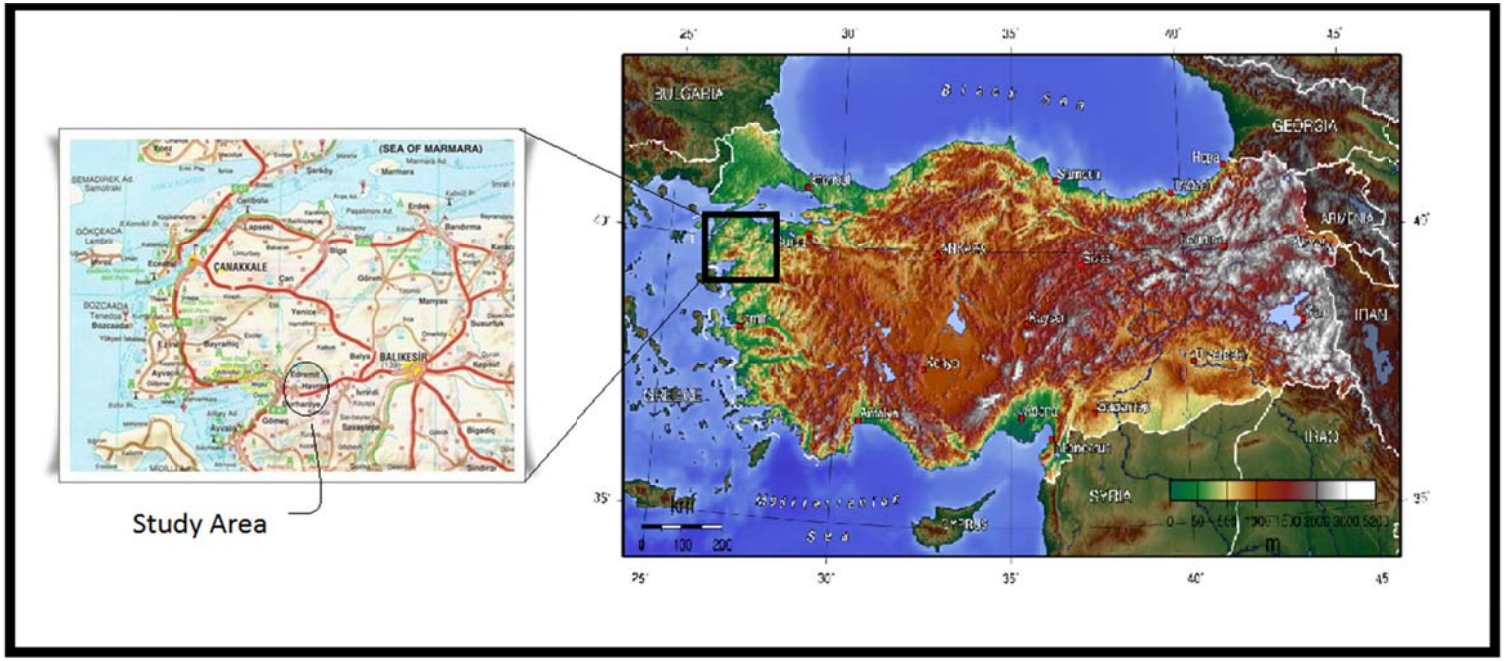

Figure 2.1 Geographical setting of Edremit geothermal field

2.2 Regional Geology

The study area, Edremit geothermal field, is located in Western Anatolia. The characteristics of this region are the E-W trending horst and grabens which includes minor cross-cutting grabens trending NE to NW (Figure 2.3). The horsts and grabens are lows and highs bounded by active normal faults. These are also NE-SW striking active dextral strike slip faults to the northwest of the Edremit.

The neotectonic deformation of Western Anatolia commenced when the Arabian Plate and Eurasian Plate collided during late Miocene. This resulted in the formation of dextral North Anatolian Fault Zone and sinistral East Anatolian Fault Zone which leads to the westward movement of the Anatolian plate along these boundary structures (Figures 2.2 and 2.3).

Western Anatolia is intensely studied. However, significant arguments are made on the neotectonic development of extensional structures. Three models are considered. Dewey and Şengör (1979) (also Şengör 1979, 1980, 1987; Şengör et al. 1985) claims that Arabia and Eurasia collided during late Serravalian time (about 12 Ma) and lead to the westward movement of Anatolian plate along its boundary structures (right lateral North Anatolian fault zone and left lateral East Anatolian fault zone) which are right lateral and left lateral strike slip faults, respectively); tectonic escape is considered as the extension of the brittle crust and therefore the formation of horst and graben system in Western Anatolia. McKenzie (1978), Le Pichon & Angelier (1979, 1981) Kissel & Laj (1988), and Meulenkamp et al. (1988) suggested back arc spreading model for the Aegean. The extension was attributed to the south-southwestward movement of the Aegean trench system: subduction roll-back. This forms the horst and graben system in the back arc region (from Aegean to Western Anatolia). The initiation age of Hellenic subduction roll-back, however, is a matter of debate. Proposals range between 5 Ma and 60 Ma. The third is the orogenic collapse model proposed originally by Dewey (1988), Seyitoğlu & Scott (1992) and Seyitoğlu et al. (1992). This model

argues for spreading and thinning of the overthickened crust subsequent to Palaeogene crustal thickening during the closure of the Neotethyan ocean across the İzmir-Ankara suture by the late Oligocene to Early Miocene. Koçyiğit et al. (1999) combined these three models and suggested that extension in Western Anatolia is episodic and comprises two-stages namely core-complex formation in the footwall of low-angle normal faults (detachment faults) during orogenic collapse and sugsequent modern graben formation along high-angle normal faults.

The geology of Turkey is very complex as it is located in the Alpine-Himalayan belt near the intersection of Africa, Arabia and Eurasia. These lands were once located at the suture zone of two megacontinents, Gondwana (south part) and Laurasia (north part). Turkey is made up of bits and pieces derived from the two megacontinents; they were later amalgamated during Alpine orogeny when Arabian plate and Anatolia collided. During this process the Tethys oceans that were once formed, closed consequently (Bozkurt and Mitwede, 2001). Western Turkey consists of Anatolide-Tauride Platform, including the Menderes Massif in the south and the Sakarya Continent, in the north. The İzmir-Ankara Neotethyan Suture forms the boundary between the two.

The Menderes Massif contains three partite sequence. Precambrian gneiss basement called as Gneissic core and a cover rocks of Paleozoic “schist envelope”. and then, Mesozoic-Cenozoic “marble envelope”. The Massif was subjected to green schist to amphibolite facies metamorphism conditions in Middle Eocene, the metamorphic grade drops gradually away from the core (Candan et al. 2011; Dora 2011; Erdoğan et al. 2011; Koralay et al. 2011 and references therein for further reading)..

The other block, Sakarya continent, consists of nonmetamorphosed to irregularly metamorphosed-especially to greenschist facies-, strongly deformed and overlapped basement over clastic and carbonate sedimentary cover rocks (Bingöl et al., 1975; Şengör and Yılmaz, 1981; Koçyiğit, 1991; Okay, 1989; Genç and Yılmaz, 1995; Yılmaz et al., 1995; Okay et al., 1996; Göncüoğlu et al., 2000;

Robertson and Ustaömer, 2012 and references therein). Other tectonic units of Anatolides include the Afyon Zone, Tavşanlı Zone, Bornova flysch, Lycian Nappes and the readers are referred to recent literature for further reading (Okay 2011; Göncüoğlu 2011 ; Okay et al. 2012 and references therein).

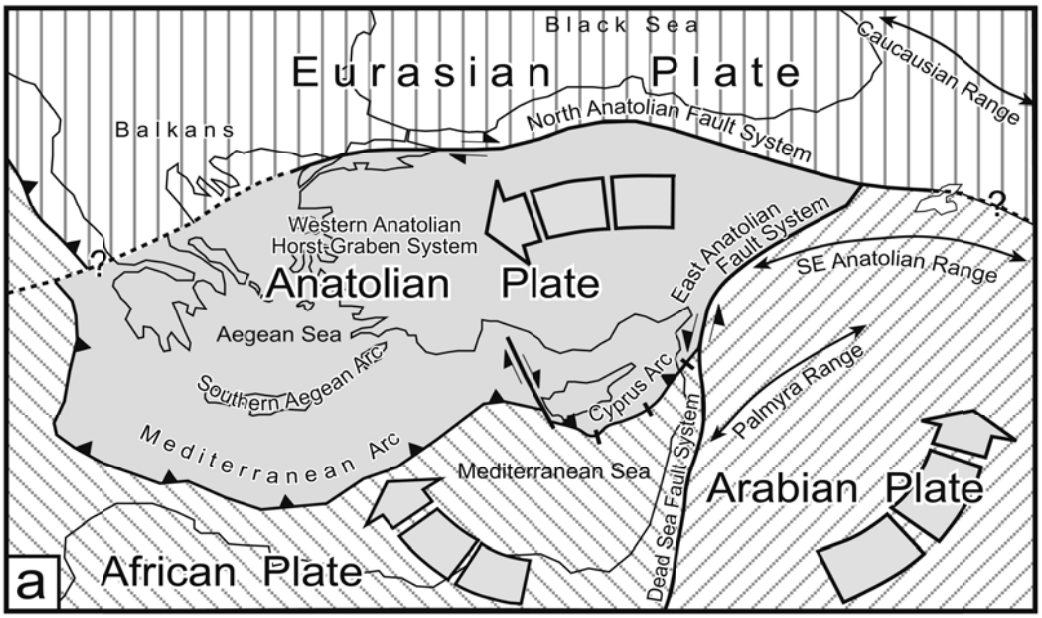

Figure 2.2 Map showing major tectonic movements in western Anatolia (Bozkurt and Rojay, 2005)

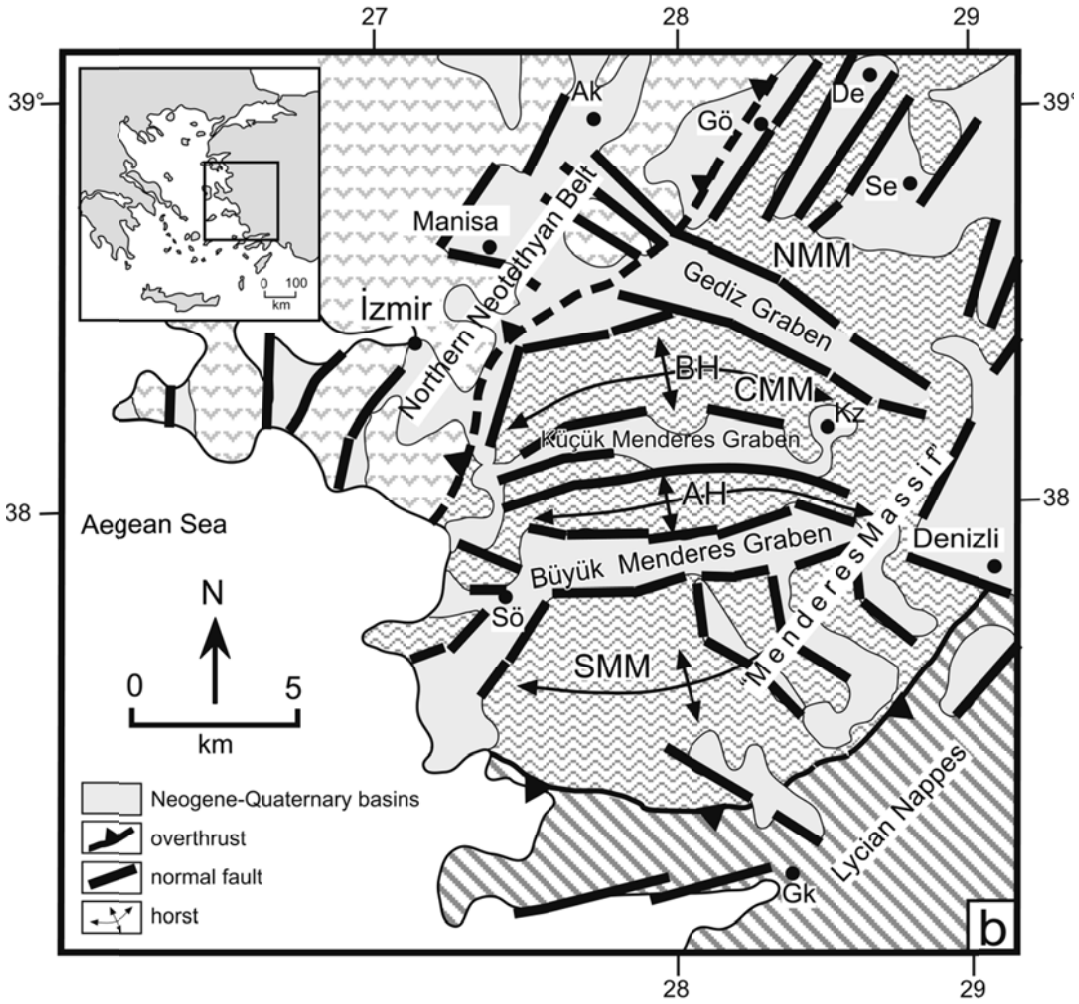

Figure 2.3 Map showing neotectonics of western Anatolia (AH- Aydın horst, Ak- Akhisar, BH- Bozdağ horst, De- Demirci, Gk- Gökova, Gö- Gördes, Kz- Kiraz, Sö- Söke, Se- Selendi, NMM- northern Menderes Massif, CMM- central Menderes Massif, SMM- southern Menderes Massif) (Bozkurt and Rojay, 2005)

2.3 Local Geology of the Study Area

The main units from bottom to top is listed as Kazdağ Group, Karakaya Formation, Bilecik Formation, Eybek Granodiorite, Hallaçlar Formation, Ballıca Formation and Plio-Quaternary deposits (Bingöl et al., 1973) (see Figures 2.4 and 2.5).

The Kazdağ Group or Kazdağ Massif lies at the bottom of the Edremit geothermal field (Figure 2.5). This group is a high grade metamorphic core complex that outcrops in Kazdağları. It contains even intercalation of amphibole bearing gneiss and marble horizons (as part of Fındıklı Formation), meta-opholitic rocks (as part of Tozlu Formation) (Bingöl et al., 1975) metacarbonates (as part of Sarıkız Marble) (Bingöl et al. ,1975), and gneisses (as part of Sutuven Formation) (Bingöl, 1969); (Duru et al., 2004). Kazdağ Group is exposed as a doubly plunging, NE-SW trending anticlinorium. The metamorpics of Kazdağ are in tectonic contact with other rock units. The metamorphism took place in Oligo-Miocene (Okay et al., 1991; Okay and Satır, 2000).

The second unit, Karakaya Formation, is underlain by the Kazdağ Massif (Bingöl et al. ,1973) (Figure 2.5). The age of this unit is early Triassic and it is exposed in the north of Edremit geothermal field. This formation is 250 meters thick and consists of two groups of units and they show lateral and vertical facies changes. The first unit group includes mudstones, radiolarites and spilitic basalts while the second group contains alternation of quartzite, siltstone, sandstone and conglomerate (Avşar, 2011).

The third unit on the study area is Bilecik Formation and it unconformably overlies the Karakaya Formation (Altınlı., 1973) (Figure 2.5). This unit correlates with the Alancık Formation (Bingöl et al. ,1973). It is a 130 meters thick unit and consists of bioclast, oolites, and sandy limestone with many intraclasts; a Late Jurassic to Early Cretaceous age is assigned to this unit (Bingöl et al, 1973; MTA 2007).

The fourth unit is Oligocene Eybek granodiorite and it intrudes the Bilecik Formation. The age of this unit is stated as Oligocene. (Krushensky, 1976; Ercan et al., 1984). It correlates with other intrusives like Kozak, Evciler, Kestenbol, Karabiga and Ilıca granitoids, in northwest Anatolia simply because they are similar in age, lithology and several other petrographic features (Sarp et al., 1998; Genç and Altunyanak, 2007).

Eybek granodiorite is covered by the fifth unit, Hallaçlar Formation which also overlies Bilecik Formation. The age of the formation is considered as Late Oligocene-Early Miocene and the thickness is measured as 400 meters. Çan volcanics is equivalent of this formation. It contains agglomerate, andesite, tuff, dacite, and rhyo-dacite. High alteration, particularly argilization and silicification is observed (Koç et al., 1994). Plutonic activity had once been the dominant motion in the study area. This formation is thought to be the secondary stage of magmatism in the region (Ercan et al., 1985).

The sixth unit considered, Ballıca Formation, overlies Hallaçlar Formation with an unconformity. The age of this formation is assigned as Middle-Late Miocene and it is 60 meters thick. This formation is exposed in the south of the region. It includes clayey limestone, marl, conglomerate, siltstone, and sandstone. Some unconsolidated sediments like sand and gravel with clayey matrix are observed. This formation is correlated with İlyasbaşı Formation of MTA (2007); (Ercan et al., 1985).

The last unit overlying Ballıca Formation is the Plio-Quaternary sediments. They consist of unconsolidated mudstone, sandstone, and conglomerate (Avşar, 2011).

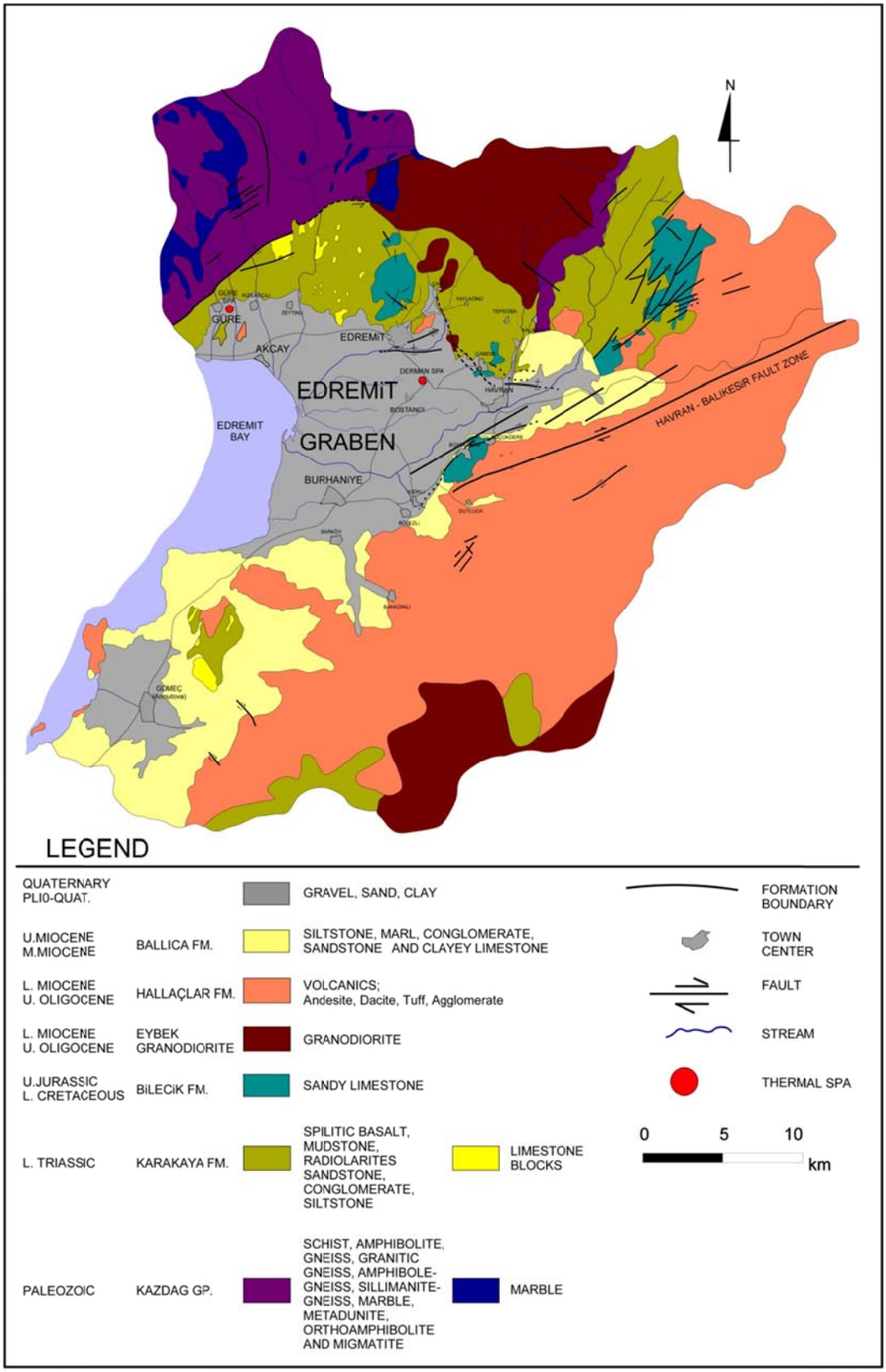

Figure 2.4 Geological map of Edremit geothermal field (Avşar, 2011)

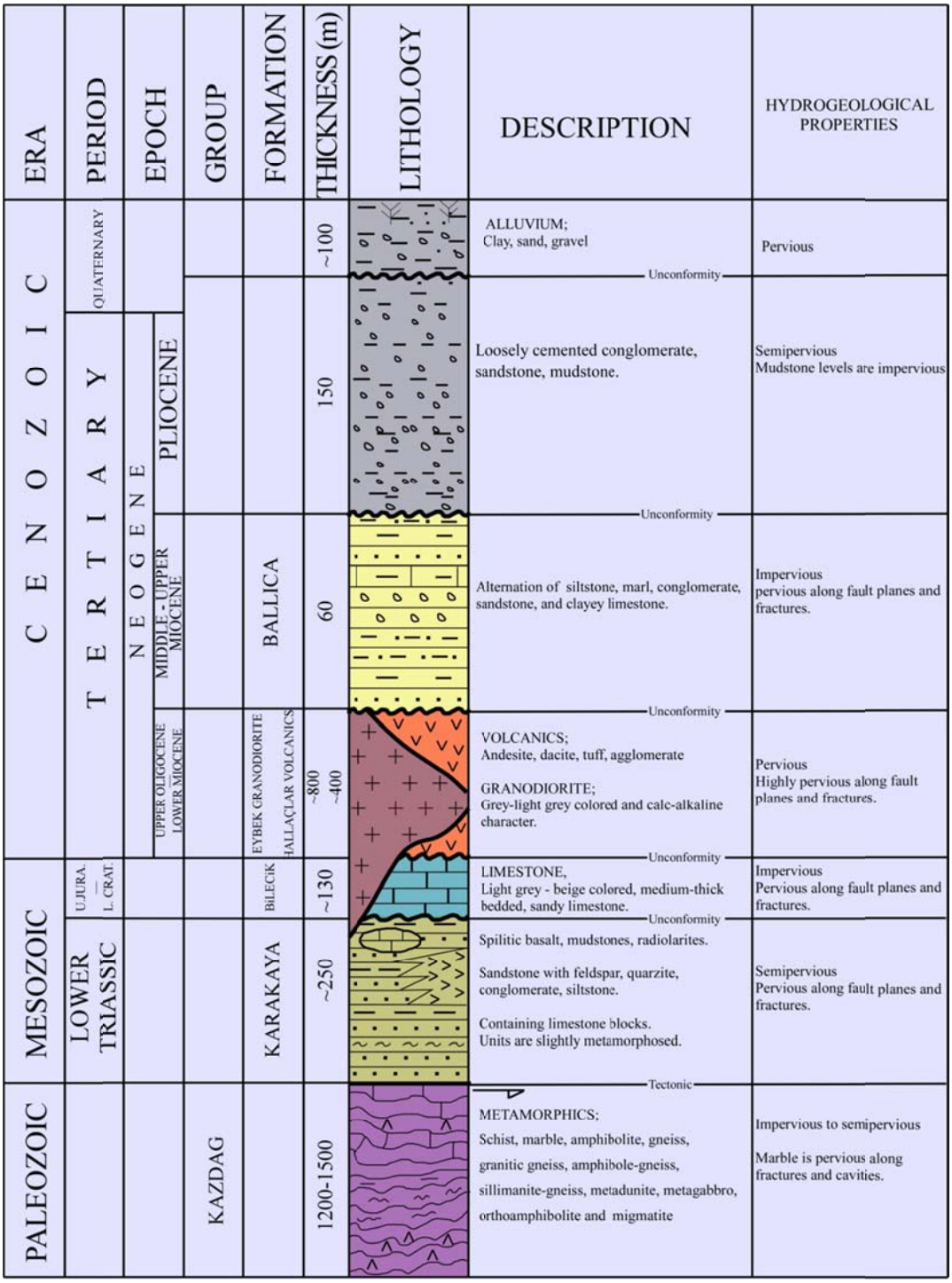

Figure 2.5 Generalized columnar section of the Edremit geothermal field (Avşar, 2011)

2.4 Hydrogeology of the Edremit Geothermal Field

The drainage area of Edremit plain is 1230 km^2. Five important streams in the area are Havran, Edremit, Karınca, Kızılkeçili, and Zeytinli stream. Of these five streams, Edremit and Havran are the major sources that provide water for the area. Edremit and Havran streams have drainage basins of 534 and 174.5 km^2, respectively. DSİ (1977) reports that hydraulic budget of the Edremit plain is calculated as $85x10^6$ m^3/year. Recharge of Edremit plain is from precipitation ($33.5x10^6$ m^3/year) and surface runoff ($51.5x10^6$ m^3/year) while discharge of the plain is through artificial discharge ($28.5x10^6$ m^3/year), evapotranspiration ($9x10^6$ m^3/year), discharge to the sea ($31x10^6$ m^3/year), and discharge by the streams ($16.5x10^6$ m^3/year). Since DSİ (1977) is relatively old, these results may be different at present due to the change in climate and due to opening of new wells in the area.

The system contains two aquifers and a thin relatively impervious layer in between. The upper aquifer is a relatively cold, shallower unconfined aquifer. It consists of Plio-Quaternary units. The impervious layer comprises Ballıca Formation and serves as an aquiclude for the upper and lower aquifers lying above and below. The lower aquifer is a relatively hot, deeper confined aquifer. This layer consists of pervious conglomerate and agglomerate units.

Currently there exist 3 wells that are usable (ED-1, ED-3 and EDJ-3) drilled by MTA. Since mass flow rate of ED-2 is significantly low, this well is shut. Three wells EDJ-4, ED-5, and EDJ-7 are pumped but they are not connected to system. Wellhead production temperature is about 60^oC and mass flow rates fluctuate between 18 and 86 kg/s (Table 2.2).

The other wells are drilled by DSİ, İB, and non-governmental miscellaneous firms. Data about these wells are given in Table 2.3.

Table 2.2 Explanation of the well data in Edremit geothermal field (Coşkun et al., 2009)

Name	Depth (m)	Wellhead Temp (^{o}C)	Flow Rate (kg/s)	Type/Condition
ED-1	195.60	60.00	75	Production/Operating
ED-2	496.50	55.00	2	Closed
ED-3	495.00	59.00	18	Production/Operating
EDJ-3	266.00	60.00	86	Production/Operating
EDJ-4	296.00	49.00	86	Production/Out of Service
EDJ-5	216.00	58.70	45	Production/Out of Service
EDJ-7	246.00	58.30	30	Production/Out of Service

Table 2.3 Data about the wells in Edremit geothermal field according to the temperature (L=lower aqui. U= upper aqui.) (Avşar, 2011)

Aqui.	Well No.	Drilled by	Drilling Date	Easting	Northing	Elev (m)	Depth (m)	Temp (^{o}C)
L	ED-3	MTA	2001	503639	4380394	22	495	62
L	ED-1	MTA	2000	503718	4380329	22	189	62
L	EDJ-3	İB	2005	503634	4380252	21	266	59
L	EDJ-2	İB	2008	503916	4380049	24	300	58
L	EDJ-5	İB	2005	504054	4380273	23	216	55
U	DERMAN	M.	-	503731	4380197	22	100	53
U	ENTUR	M.	2000	503743	4380178	22	90	51
L	EDJ-7	İ.B.	2005	503968	4380402	23	246	51
L	EDJ-4	İ.B.	2005	503458	4380136	19	296	50
L	ED-2*	M.T.A	2001	504014	4380293	23	496	47
L	EDJ-8	İ.B.	2007	503815	4380491	23	250	43
U	YAĞCI	M.	-	503729	4380591	23	100	42
U	DSİ-6	DSİ	1970	503753	4379919	24	95	39
U	DOĞANDERE	M.	-	503753	4379919	24	30	32

Table 2.3 (Continued)

U	DSİ-9	DSİ	1974	502958	4380668	20	122	32
U	HASTANE	DSİ	1975	504099	4381130	28	90	31
U	DSİ-5	DSİ	1970	503949	4380066	24	91	30
U	DSİ-7	DSİ	1970	504088	4379653	22	132	21
U	DSİ-8	DSİ	1972	505195	4380605	26	83	18
U	EMİNKUYU**	DSİ	-	503129	4382054	28	-	18
U	EMİNDSİ	DSİ	1975	502824	4382144	24	100	12

*Non-operational well

CHAPTER 3

NUMERICAL MODELING

3.1 Introduction

Edremit field is one of the important geothermal fields of Turkey. In order to investigate its geothermal potential, sustainability and reinjection possibilities a numerical model is established. The model tries to simulate a geothermal system consisting of a colder unconfined, and a hotter confined aquifer separated by a rather thin and comparatively impervious layer in between. At present it is not yet clear if there is a hydraulic relation between the two aquifers. In addition to these a couple of faults are present in the area. There are several wells drilled into these aquifers producing cold and hot water from the aquifers depending on their depths. In order to simulate this geothermal system a two dimensional, cross sectional numerical model is built. After setting up the model, various boundary conditions are applied and the model results are compared with the observed during calibration studies (Figure 3.1).

3.2 Conceptual Model

A conceptual model of the geothermal system has been prepared by using previous studies related to the Edremit valley and the geological models proposed by Avşar (2011). The conceptual model visualizes that the Edremit Geothermal System consists of a colder unconfined, and a hotter confined aquifer separated by a rather thin and comparatively impervious layer in between (Figure 3.1). The upper unit is the unconfined aquifer which contains alluvium, unconsolidated mudstone, sandstone and conglomerate. This aquifer carries relatively cold water in it. The

lower confined aquifer transmits hot water. It comprises highly permeable conglomerate and agglomerate. A thin quite impervious layer lies between those two aquifers. This layer serves as a semi pervious layer for both of the aquifers. The geothermal system is heated from bottom and energy is stored in the lower aquifer yielding hot water production from wells drilled into this aquifer. The upper aquifer is rather cool and it produces cold water. However some of the wells drilled into upper aquifer are producing warm water probably due to a mixing of cold water with hot water. This is also thought by mixing through a fault system that cuts both aquifers and it is verified by wells drilled near to fault system yield hot water. Data about these wells are given in Table 3.1. There are several wells drilled into these aquifers producing cold and hot water from the aquifers depending on their depths.

Careful inspection of the present conditions in the Edremit valley shows that the wells are located at the central part and they cover a small area as compared to the whole valley. Considering this fact a smaller area closer to the production wells is chosen and a cross sectional numerical model is built in order to examine variation of the pressure and temperature in the geothermal system. In doing this a line of section (A-A') is selected in the basin where several wells are located (Figure 3.2) and a cross sectional mesh consisting of 14400 quadrilateral elements with 14739 nodes is constructed. In this way among 22 wells drilled in the area 7 of them are located at the cross section which would be used in the calibration studies. The cross sectional model is located along the line of section and it is designed to be 2600 m long and 500 m deep. The depth of the model is chosen to be 500 meters to use the information of the deepest well (495 m) drilled at the study area. This size is so selected because the cross section contains all the relatively warmer wells from north to south and the hottest two wells in the middle including a major fault in between. The fault zone (dipping 80 degrees) has approximately 20 meters width along the cross section and it is assumed to be vertical in the mesh construction (Figure 3.2 and Figure 3.3).

Table 3.1 Data about the Wells Used in the Model

Aqui.	Well No.	Node Number	Element on the Left	Element on the Right	Distance to the Origin (m)	Elev (m)	Depth (m)	Temp (^{o}C)
U	DSİ-9	1581	1500	1550	300	20	122	32
U	YAĞCI	7191	7000	7050	1400	23	100	42
L	ED-3	8313	8100	8150	1620	22	495	62
L	ED-1	10353	10100	10150	1740	22	189	62
U	DERMAN	10863	10600	10650	1840	22	100	53
U	ENTUR	11169	10900	10950	1900	22	90	51
U	DSİ-6	12699	12400	12450	2200	24	95	39

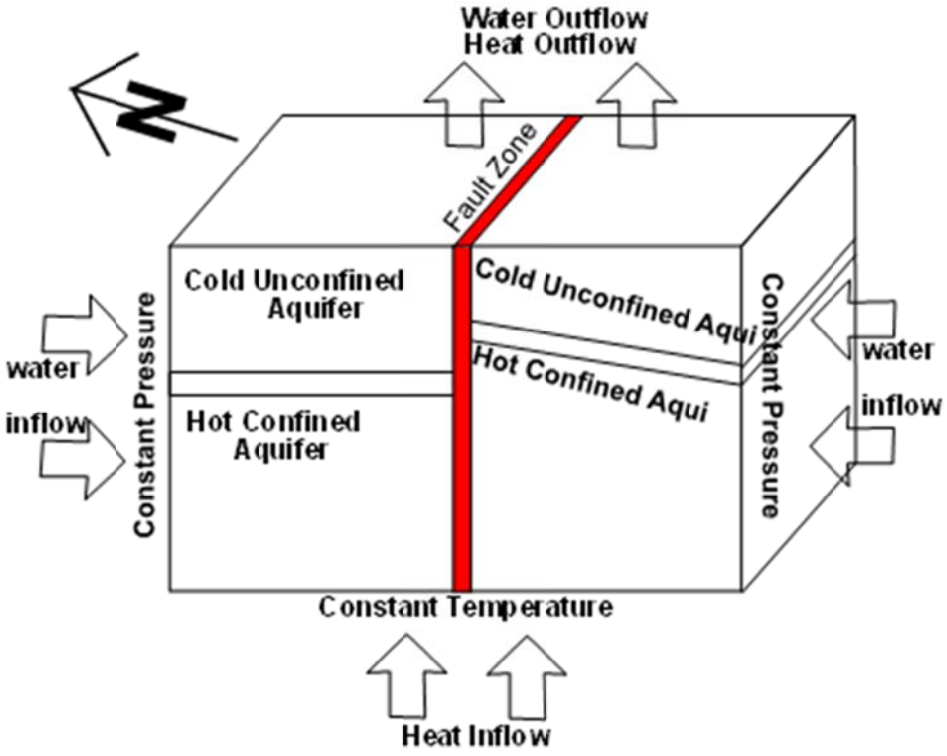

Figure 3.1 Block Diagram Showing the Conceptual Model and Boundary Conditions Simulated in the Model (not to scale)

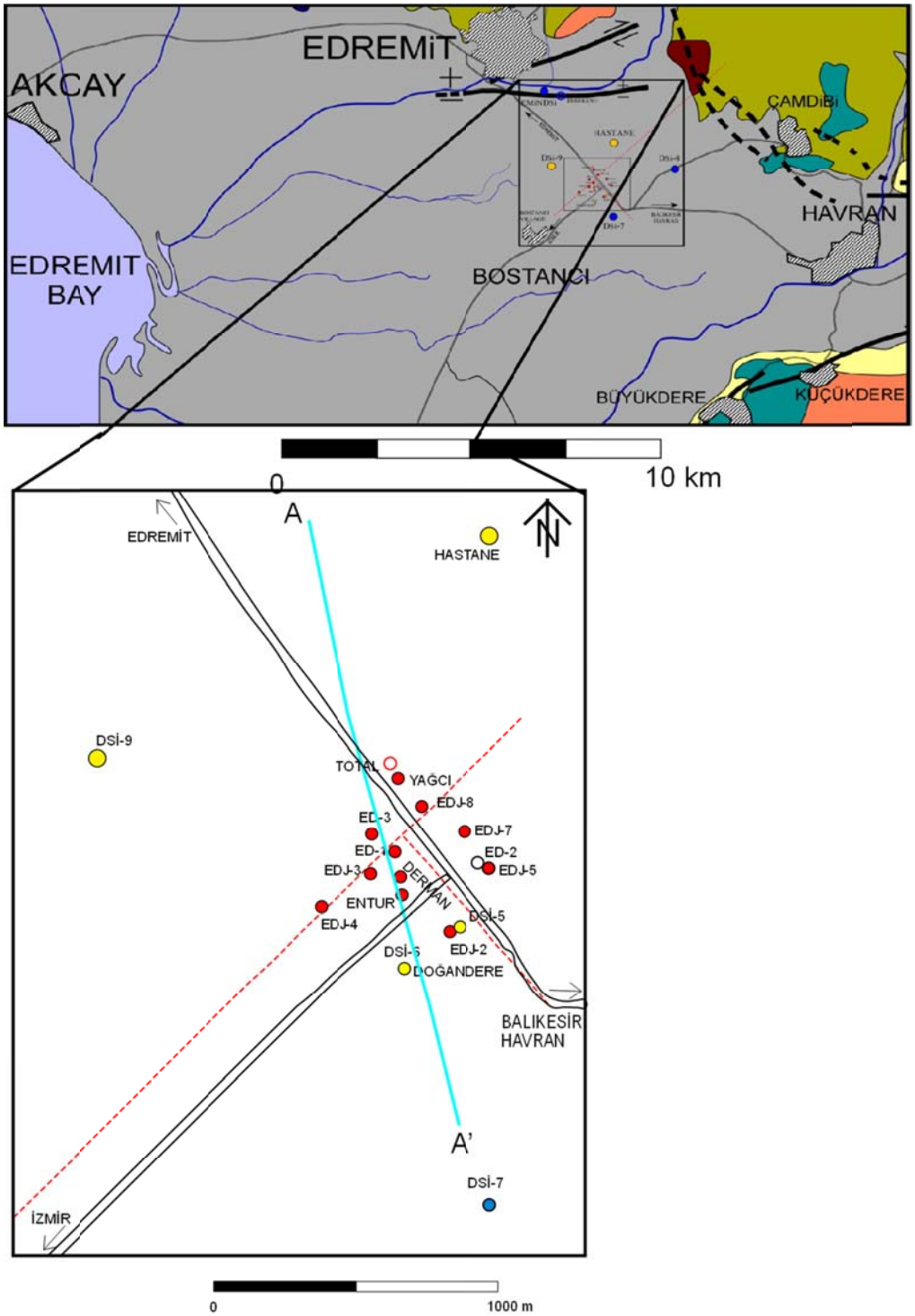

Figure 3.2 Map showing the well locations (red circles meaning hot geothermal wells, yellow circles correspond to the warm wells and blue circle is used to denote cold water wells), faults (red dashed lines) and line of section A-A' used in the conceptual model (map modified from Avşar, 2011)

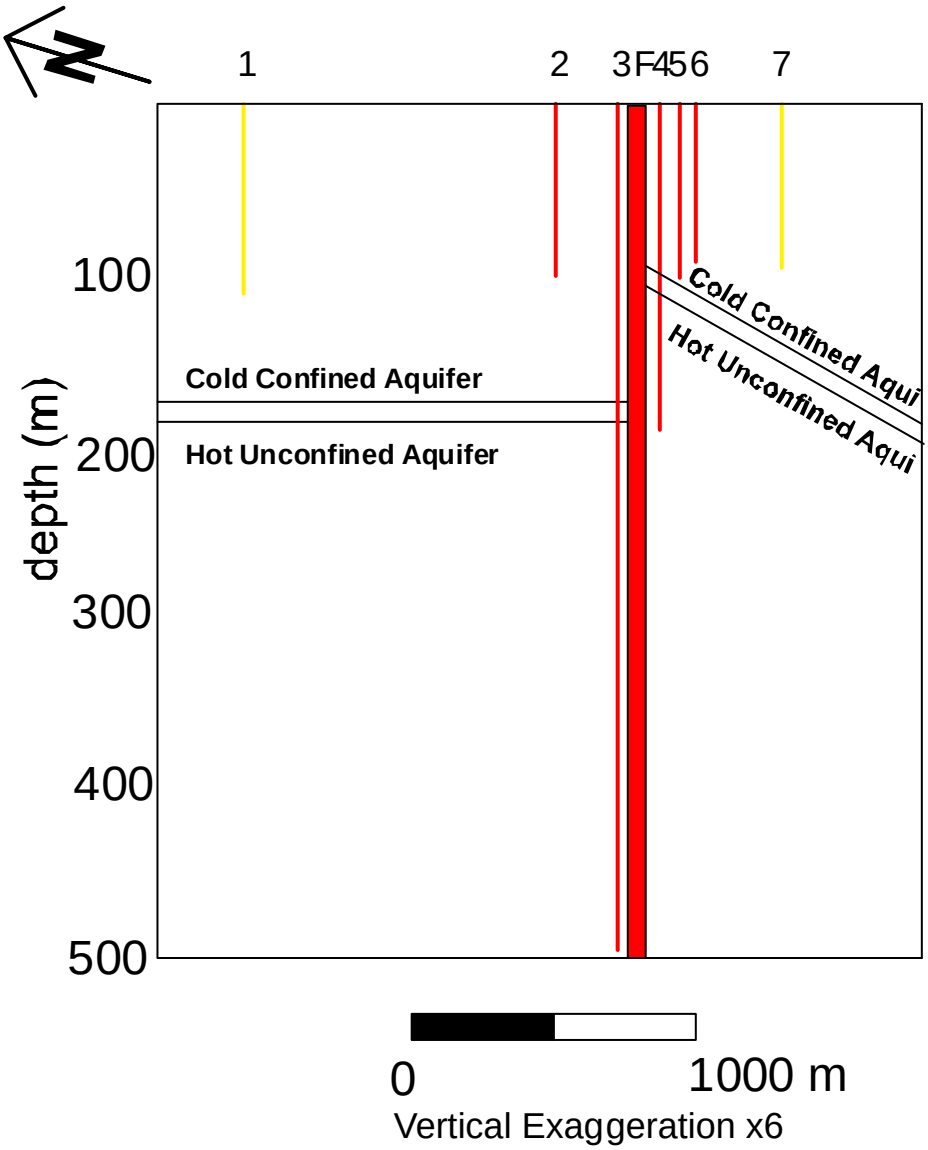

Figure 3.3 Cross Section Showing the Depth and Type of Aquifers and the Fault Zone in the Model (Numbers show the well names 1-DSİ-9, 2-YAĞCI, 3-ED-3, F-FAULT ZONE, 4-ED-1, 5-DERMAN, 6-ENTUR, and 7-DSİ-6, respectively)

In the construction of the cross sectional mesh several trial runs are made to optimize the mesh size for oscillation free solution. This study proposed that 10 mx10 m elements would be suitable and hence the elements are generally assigned this size throughout the mesh. However, in the fault zone finer elements (1 m x 10 m), and next to the fault zone 5 m x 10 m elements are used. Considering higher flow rate and major heat transfer along the fault zone, that area is highly refined in element size.

After setting up the conceptual and the numerical model, various boundary conditions are applied and the model results are compared with the observed pressure and temperature values during calibration studies. During calibration and simulation studies the Program SUTRA (Voss, 1984) is utilized and the computations are done by this program. SUTRA is a two dimensional, areal and transient finite element numerical model, and it is coded by USGS. It has been utilized to solve the flow equation and the energy equation in a coupled manner, to determine distribution of the unknowns (pressure and temperature) throughout the geothermal reservoir. The program (SUTRA) uses a hybrid galerkin-finite-element and integrated-finite-difference methods with two-dimensional quadrilateral finite elements and finite-difference time discretization to solve for two-dimensional areal or cross-sectional simulations.

3.3 Boundary Conditions

In order to complete the numerical model and perform a calibration study boundary conditions, for pressure and temperature variables, are defined (Figure 3.1). In terms of pressure the northern and the southern side boundary nodes are assigned according to the estimated pressures corresponding to the hydraulic pressures at the related depths. The hydraulic heads at A and A' on the surface are assumed to be 10 m and 5 m respectively by considering the nearby wells in the area. Starting from these surface boundary nodes the hydraulic pressures are computed for each boundary node down to the bottom of the model and they are

assigned as constant boundary pressures. The upper surface nodes are left as free boundary nodes in terms of the pressure variable.

Conceptual model assumed that the system is heated from bottom by means of a continuous heat inflow (recharge) and this keeps the temperatures at about 60 degrees Celcius. Therefore constant temperatures of 60^{o}C are assigned at these nodes. The geothermal system is losing heat to the atmosphere from the surface nodes and additionally hot water is discharged through some nodes (point discharges) representing past hot water springs. Hence these conditions are represented by means of heat outflow from the surface boundary. Along the northern and southern side boundaries the model requires temperatures of inflowing water into the reservoir. Considering the whole geothermal system, it is assumed that the model is supported from the side boundaries hence constant temperatures are assigned along the related boundary nodes. These temperatures are 60^{o}C at the bottom nodes and gradually decrease to 30^{o}C at the surface nodes.

3.4 Model Calibration

After applying the boundary conditions to the numerical model, a calibration study is performed to simulate initial state of the geothermal system. This is started by assuming a cool and empty reservoir and it is continually heated from below and let the system to reach its present conditions. This numerical procedure is continuously repeated by using the boundary conditions and appropriate physical parameters unless a match is obtained between the computed and the observed pressures and the temperatures. During calibration runs different physical parameters of the aquifer and different temperature and pressure nodal values are tried and the computed pressures and the temperatures are compared with the observed ones at some wells. Finally, difference between the observed and computed pressure and temperature values are minimized and consequently the model is calibrated. At the end of the calibration the coefficient of determination, % Bias, and the root mean square error (RMSE) are used to evaluate the

significance of the calibration. The definitions and mathematical formulae of these terms are given below:

$$r = \frac{n*(\sum(SIM*OBS)) - \sum OBS * \sum SIM}{\sqrt{\left[n*\sum(OBS)^2 - (\sum OBS)^2\right] * \left[n*\sum(SIM)^2 - (\sum SIM)^2\right]}}$$

$$\%Bias = \frac{\sum(SIM - OBS)}{\sum OBS} * 100$$

$$RMSE = \sqrt{\frac{\sum(SIM - OBS)^2}{n}}$$

$$RMS = \frac{RMSE}{\left(\frac{\sum OBS}{n}\right)} \qquad \%Error = RMS * 100$$

$$F = \frac{(n-2)*r^2}{1-r^2}$$

where n is the number of observations, SIM represents the simulated values and OBS means the observed ones.

R^2 is a statistic that gives some information about the goodness of fit of a model. Coefficient of determination is a statistical measure of how well the regression line estimates the real data points. That coefficient of determination is 1 show that the regression line exactly matches the data. Percent bias measures the average tendency of the simulated values to be larger or smaller than their observed ones. The ideal value of % Bias is 0.0, with absolute small values indicating accurate model simulation. Positive values show overestimation bias, while negative values point out underestimation bias. The root-mean-square error (RMSE), on the other hand, is a generally used measure of the differences between values predicted by a model and the values actually observed. RMSE, RMS and % error is a good measure of accuracy and it needs to be 0.0 for a perfect match. Thus, for an ideal calibration, the coefficient of determination should be 1.0 (slope angle of the graph

should be 45^0), % Bias and RMSE is 0.0. Therefore, the more the results approach the ideal situation, the better the model is calibrated.

In order to calibrate the Edremit geothermal system to its initial state, the initial reservoir rock and fluid parameters (Table 3.2) are used in the simulator. Some of these parameters are taken from the literature (Voss, 1984) and the others are tried in the calibration runs. In this study the permeability of the reservoir changes from 1.52×10^{-12} m^2 in the relatively impervious layer to 3.04×10^{-11} m^2 in the fault zone. In order to calibrate the initial state of the geothermal system, a cool and empty reservoir has been started to heat for a period of 44000 days (about 120 years) by using the appropriate boundary and initial conditions. The system is calibrated by using a dynamic solution algorithm and the solutions are made matching the observed values at the observation wells.

Table 3.2 Parameters of fluid and reservoir rock

Parameter	Value	Unit
Fluid Compressibility	4.47×10^{-10}	$(kg/ms^2)^{-1}$
Fluid Specific Heat	4182	J/kg^0C
Fluid Thermal Conductivity	0.001	J/m^0Cs
Fluid Base Density	1000	kg/m^3
Fluid Viscosity	$\mu(T)=(239.4 \times 10^{-7}) \times 10^{(248.37/(T+133.15))}$	kg/ms
Solid Matrix Compressibility	1.00×10^{-10}	$(kg/ms^2)^{-1}$
Solid Grain Specific Heat	840	J/kg^0C
Porosity of Reservoir Rock	10	%
Permeability of Reservoir Rock	1.52×10^{-12} - 3.04×10^{-11}	m^2

The system is simulated for 44000 days (about 120 years) for the heating of complete reservoir and the calibration results are given in Tables 3.3, 3.4, 3.5, 3.6 and from Figures 3.4 to Figures 3.9. These tables and figures clearly show the success of the calibration study, and they highlight the match of the variables. In addition to these figures and tables a statistical analysis is made to verify the success of the calibration. In this study correlation coefficients and goodness of fits of the calibration results are made and given in Table 3.7. This indicates a highly good matchup for the results that are simulated and the observed values from the wells nearby. Statistical test (F-test) results also show high significant relations between the simulated and the observed values (Table 3.7). Furthermore, observed temperature profile at well ED-3 has been correlated and it has been found that the simulated temperatures are highly correlated with the observed values of the well log ED-1 (Figures 3.7, 3.8, and 3.9). It can be seen in Figure 3.8 that the observed temperatures follow a two linear trend series. However, since the program allows only one thermal conductivity value for the whole reservoir, the simulated temperatures seem to have only one linear trend. Contour map of the temperatures after calibration is given in Figure 3.10.

Table 3.3 Calibrated head values at the wells (* data from Avşar, 2011)

Well	Node No.	Observed head (m)*	Computed head (m)	Dev. (m)	Dev. %	Dev.^{2} (m^2)
YAĞCI	7191	9	8.55	-0.45	-0.05	0.203
ED-3	8313	7.1	8.039	0.939	0.132	0.882
ED-1	10353	9.15	8.324	-0.826	-0.09	0.682
DSİ-6	12699	4.8	4.856	0.056	0.012	0.003
	SUM	30.05	29.769	-0.281	0.004	1.77

Table 3.4 Calibrated pressure values at the wells (* data modified from Avşar, 2011)

Well	Node No.	Observed pressure (Pa)*	Computed pressure (Pa)	Dev. (Pa)	Dev. %	Dev.^{2} $(Pa)^2$
YAĞCI	7191	88290	83875.5	-4414.5	-0.05	19487810
ED-3	8313	69651	78862.59	9211.59	0.132	84853390
ED-1	10353	89761.5	81658.44	-8103.06	-0.09	65659581
DSİ-6	12699	47088	47637.36	549.36	0.012	301796.4
	SUM	294790.5	292033.9	-2756.61	0.004	1.7×10^8

Table 3.5 Calibrated temperature values at the wells (* data from Avşar,2011)

Well	Node No.	Observed Temperature (^oC)*	Computed Temperature (^oC)	Dev. (^oC)	Dev. %	Dev.^{2} (^oC)^2
DSİ-9	1569	32	36.796	4.796	0.15	23.002
YAĞCI	7181	42	38.867	-3.133	-0.075	9.816
ED-3	8275	62	54.555	-7.445	-0.12	55.428
DERMAN	10853	53	49.175	-3.825	-0.072	14.631
ENTUR	11159	51	56.178	5.178	0.102	26.812
DSİ-6	12686	39	40.589	1.589	0.041	2.525
	SUM	279	276.16	-2.84	0.025	132.213

Table 3.6 Observed and computed temperature values of ED-3 according to depth (* from Avşar, 2011)

Node No.	Depth (m)	Observed Temperature (^oC)*	Computed Temperature (^oC)	Dev. (^oC)	Dev. %	Dev.^{2} (^oC)^2
8305	85	35	45	8.451	0.169	71.419
8297	165	38.4	46.952	3.375	0.068	11.391
8295	180	41.9	47.467	3.86	0.08	14.9
8287	265	45.6	50.167	4.567	0.1	20.857
8281	324	48.4	52.26	5.567	0.133	30.991
8278	350	50	53.375	8.552	0.223	73.137
8266	475	50.1	58.551	10	0.286	100
	SUM	353.772	309.4	44.372	1.057	322.695

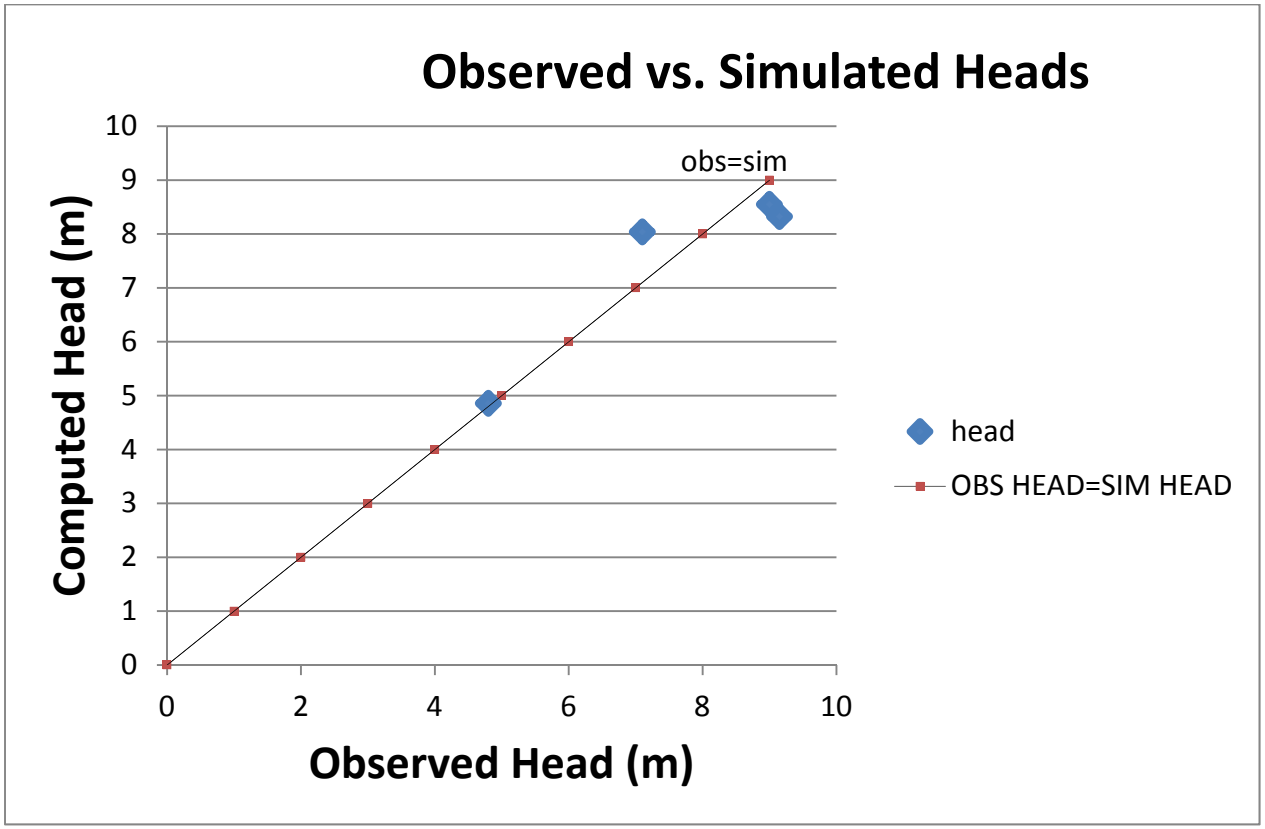

Figure 3.4 Chart showing the relation between computed heads and observed heads (the observed heads is from the static well data measured by Edremit Jeotermal A.Ş in 30/08/2008).

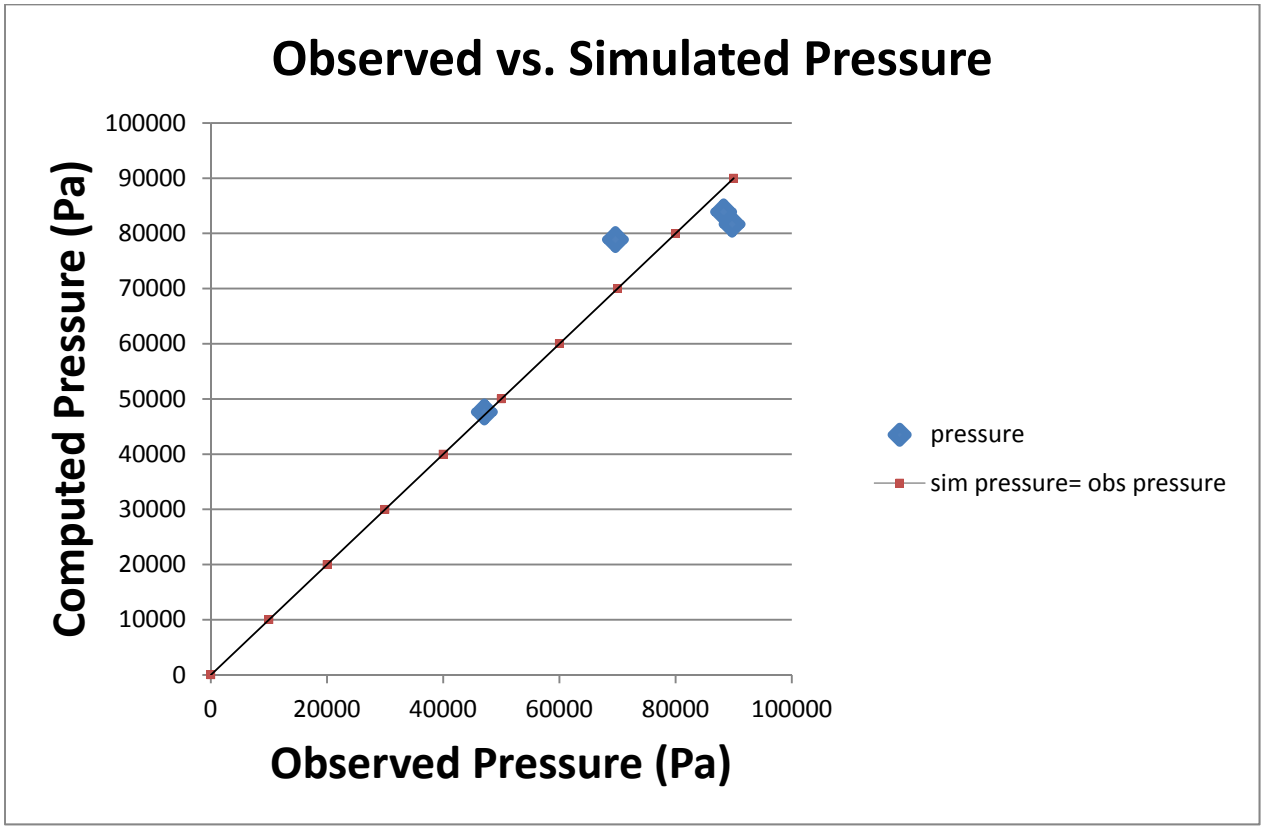

Figure 3.5 Chart showing the relation between computed pressure and observed pressure

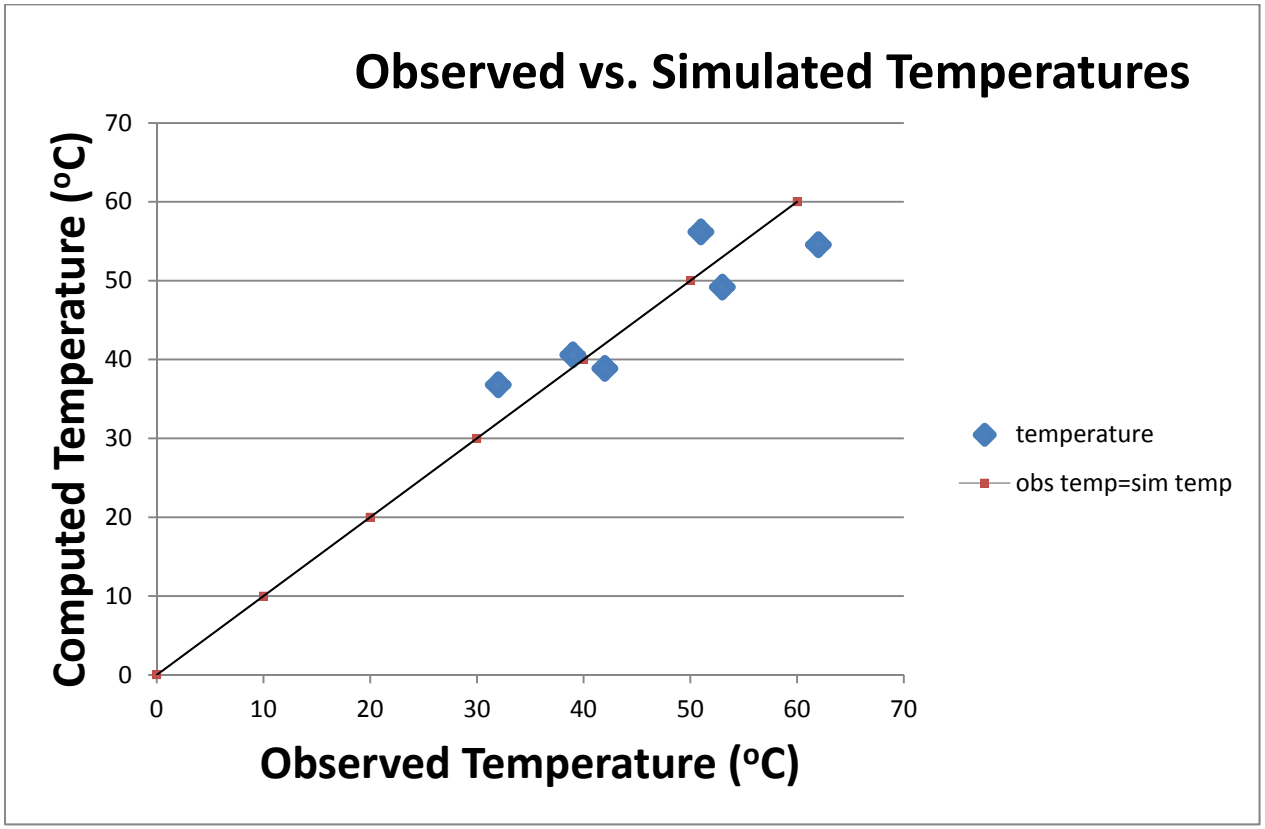

Figure 3.6 Chart showing the relation between computed and observed temperatures using the wells nearby

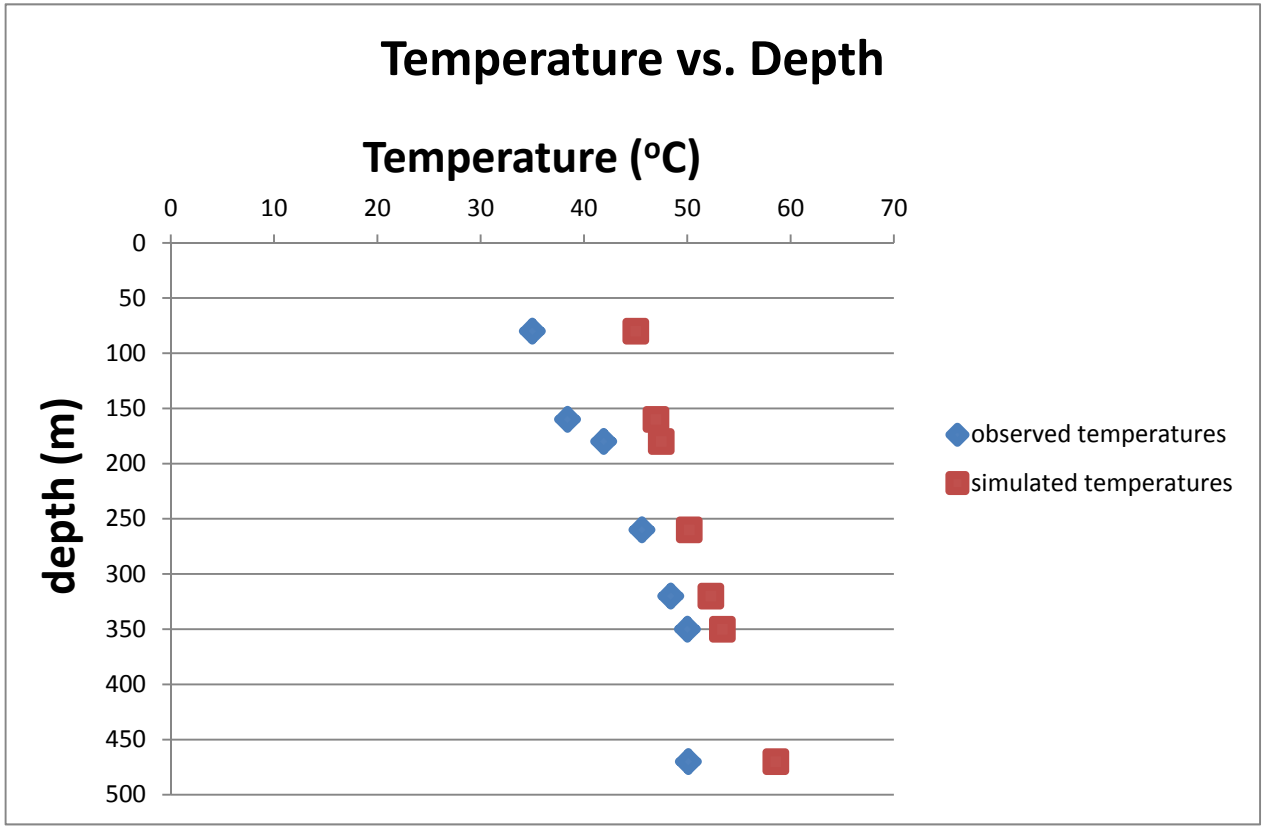

Figure 3.7 Chart showing the relation of the observed and simulated temperatures of the well ED-3 with depth (The observed values are taken from the well log of ED-3 seen in Figure 3.9)

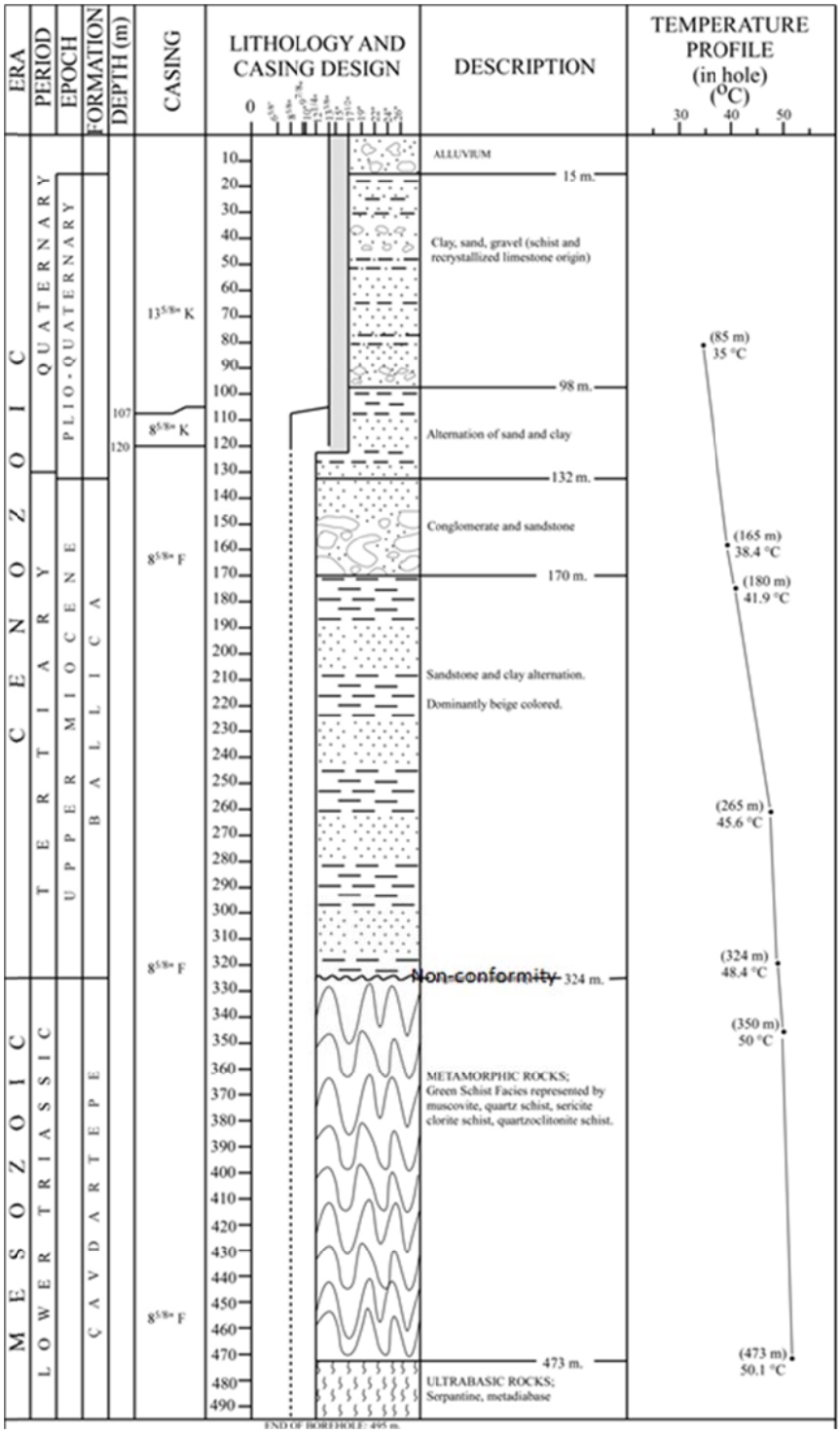

Figure 3.8 Borehole log of the well ED-3 (modified from Avşar, 2011)

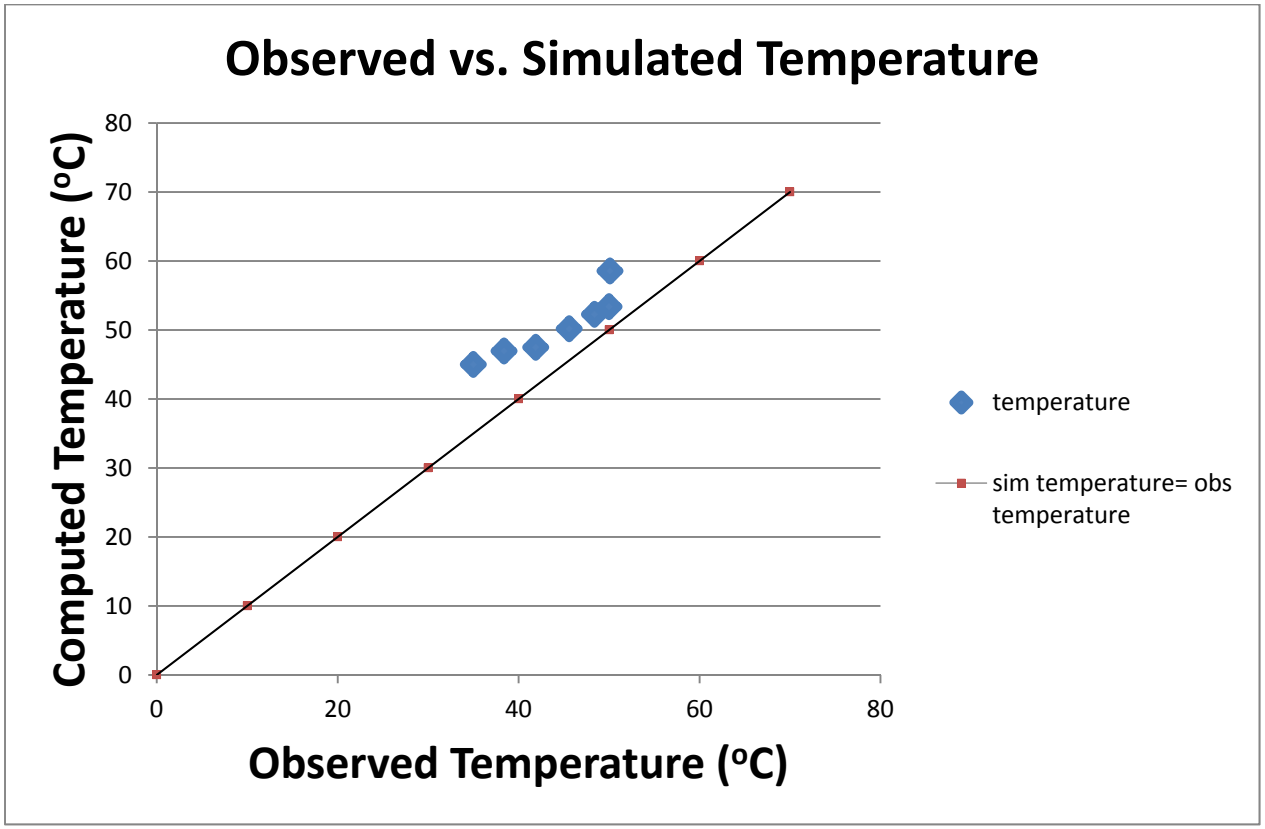

Figure 3.9 Chart showing the relation between the simulated temperatures and temperatures observed from the borehole log of ED-3.

Table 3.7 Statistical results of Calibration

	Calibrated Head and Pressure (m)	Calibrated Temperature (^oC)	Calibrated Temperature of ED-3 (^oC)
R	0.93	0.90	0.906
R^2	0.864	0.792	0.82
% Bias	-0.935	-1.018	14.341
RMSE	0.665 (head) 6525 (pressure)	4.694	6.79
RMS	0.089	0.101	0.154
% Error	8.854	10.095	15.361
F	12.813	15.211	18.269
Error calculated from F-dist	6.99 %	1.754 %	1.29 %

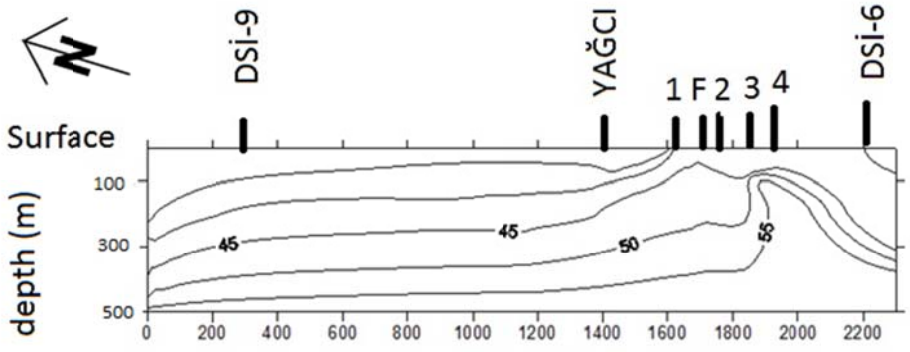

Figure 3.10 Contour map of temperatures after calibration (numbers show the well names 1- ED-3, F- Fault zone, 2-ED-1, 3-DERMAN and 4-ENTUR)

CHAPTER 4

NUMERICAL APPLICATIONS

4.1 Introduction

This chapter gives information about some possible scenarios after making the calibration. These scenarios give predictions about what will happen to the system after years without any change in the system, how will temperature and pressure change after many years, what will be the result of a pumping well in the system, and at what location it should be placed, what could be the injection possibilities of the geothermal system, etc. For this purpose, some alternative scenarios are made and they are compared at the end of this chapter. The alternative scenarios are given in Table 4.1.

Table 4.1 Definition of alternative scenarios

Scenario	Definition
Scenario 1	Water is pumped from the wells YAĞCI, DERMAN, ENTUR and ED-3 alone at a rate of 5 kg/s
Scenario 2	Water is pumped from YAĞCI, DERMAN, ENTUR and ED-3 together
Scenario 3	80% of the pumped water is injected to the system from an newly opening well located at 70 m away from the well ED-3 while all the other wells are running

The model is simulated for another 3500 days (approximately 10 years) without making any changes after calibration to ensure that this calibration is enough. After looking at these results, it can be clearly observed that the head difference between the final and initial results are the same up to three digits while the temperature difference is 0.5 which is quite negligible.

4.2 Alternative Scenarios

4.2.1 Scenario 1

In this scenario the pumping wells YAĞCI, DERMAN, ENTUR, ED-3 are operated separately to pump at a rate of 5 kg/s in order to observe response of the aquifer to these productions. During these operations 4.182 $x10^5$ J/s amount of energy is taken from the system, by using the general heat equation

$$Q = m * c * \Delta T$$

where Q is the rate of energy gained or lost in the system, m is the rate of mass, c is the specific heat capacity and ΔT is the temperature difference between the initial and final system.

The change in temperature and hydraulic head are tabulated in Tables 4.2 through 4.5 and related figures are drawn (Figures 4.1 to 4.14).

Figures 4.1 and 4.2 show the variation in temperature and hydraulic head when water is pumped only from the well Yağcı with the mass rate of 5 kg/s and energy rate of 4.182 x 10^5. It is observed from these graphs that the hydraulic head decreases abruptly from 108.325 meters to 107.89 meters in approximately 8 hours and reach steady state while the temperature decrease affects rather slowly (about 40 days is needed to drop from 38.87^{o}C to 31.32^{o}C).

The results of the water pumping well Entur with the same mass and energy rate are given in Figures 4.3 and 4.4. These results indicate the temperature of this well at this node cools about 12^{o}C from 53.739^{o}C to 41.694^{o}C in 100 days. The hydraulic head, on the other hand, decreases rapidly as in the case of Yağcı from 104.515 meters to 104.266 meters (almost 0.30 meters) in 3.5 hours only.

At the third case, water is pumped only from the Derman well and the change of temperature and hydraulic head with respect to time are drawn in Figures 4.5 and 4.6. Figure 4.6 indicates a sharp decrease in hydraulic head (drops nearly 0.45 meters from 104.22 meters to 103.875 meters in 2.5 hours) as in the other two cases imply. The temperature of this node decreases approximately by 5 degrees from 50.285 to 45.655.

The fourth case is to pump the water only from the well ED-3 with the same mass and energy rate. Figures 4.7 through 4.14 show these temperature and pressure of these nodes with time. The hydraulic head graphs indicate an abrupt drop (nearly 0.4 meters) in 10 hours. Likewise, the temperatures decrease quite slowly but at a great difference (approximately 12^{o}C in 100 days).

Table 4.2 Temperature distribution in major nodes used in scenario 1

Time (days)	Temp at the depth of 100 m in Yağcı (^oC)	Temp at the depth of 100 m in Entur (^oC)	Temp at the depth of 100 m in Derman (^oC)	Temp at the depth of 230 m in ED-3 (^oC)	Temp at the depth of 280 m in ED-3 (^oC)	Temp at the depth of 330 m in ED-3 (^oC)	Temp at the depth of 380 m in ED-3 (^oC)
0	38.857	53.739	50.285	49.147	50.845	52.62	54.55
10	33.634	47.358	46.741	46.262	47.961	49.738	51.67
20	32.12	44.821	46.227	44.033	45.732	47.508	49.44
30	31.581	43.684	46.048	42.298	43.996	45.769	47.699
40	31.139	43.084	45.936	40.937	42.633	44.404	46.332
50	31.147	42.704	45.855	39.864	41.557	43.325	45.25
60	31.013	42.424	45.795	39.008	40.698	42.464	44.387
70	30.902	42.199	45.747	38.321	40.007	41.772	43.693
80	30.807	42.008	45.71	37.763	39.446	41.209	43.128
90	30.724	41.842	45.68	37.305	38.985	40.746	42.665
100	30.653	41.694	45.655	36.925	38.601	40.362	42.281

Table 4.3 Hydraulic head distribution in major nodes used in scenario 1

Time (hours)	Head at the depth of 100 m in Yağcı (m)	Head at the depth of 100 m in Entur (m)	Head at the depth of 100 m in Derman (m)	Head at the depth of 230 m in ED-3 (m)	Head at the depth of 280 m in ED-3 (m)	Head at the depth of 330 m in ED-3 (m)	Head at the depth of 380 m in ED-3 (m)
0	108.327	104,515	104.218	238.239	288.203	338.224	388.123
5	107.910	104,265	103.871	237.898	287.841	337.803	387.766
10	107.886	104,265	103.871	237.855	287.816	337.778	387.741
15	107.883	104,265	103.871	237.852	287.813	337.776	387.738
20	107.883	104,265	103.871	237.852	287.813	337.775	387.738
25	107.883	104,265	103.87	237.852	287.813	337.775	387.738

Table 4.4 Temperature decline in nodes used in scenario 1

Node No.	Well Name	Rate of mass (kg/s)	Rate of Energy (J/s)	Initial Temperature (44000 days) (^{o}C)	Final Temperature (44100 days) (^{o}C)	Decline (^{o}C)
7181	YAĞCI	5	418200	38.857	30.653	8.204
8275	ED-3	1.25	104550	54.55	42.481	12.269
8280	ED-3	1.25	104550	52.62	40.362	12.258
8285	ED-3	1.25	104550	50.845	38.601	12.244
8290	ED-3	1.25	104550	49.147	36.925	12.222
10853	DERMAN	5	418200	50.285	45.655	4.63
11159	ENTUR	5	418200	53.739	41.694	12.045

Table 4.5 Hydraulic head decline in nodes used in scenario 1

Node No.	Well Name	Rate of mass (kg/s)	Rate of Energy (J/s)	Initial Hydraulic Head (44000 days) (m)	Final Hydraulic Head (44001 days) (m)	Decline (m)
7181	YAĞCI	5	418200	108.327	107.883	0.376
8275	ED-3	1.25	104550	388.123	387.738	0.385
8280	ED-3	1.25	104550	338.224	337.735	0.448
8285	ED-3	1.25	104550	288.203	287.813	0.39
8290	ED-3	1.25	104550	238.239	237.852	0.387
10853	DERMAN	5	418200	104.218	103.87	0.348
11159	ENTUR	5	418200	104.515	104.265	0.25

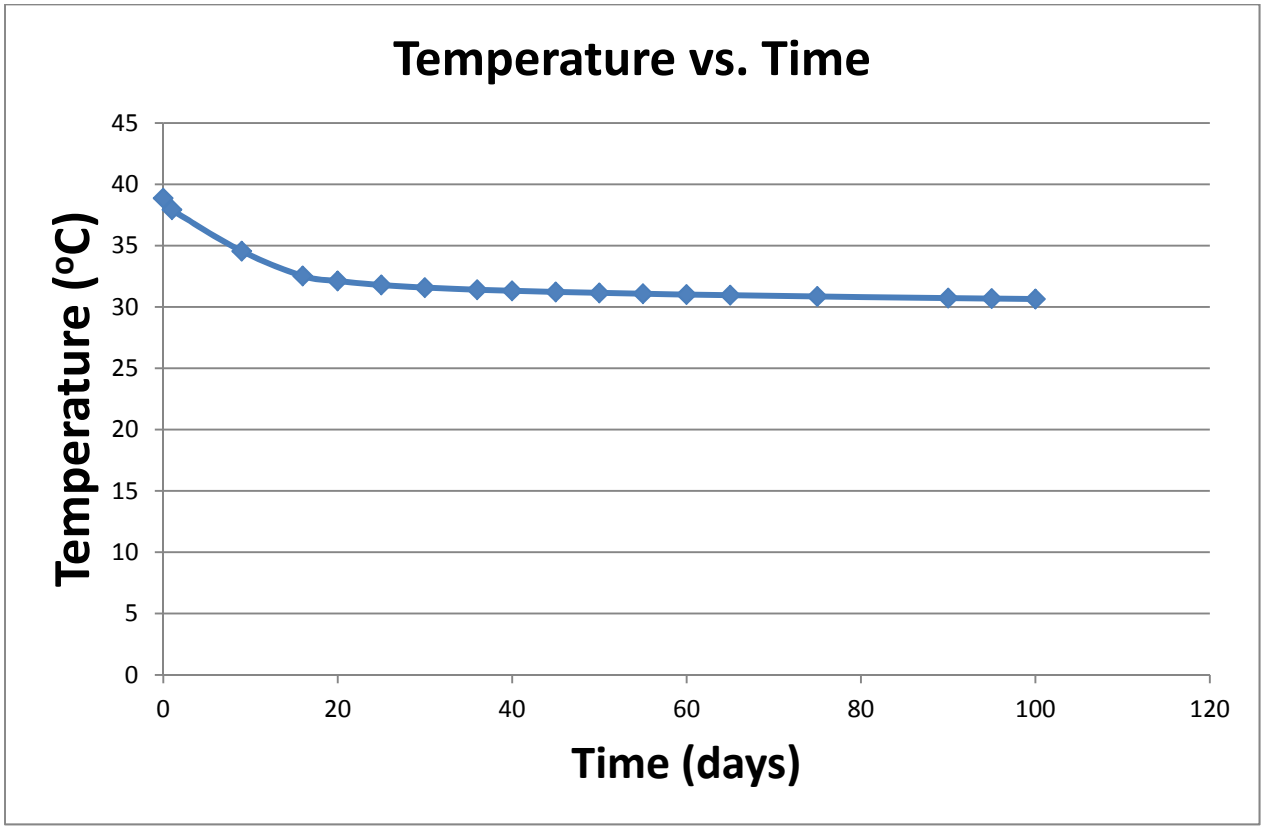

Figure 4.1 Graph showing the temperature change with time when water is pumped at a mass rate of 5 kg/s with 4.182 x 10^5 J/s of energy drawn from the system in node 7181 located at the depth of 100 meters in Yağcı

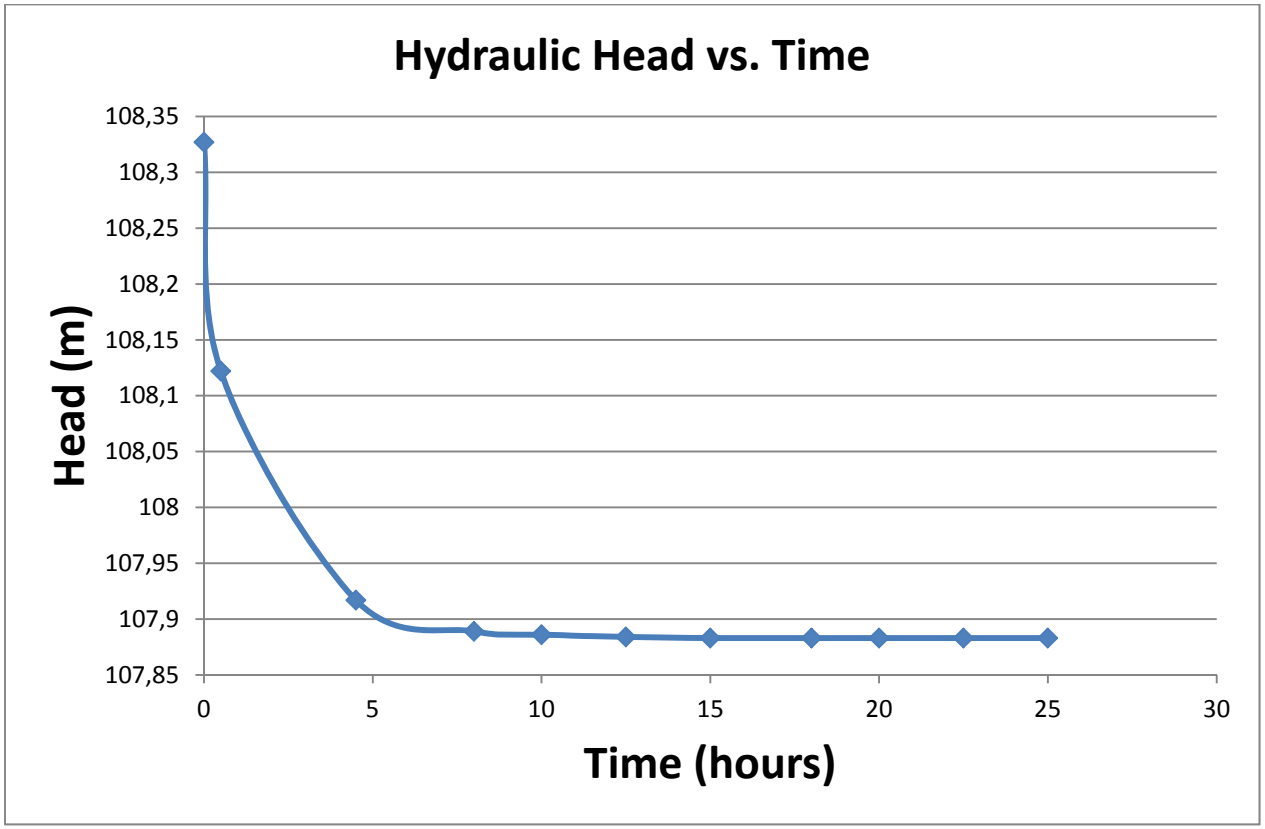

Figure 4.2 Graph showing the hydraulic head change with time when water is pumped at a mass rate of 5 kg/s with 4.182 x 10^5 J/s of energy drawn from the system in node 7181 located at the depth of 100 meters in Yağcı

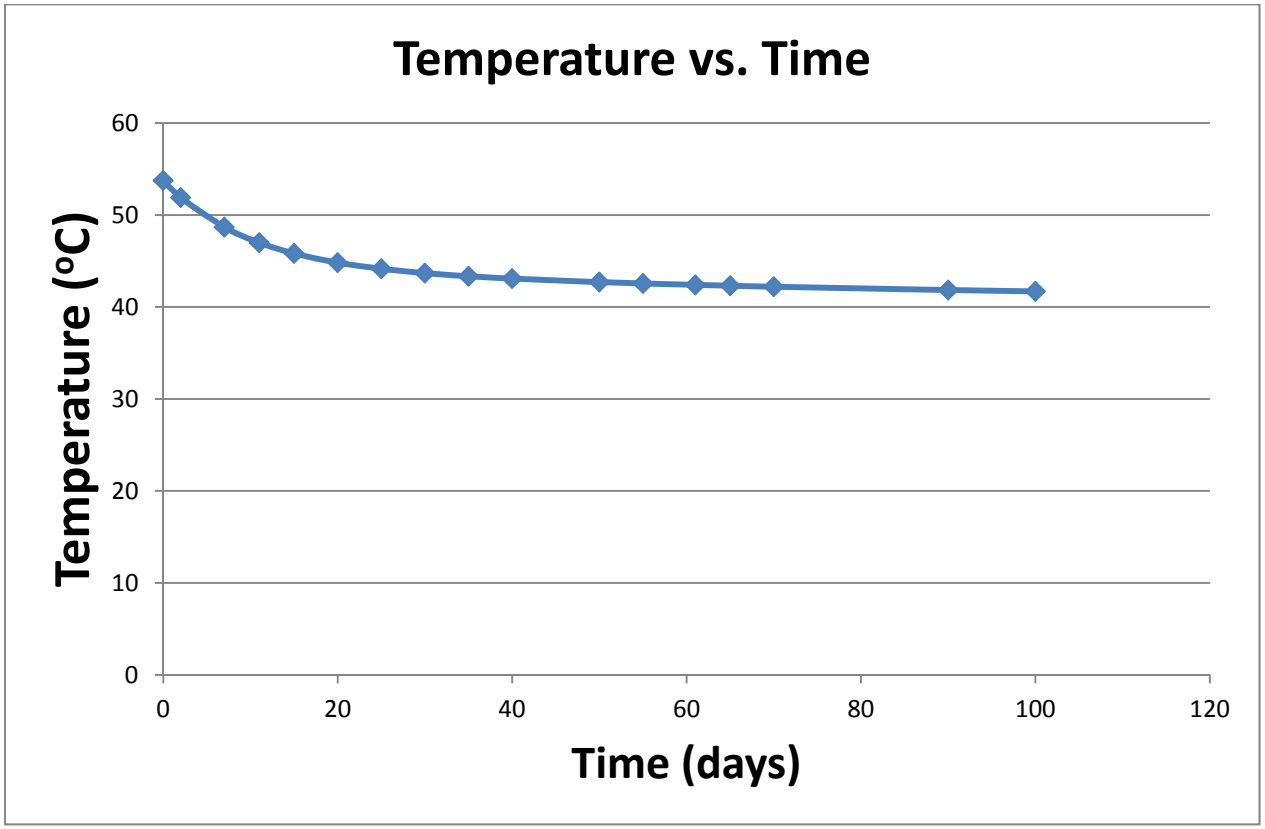

Figure 4.3 Graph showing the temperature change with time when water is pumped at a mass rate of 5 kg/s with 4.182 x 10^5 J/s of energy drawn from the system in node 11159 located at the depth of 100 meters in Entur

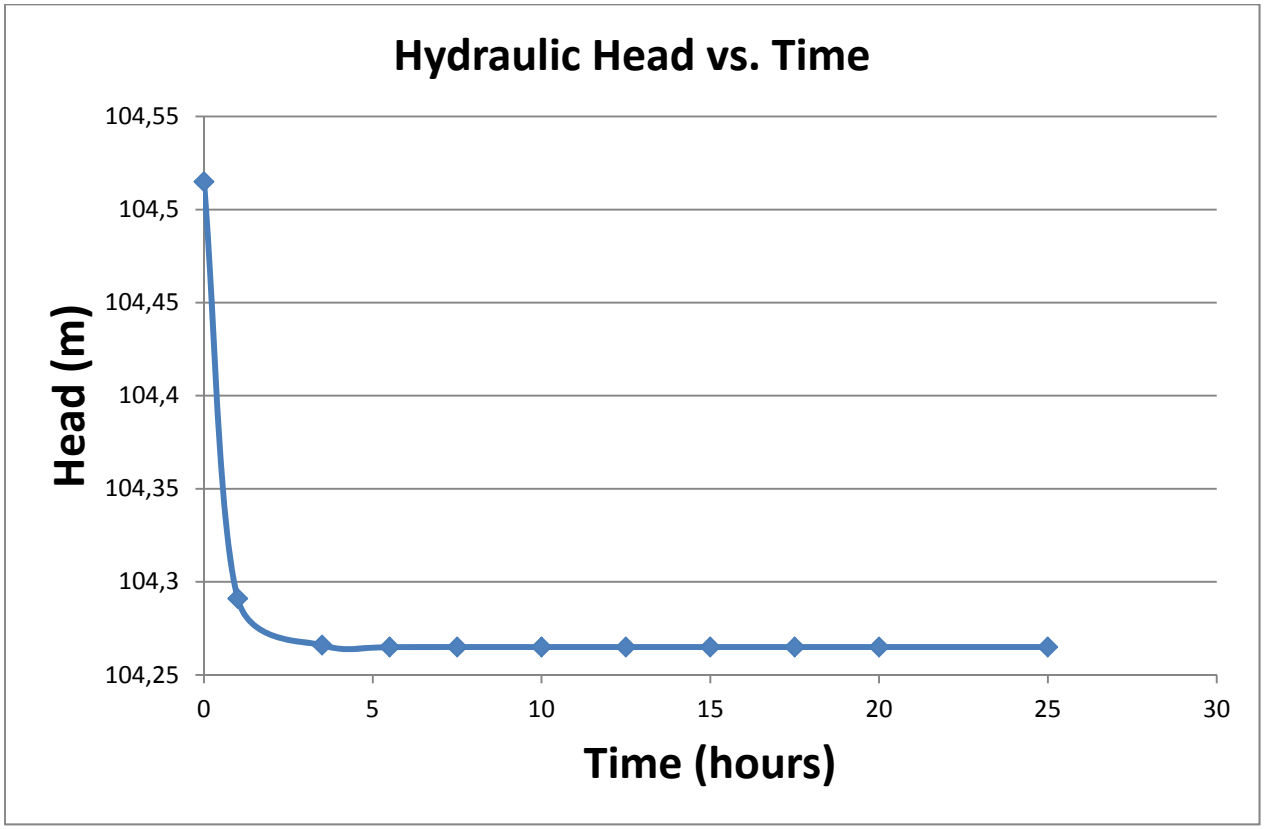

Figure 4.4 Graph showing the hydraulic head change with time when water is pumped at a mass rate of 5 kg/s with 4.182 x 10^5 J/s of energy drawn from the system in node 11159 located at the depth of 100 meters in Entur

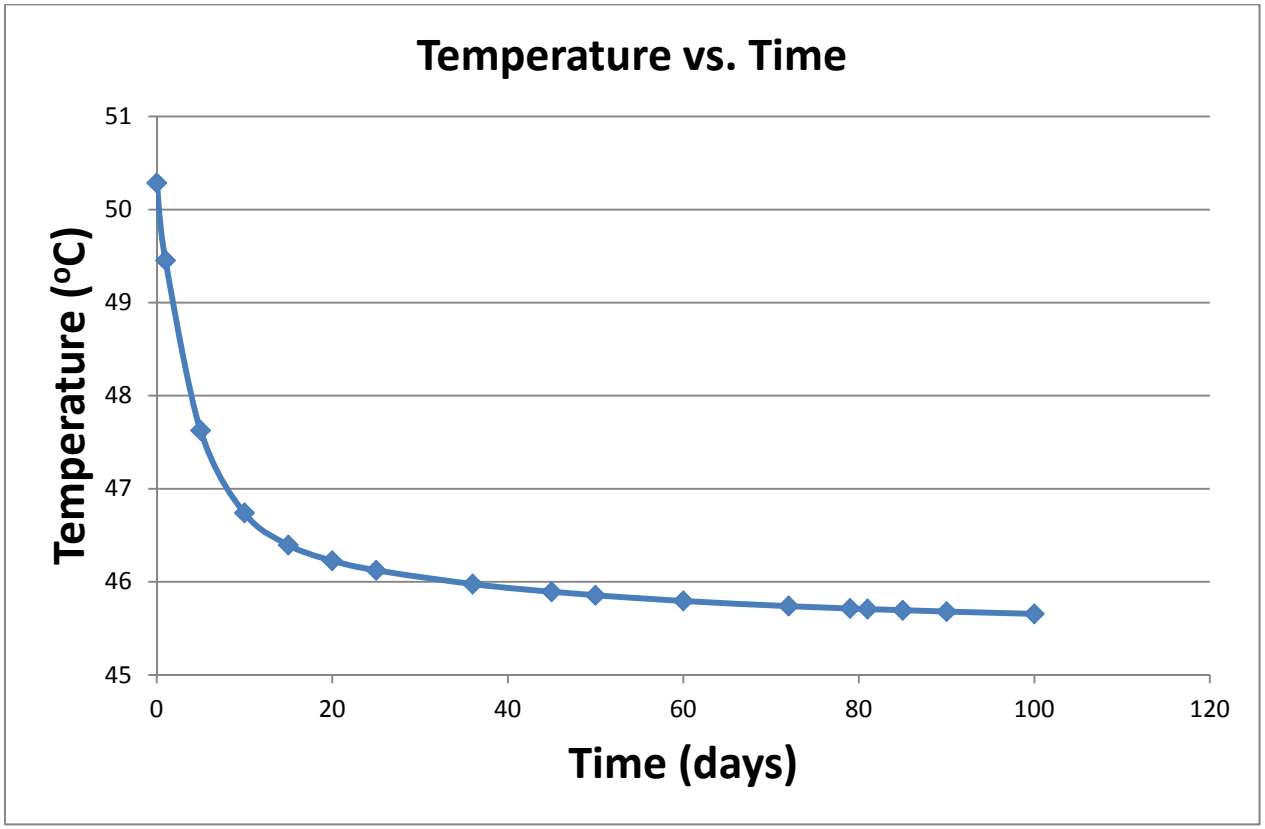

Figure 4.5 Graph showing the temperature change with time when water is pumped at a mass rate of 5 kg/s with 4.182 x 10^5 J/s of energy drawn from the system in node 10853 located at the depth of 100 meters in Derman

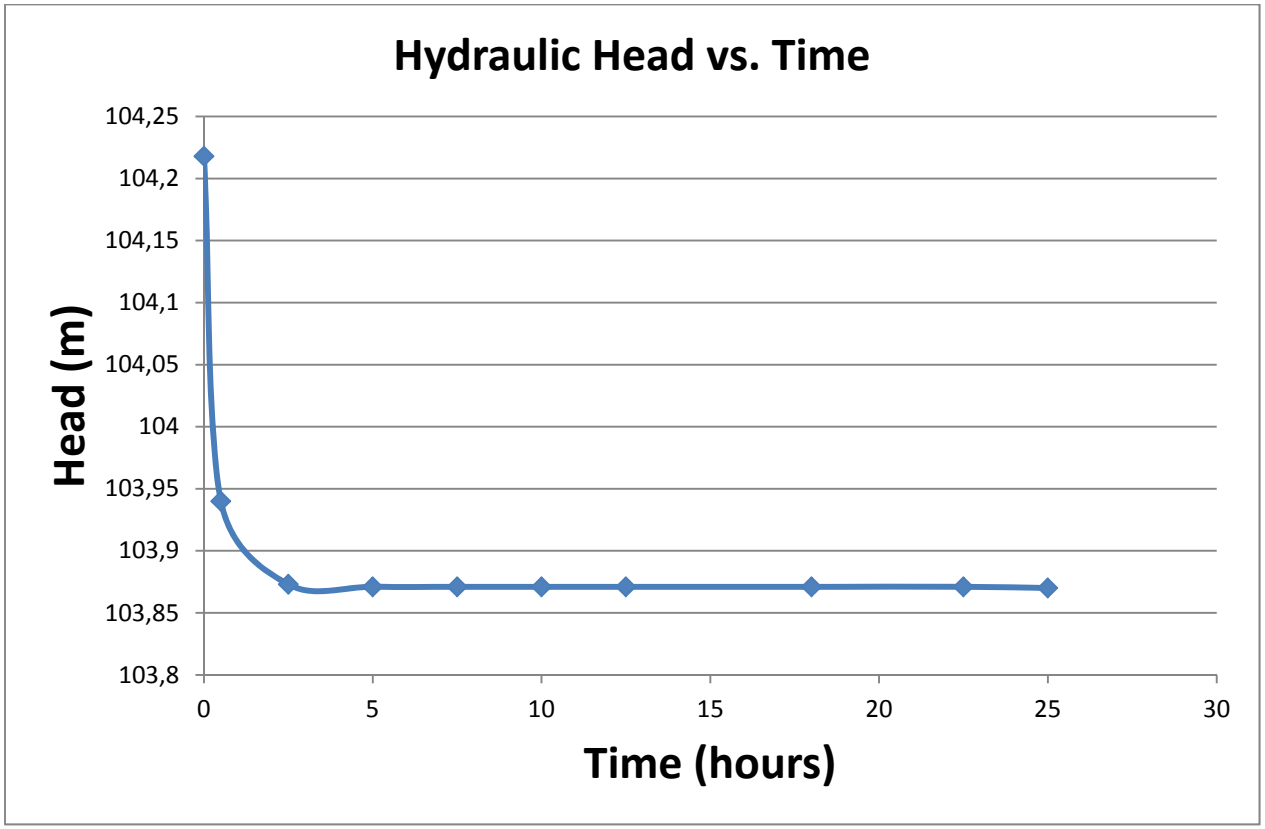

Figure 4.6 Graph showing the hydraulic head change with time when water is pumped at a mass rate of 5 kg/s with 4.182 x 10^5 J/s of energy drawn from the system in node 10853 located at the depth of 100 meters in Derman

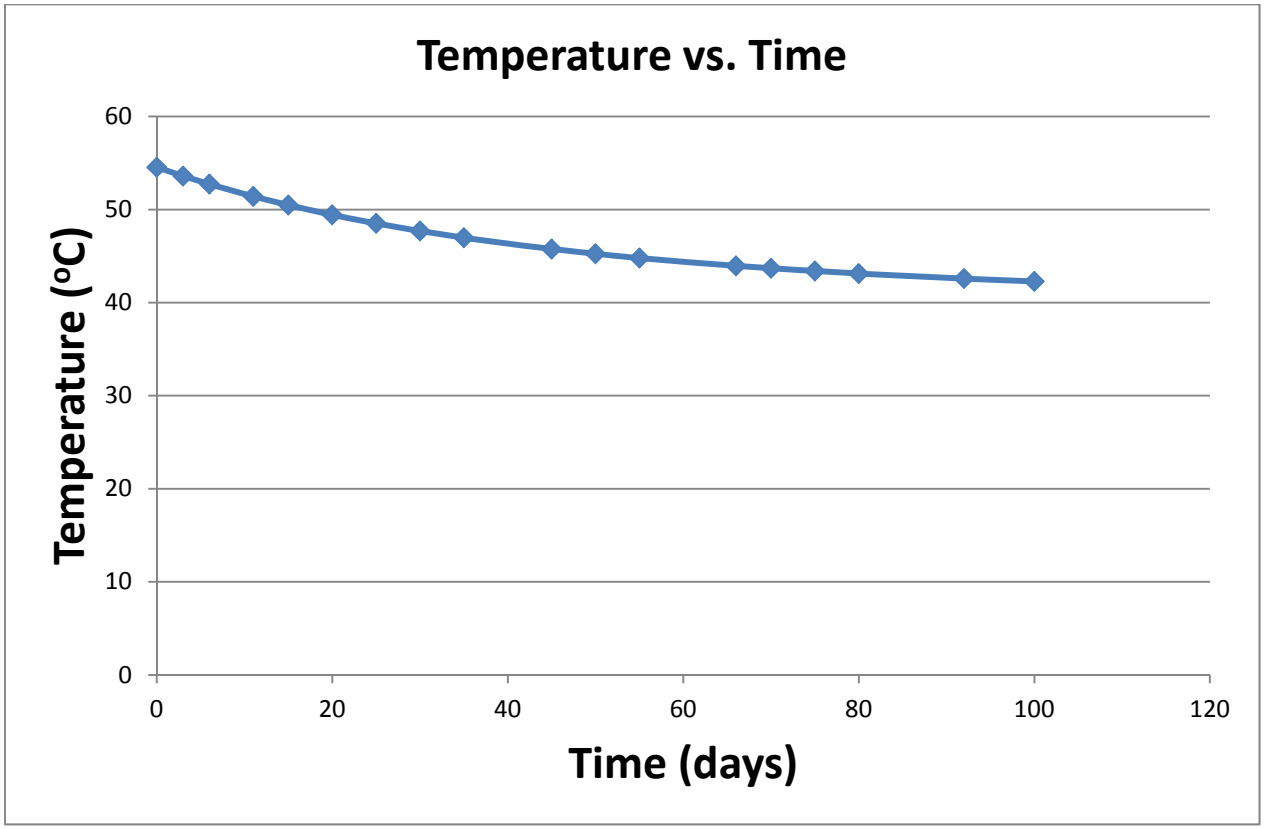

Figure 4.7 Graph showing the temperature change with time when water is pumped at a mass rate of 1.25 kg/s with 1.0455 x 10^5 J/s of energy drawn from the system in node 8275 located at the depth of 380 meters in ED-3

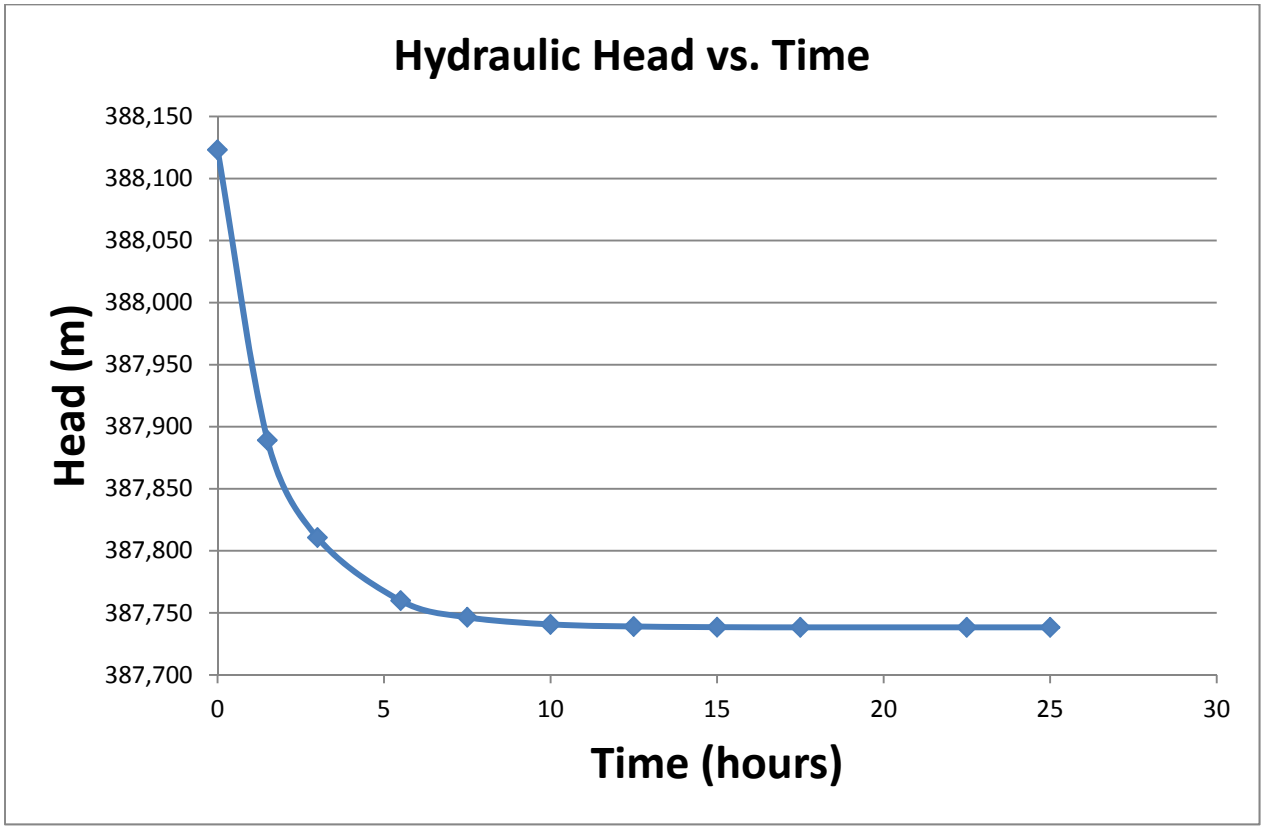

Figure 4.8 Graph showing the hydraulic head change with time when water is pumped at a mass rate of 1.25 kg/s with 1.0455 x 10^5 J/s of energy rate drawn from the system in node 8275 located at the depth of 380 meters in ED-3

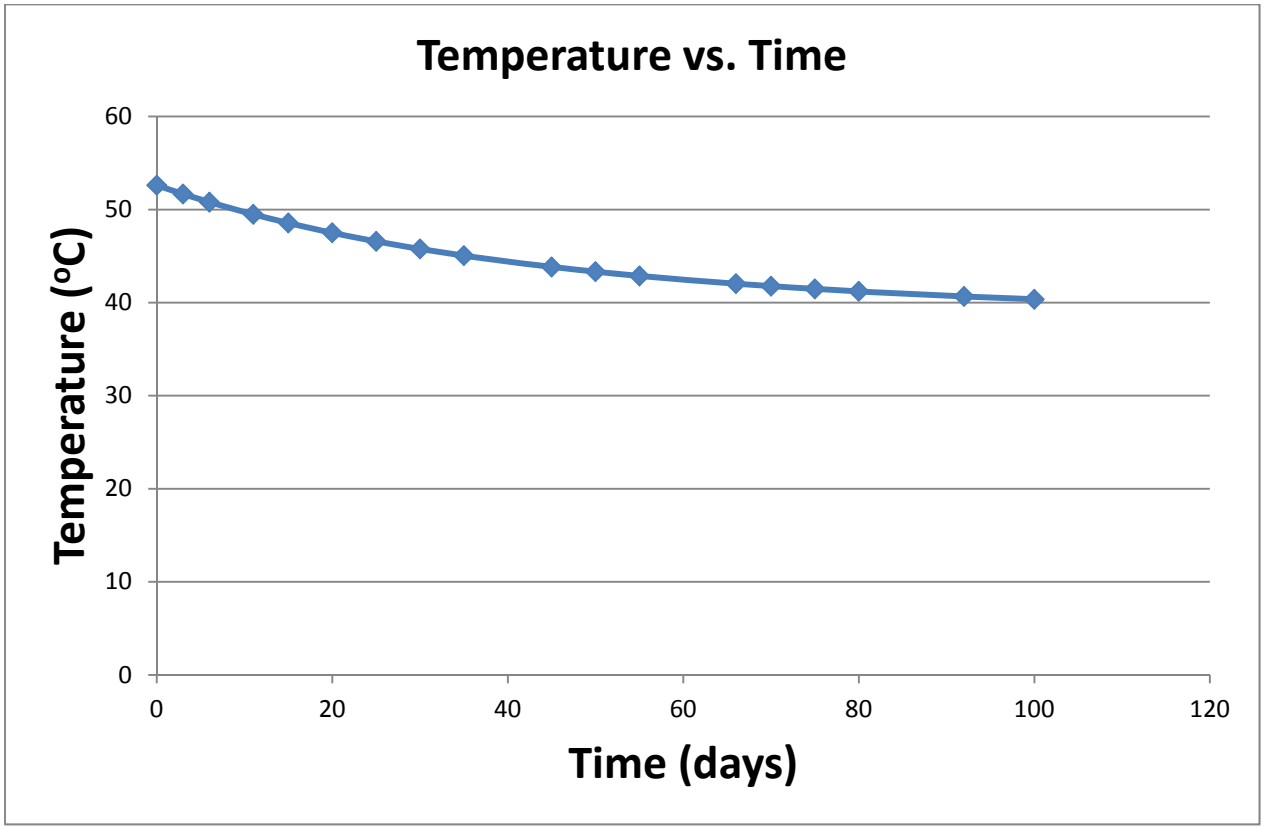

Figure 4.9 Graph showing the temperature change with time when water is pumped at a mass rate of 1.25 kg/s with 1.0455 x 10^5 J/s of energy drawn from the system in node 8280 located at the depth of 330 meters in ED-3

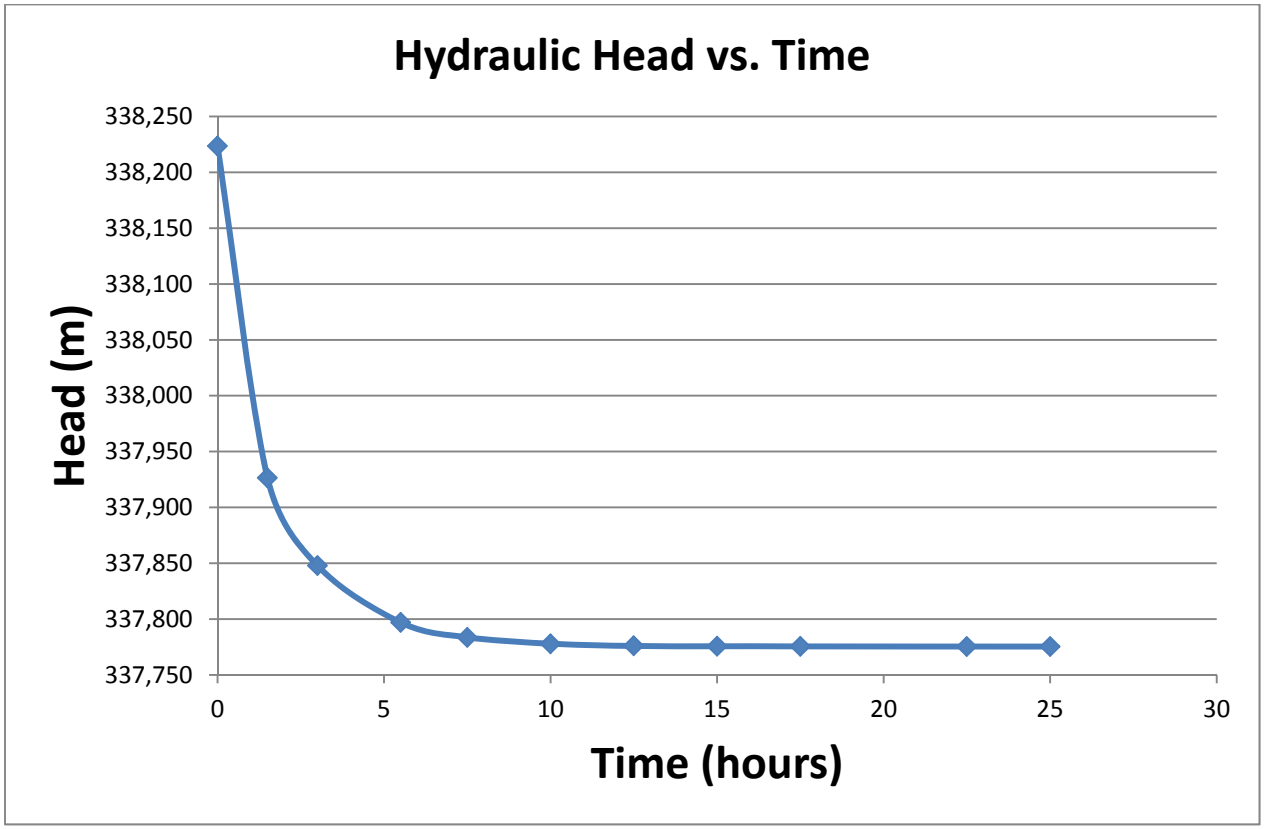

Figure 4.10 Graph showing the hydraulic head change with time when water is pumped at a mass rate of 1.25 kg/s with 1.0455 x 10^5 J/s of energy rate drawn from the system in node 8280 located at the depth of 330 meters in ED-3

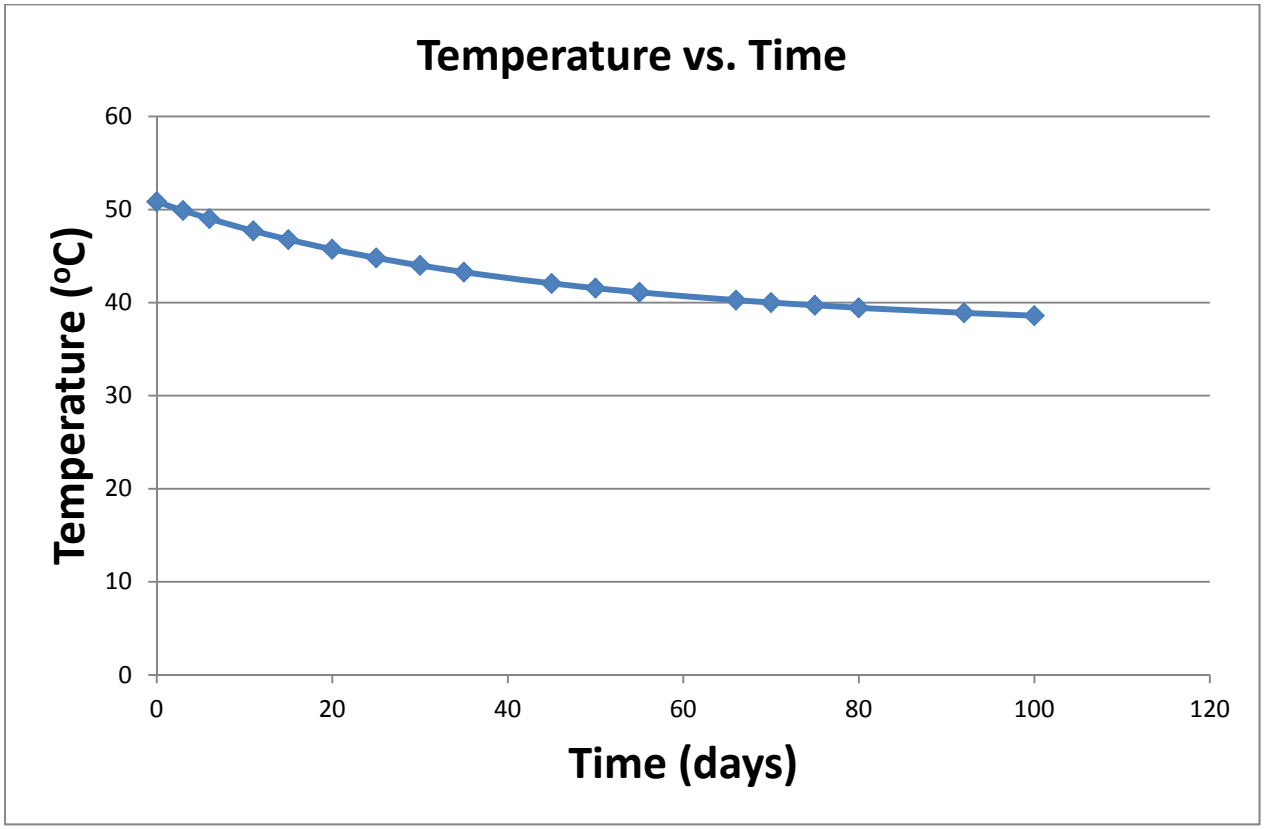

Figure 4.11 Graph showing the temperature change with time when water is pumped at a mass rate of 1.25 kg/s with 1.0455 x 10^5 J/s of energy drawn from the system in node 8285 located at the depth of 280 meters in ED-3

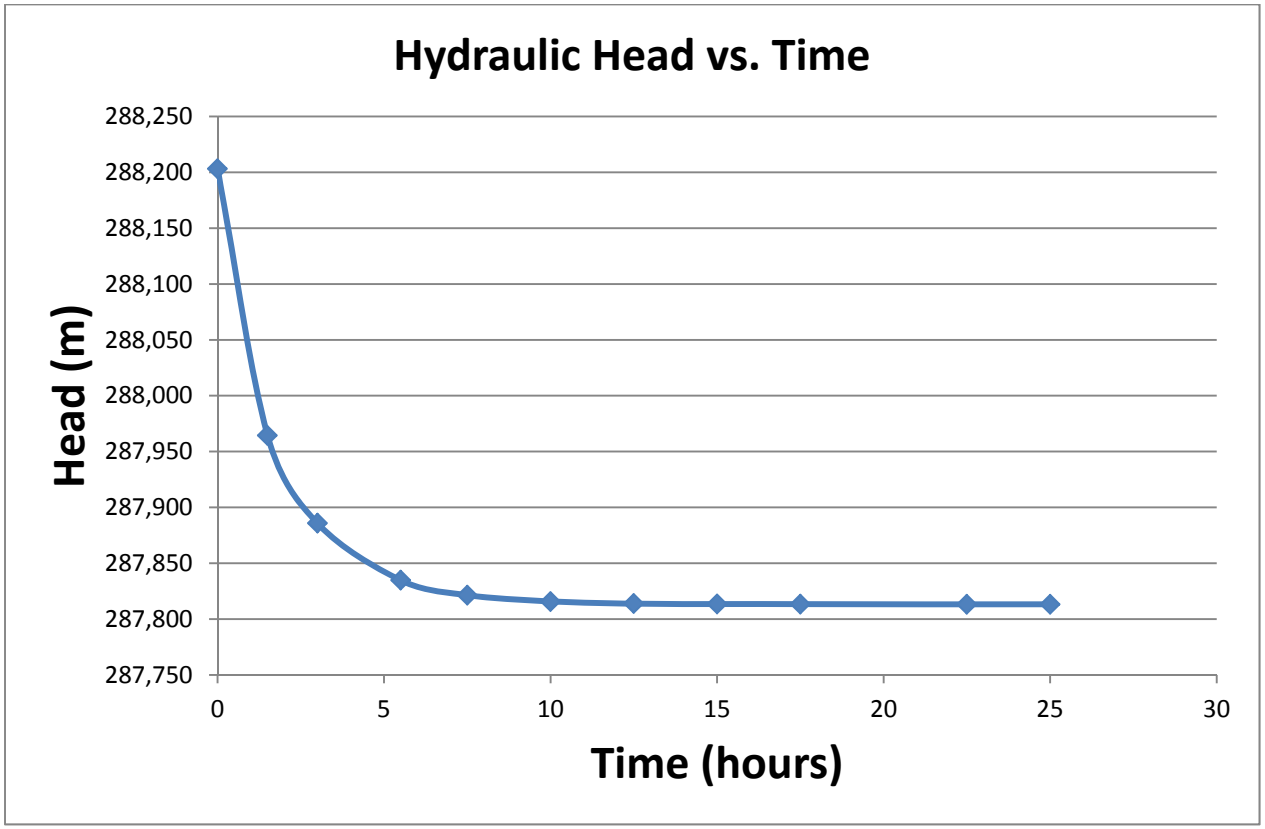

Figure 4.12 Graph showing the hydraulic head change with time when water is pumped at a mass rate of 1.25 kg/s with 1.0455 x 10^5 J/s of energy rate drawn from the system in node 8285 located at the depth of 280 meters in ED-3

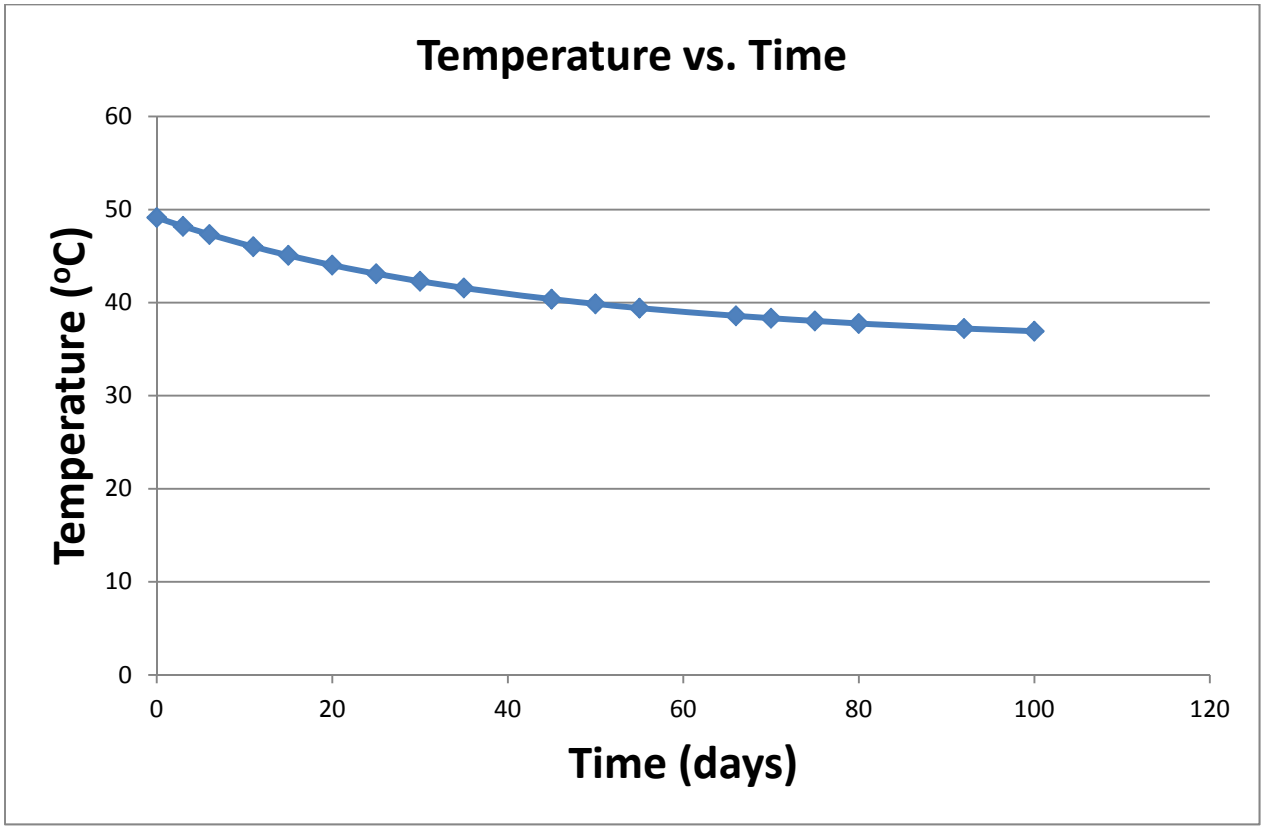

Figure 4.13 Graph showing the temperature change with time when water is pumped at a mass rate of 1.25 kg/s with 1.0455 x 10^5 J/s of energy drawn from the system in node 8290 located at the depth of 230 meters in ED-3

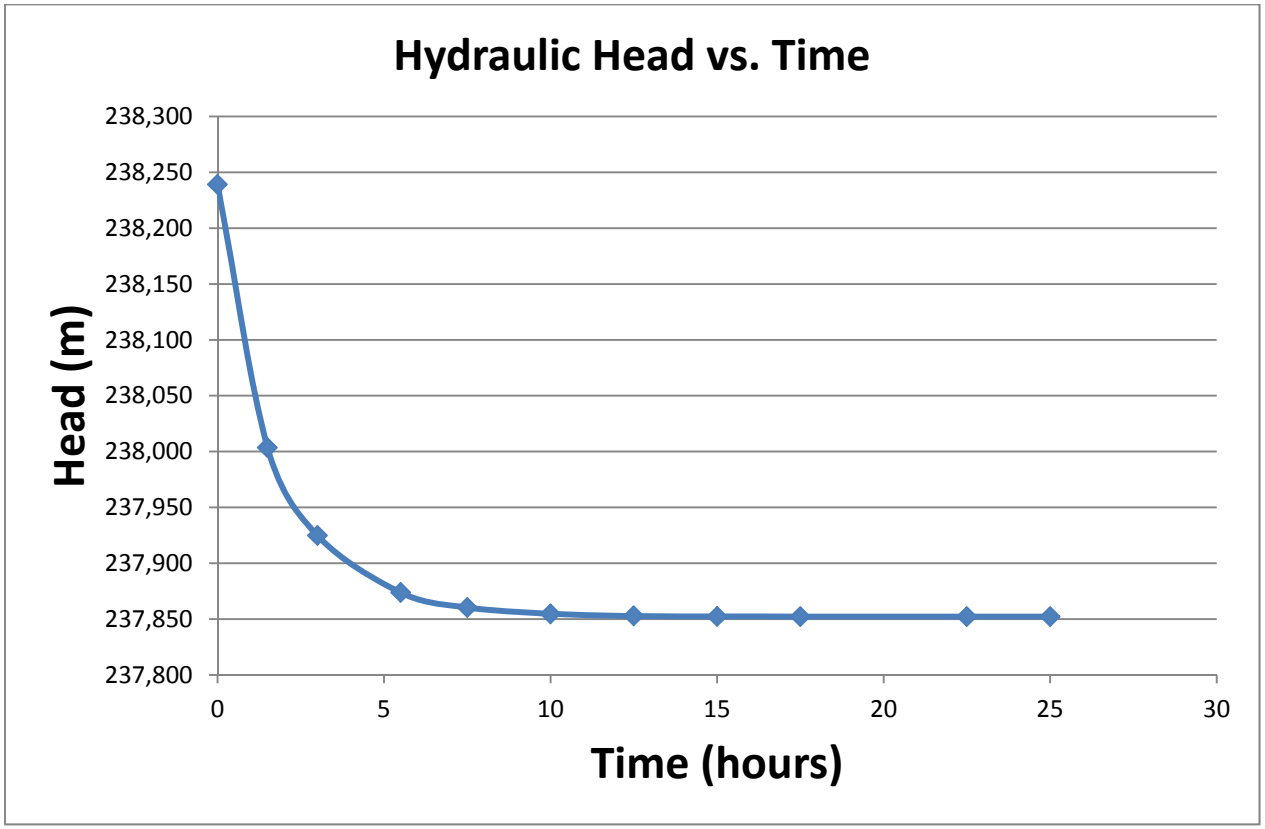

Figure 4.14 Graph showing the hydraulic head change with time when water is pumped at a mass rate of 1.25 kg/s with 1.0455 x 10^5 J/s of energy rate drawn from the system in node 8290 located at the depth of 230 meters in ED-3

4.2.2 Scenario 2

In this scenario, all the wells are operated simultaneously at the same rate of their individual productions to examine the effect of production in the reservoir.

The variation of temperature and hydraulic head with respect to time in the specific nodes used in scenario 2 is given from Tables 4.6 to 4.9 and from Figures 4.15 to 4.21.

Figures 4.15 and 4.16 show the variation in temperature and hydraulic head of the pumping well Yağcı when all the pumping wells are running. It is observed from these figures that pressure declines abruptly from 108.325 to 103.75 meters in approximately 10 hours. As in the other cases the temperature decreases rather slowly from 38.9^{o}C to 30.5^{o}C.

The change in temperature and hydraulic head of the pumping well Entur used in this scenario is drawn in Figures 4.17 and 4.18. These figures indicate a sharp hydraulic head decline from 104.5 to 103.7 meters in approximately 8 hours and a relatively slow cooling 53.75^{o}C to 41^{o}C in 100 days.

Figures 4.19 and 4.20 indicate the change in temperature and hydraulic head of the well Derman used in this scenario. The hydraulic head drops from 104.2 meters to 103.4 meters in nearly 7.5 hours. The temperature, on the other hand, decreases from 50.3^{o}C to 45.6^{o}C in 100 days.

The results of the decrease in temperature and hydraulic head are given in Tables 4.8, 4.9, 4.14, 4.15, 4.16 and 4.17.

Table 4.6 Temperature distribution in major nodes used in scenario 2

Time (days)	Temp at the depth of 100 m in Yağcı (^{o}C)	Temp at the depth of 100 m in Entur (^{o}C)	Temp at the depth of 100 m in Derman (^{o}C)
0	38.857	53.739	50.285
10	33.618	47.261	46.716
20	32.091	44.622	46.177
30	31.544	43.406	45.973
40	31.274	42.747	45.838
50	31.096	42.322	45.734
60	30.957	42.009	45.651
70	30.841	41.758	45.582
80	30.741	41.547	45.522
90	30.655	41.365	45.471
100	30.579	41.205	45.425

Table 4.7 Hydraulic head distribution in major nodes used in scenario 2

Time (minutes)	Head at the depth of 100 m in Yağcı (m)	Head at the depth of 100 m in Entur (m)	Head at the depth of 100 m in Derman (m)	Head at the depth of 230 m in ED-3 (m)	Head at the depth of 280 m in ED-3 (m)	Head at the depth of 330 m in ED-3 (m)	Head at the depth of 380 m in ED-3 (m)
0	108.327	104,515	104.218	238.239	288.203	338.165	388.123
100	105.061	103.83	103.506	236.168	286.156	336.141	386.122
200	104.286	103.758	103.43	235.372	285.361	335.347	385.324
300	103.963	103.73	103.4	235.040	285.03	335.017	384.998
400	103.829	103.719	103.388	234.902	284.892	334.879	384.861
500	103.773	103.714	103.383	234.845	284.835	334.822	384.803
600	103.749	103.712	103.381	234.821	284.811	334.798	384.78
700	103.739	103.711	103.38	234.811	284.801	334.788	384.77
800	103.735	103.711	103.379	234.807	284.797	334.784	384.765
900	103.733	103.71	103.379	234.805	284.795	334.782	384.764
1000	103.732	103.71	103.379	234.804	284.794	334.781	384.763
1100	103.732	103.71	103.379	234.804	284.794	334.781	384.763
1200	103.731	103.71	103.379	234.804	284.794	334.781	384.763
1300	103.731	103.71	103.379	234.804	284.794	334.781	384.763
1400	103.731	103.71	103.378	234.804	284.794	334.781	384.762
1500	103.731	103.71	103.378	234.804	284.794	334.781	384.762

Table 4.8 Temperature decline in nodes used in scenario 2

Node No.	Well Name	Rate of mass (kg/s)	Rate of Energy (J/s)	Initial Temperature (44000 days) (^{o}C)	Final Temperature (51000 days) (^{o}C)	Decline (^{o}C)
7181	YAĞCI	5	418200	38.857	30.614	8.243
8275	ED-3	1.25	104550	54.55	37.768	16.782
8280	ED-3	1.25	104550	52.62	35.479	16.871
8285	ED-3	1.25	104550	50.845	33.545	17.3
8290	ED-3	1.25	104550	49.147	31.83	17.317
10853	DERMAN	5	418200	50.285	45.59	4.695
11159	ENTUR	5	418200	53.739	33.916	19.823

Table 4.9 Hydraulic head decline in nodes used in scenario 2

Node No.	Well Name	Rate of mass (kg/s)	Rate of Energy (J/s)	Initial Hydraulic Head (44000 days) (m)	Final Hydraulic Head (51000 days) (m)	Decline (m)
7181	YAĞCI	5	418200	108.327	107.463	0.864
8275	ED-3	1.25	104550	388.123	387.32	0.803
8280	ED-3	1.25	104550	338.224	337.354	0.87
8285	ED-3	1.25	104550	288.203	287.389	0.814
8290	ED-3	1.25	104550	238.239	237.424	0.815
10853	DERMAN	5	418200	104.218	103.561	0.657
11159	ENTUR	5	418200	104.515	103.866	0.649

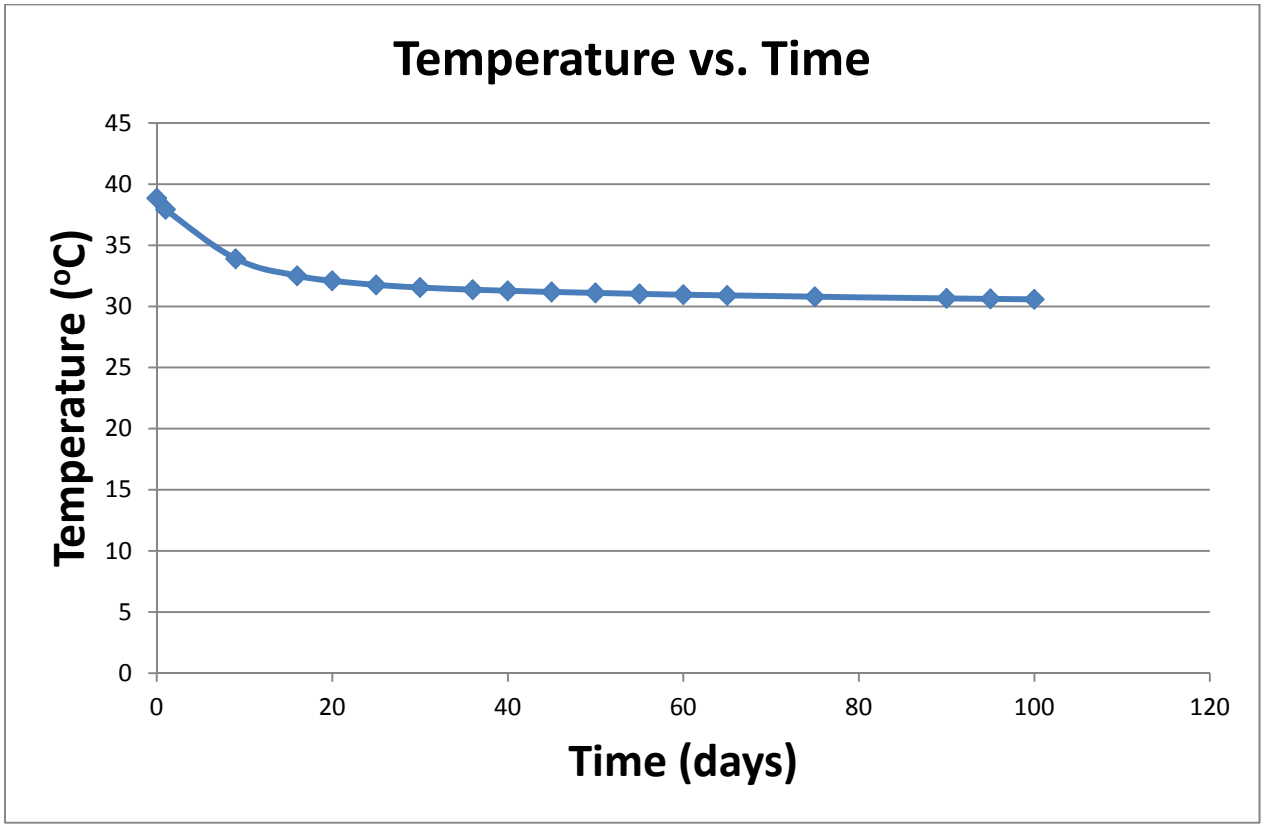

Figure 4.15 Graph of change in temperature of node 7181 located in well Yağcı with time when all wells mentioned in scenario 2 are working

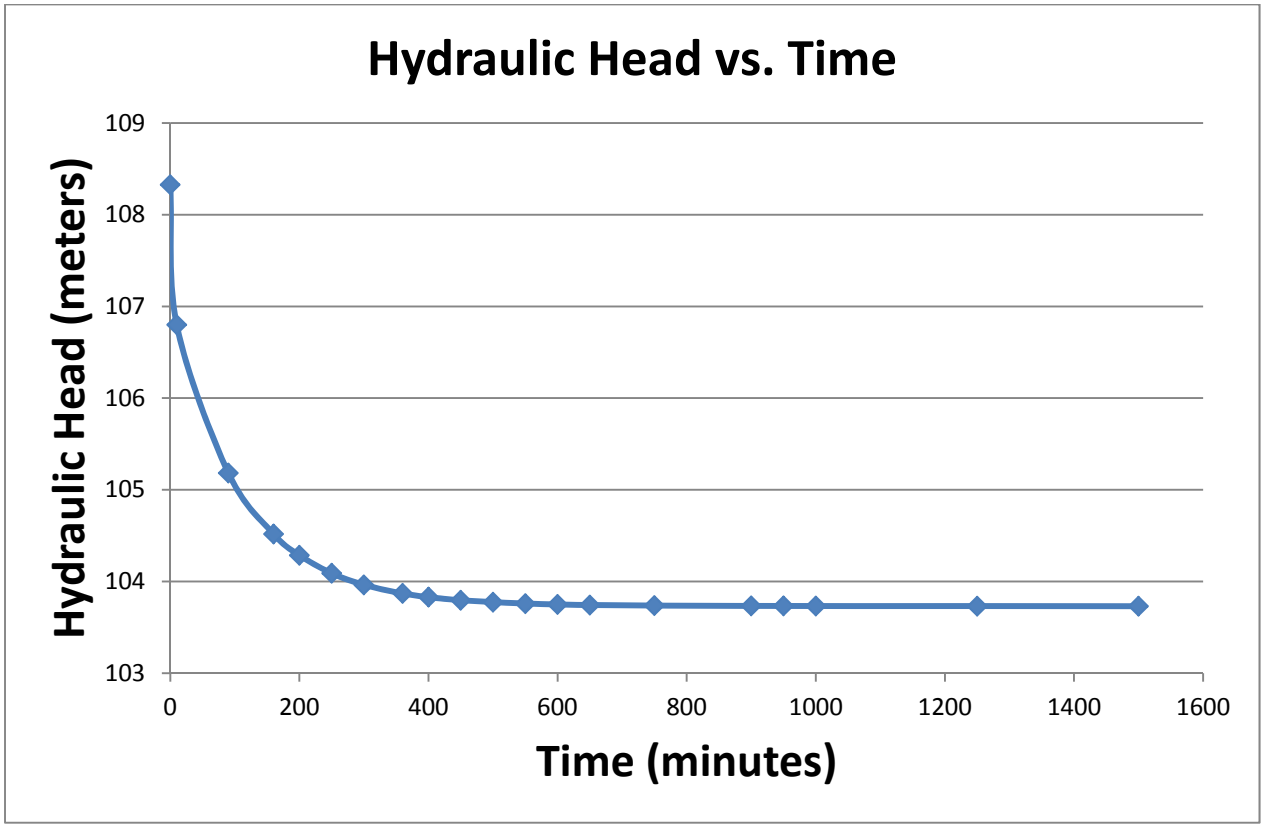

Figure 4.16 Graph of change in hydraulic head of node 7181 located in well Yağcı with time when all wells mentioned in scenario 2 are working

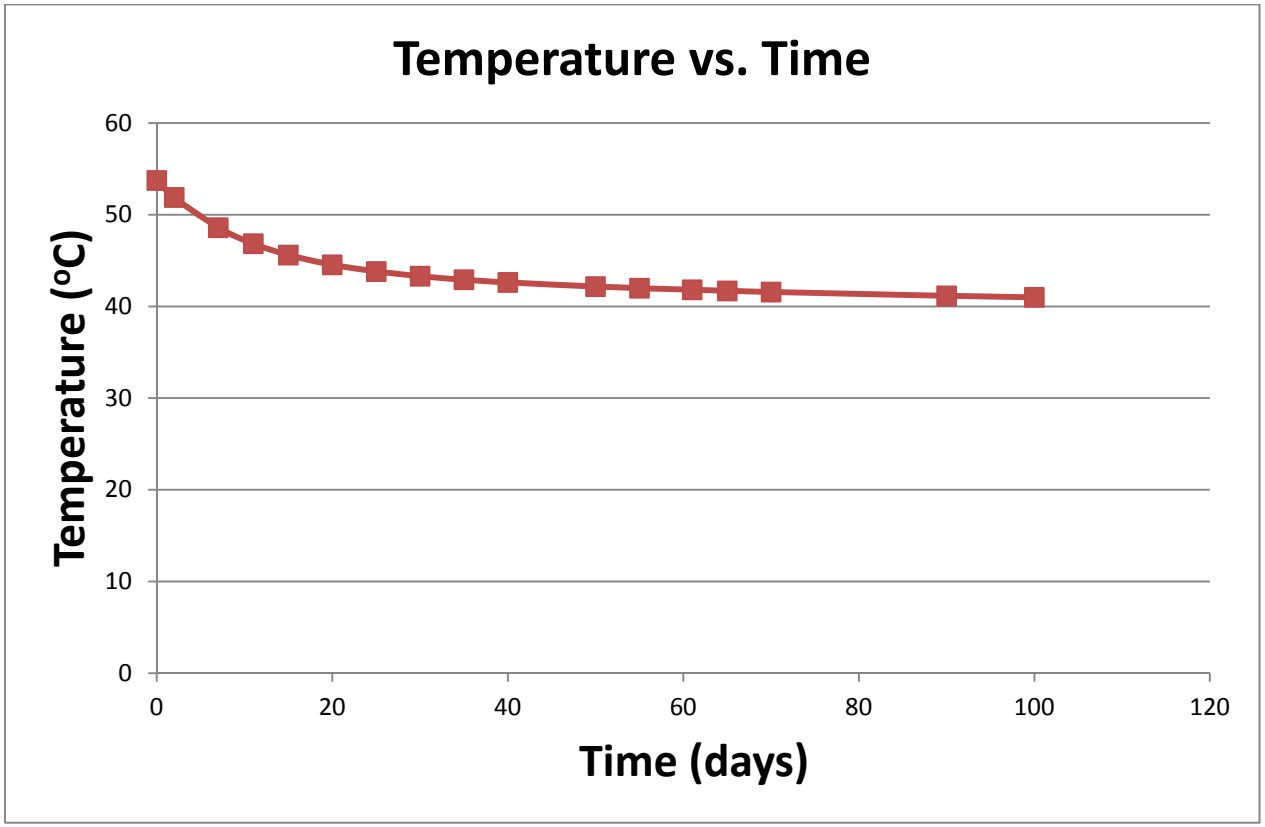

Figure 4.17 Graph of change in temperature of node 11159 located in well Entur with time when all wells mentioned in scenario 2 are working

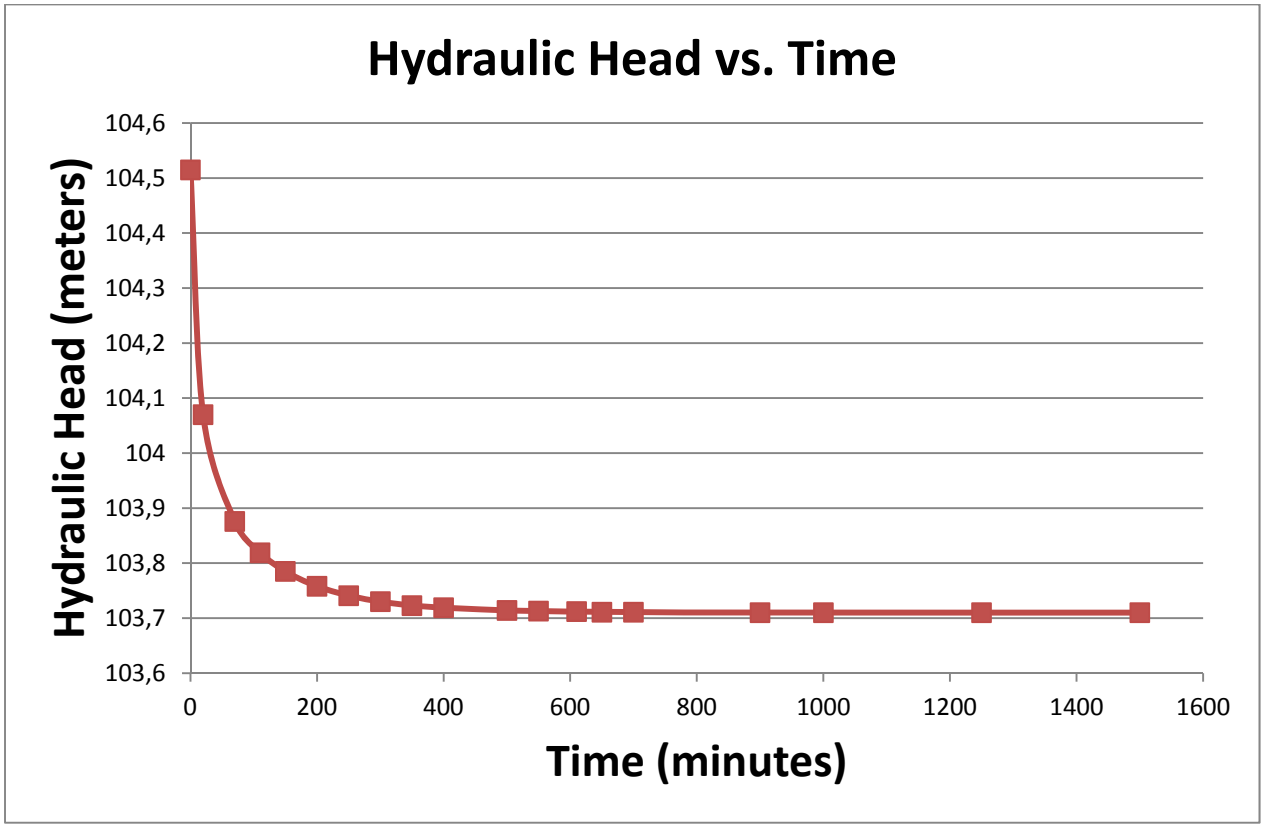

Figure 4.18 Graph of change in hydraulic head of node 11159 located in well Entur with time when all wells mentioned in scenario 2 are working

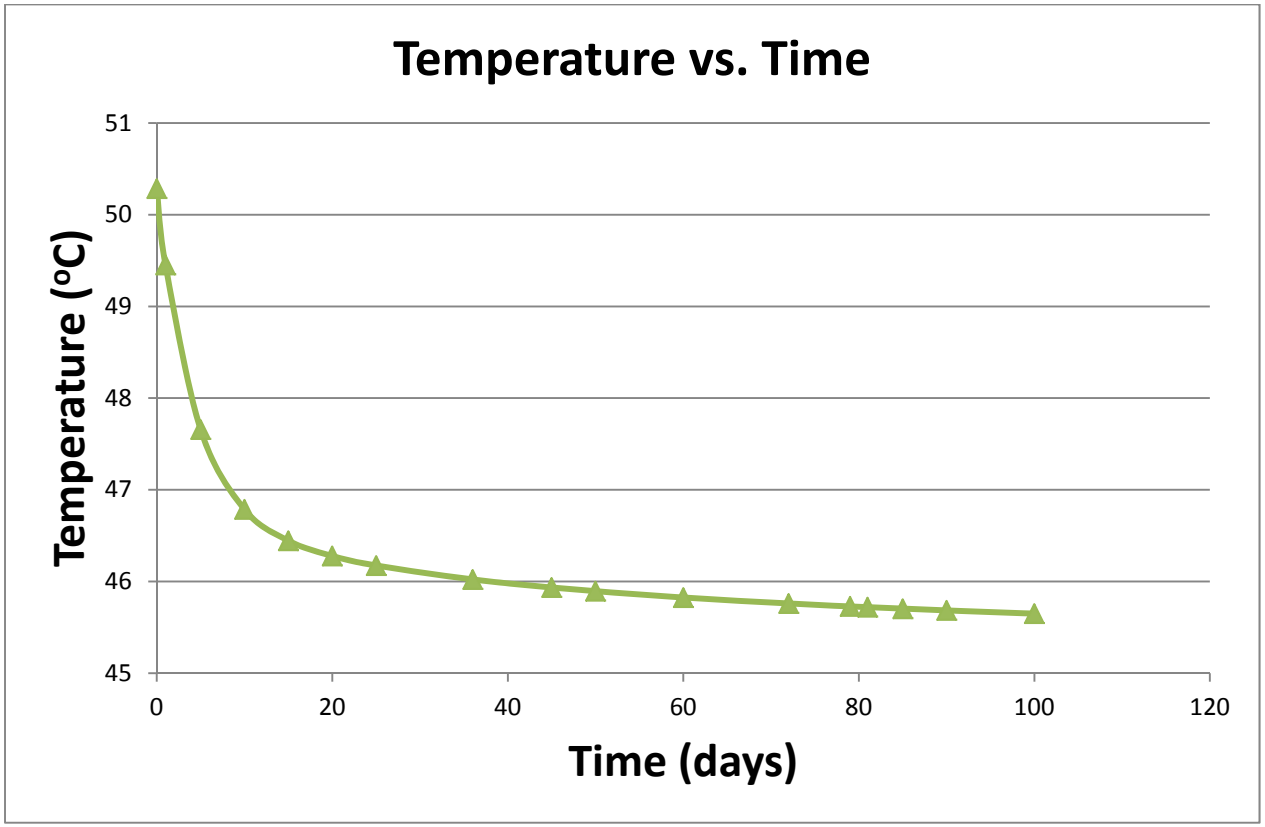

Figure 4.19 Graph of change in temperature of node 10853 located in well Derman with time when all wells mentioned in scenario 2 are working

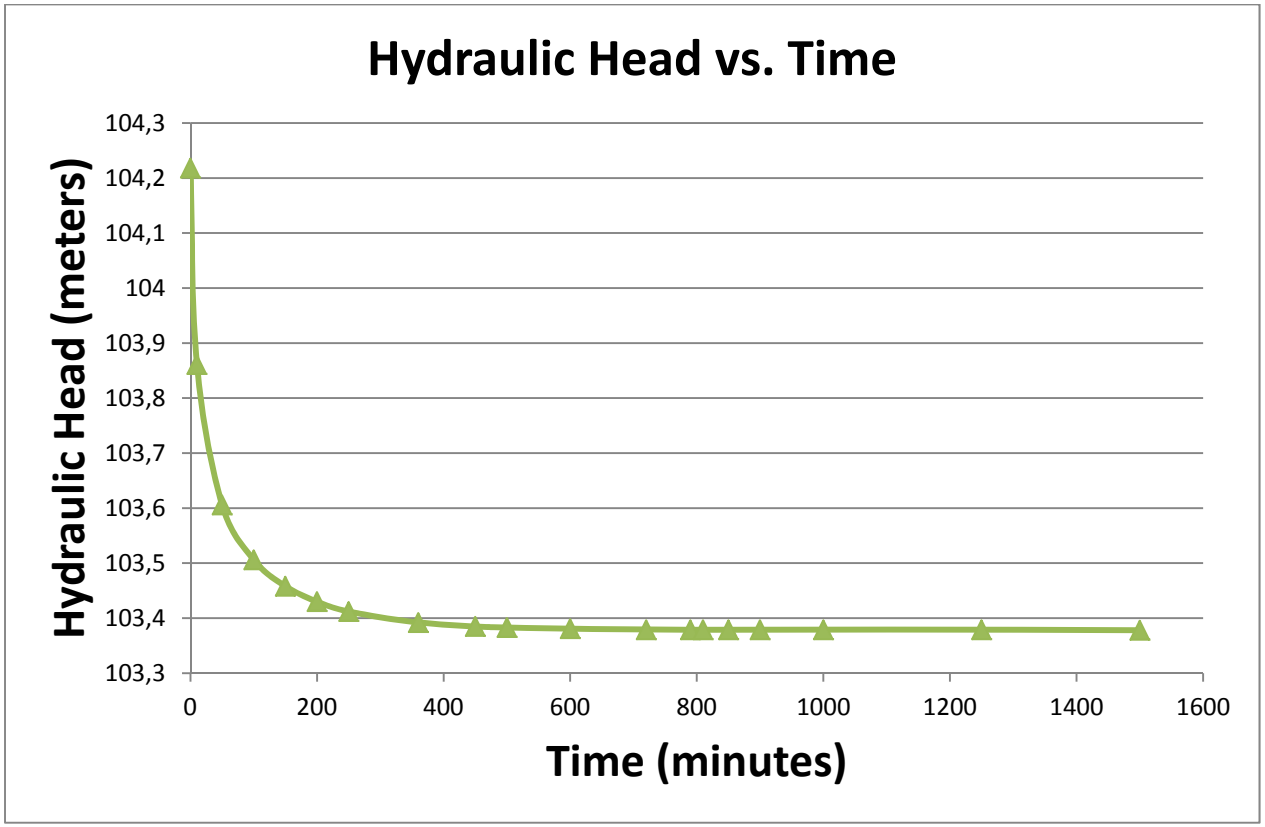

Figure 4.20 Graph of change in hydraulic head of node 10853 located in well Derman with time when all wells mentioned in scenario 2 are working

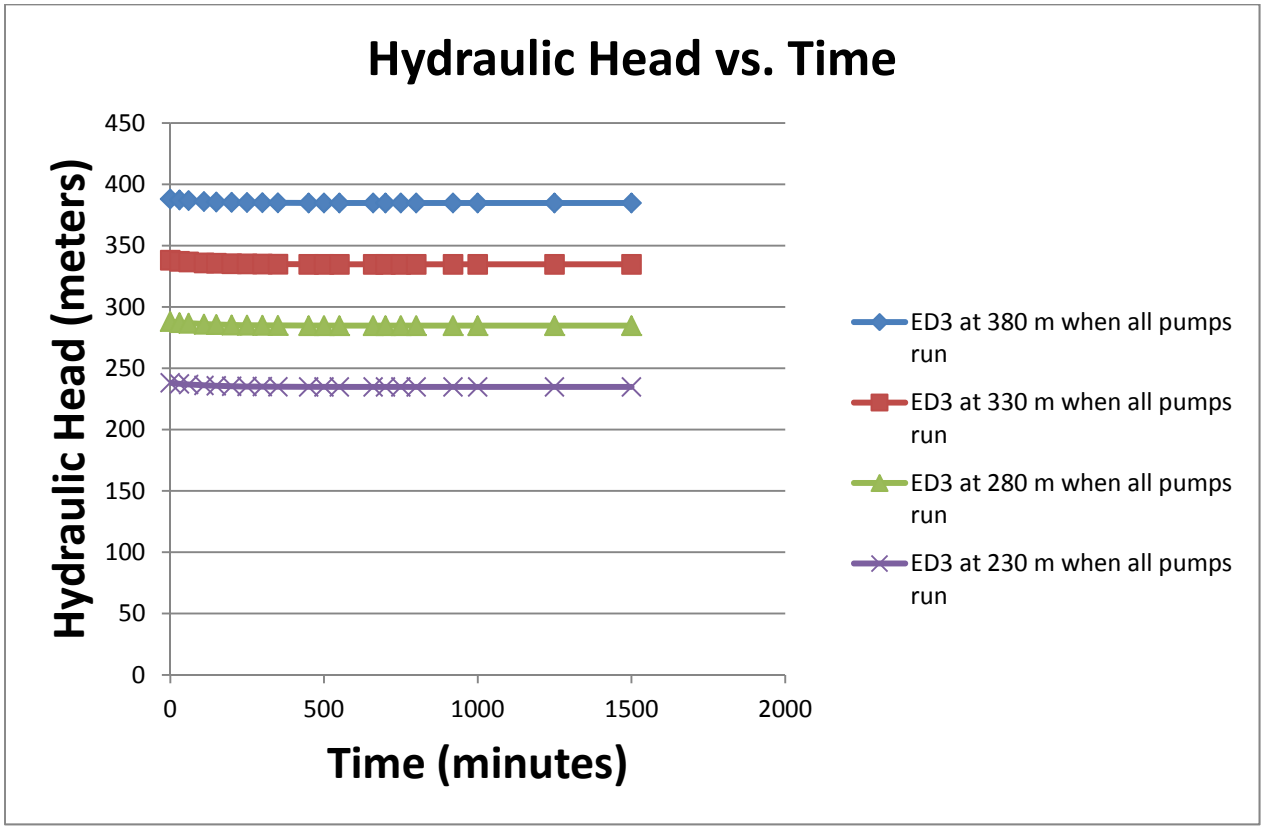

Figure 4.21 Graph of change in hydraulic head of nodes 8275, 8280, 8285, and 8290 located in well ED-3 with time when all wells mentioned in scenario 2 are working

4.2.3 Scenario 3

In this scenario, all the pumping wells mentioned in scenario 2 are working. In addition to this, a new is opened 70 meters away from well ED-3 and 80% of the water pumped is injected to the system from this well with the temperature of the injected water being 20^{o}C.

The results are tabulated in Tables 4.10 through 4.13 and drawn in Figures 4.22 through 4.29.

.

Figures from 4.22 to 4.29 indicate the variation of temperature and hydraulic head with respect to time. These figures indicate that since the water is injected into the aquifer at these nodes, hydraulic head increases abruptly 0.5 meters in almost 10 hours. Temperature results, on the other hand, cools slowly about 30^{o}C in 100 days because the injected temperature of the water is 20^{o}C.

Table 4.10 Temperature distribution in major nodes used in scenario 3

Time (days)	Temp at the depth of 230 m in the injection well (^{o}C)	Temp at the depth of 280 m in the injection well (^{o}C)	Temp at the depth of 330 m in the injection well (^{o}C)	Temp at the depth of 380 m in the injection well (^{o}C)
0	48.519	50.22	52.046	54.059
10	40.283	41.507	42.814	44.255
20	35.759	36.73	37.758	38.884
30	33.168	34	34.869	35.816
40	31.594	32.344	33.118	33.956
50	30.564	31.26	31.974	32.74
60	29.832	30.489	31.159	31.874
70	29.268	29.895	30.53	31.206
80	28.805	29.405	30.011	30.656
90	28.407	28.982	29.563	30.18
100	28.053	28.605	29.163	29.756

Table 4.11 Hydraulic head distribution in major nodes used in scenario 3

Time (minutes)	Head at the depth of 230 m in the injection well (m)	Head at the depth of 230 m in the injection well (m)	Head at the depth of 230 m in the injection well (m)	Head at the depth of 230 m in the injection well (m)
0	238.285	288.25	338.221	388.169
100	238.658	288.634	338.595	388.542
200	238.745	288.721	338.682	388.629
300	238.782	288.757	338.718	388.665
400	238.797	288.772	338.733	388.68
500	238.803	288.778	338.74	388.687
600	238.806	288.781	338.742	388.689
700	238.807	288.782	338.743	388.69
800	238.807	288.782	338.744	388.691
900	238.808	288.783	338.744	388.691
1000	238.808	288.783	338.744	388.691
1100	238.808	288.783	338.744	388.691
1200	238.808	288.783	338.744	388.691
1300	238.808	288.783	338.744	388.691
1400	238.808	288.783	338.744	388.691
1500	238.808	288.783	338.744	388.691

Table 4.12 Temperature decline in nodes used in scenario 3

Node No.	Well Name	Rate of mass (kg/s)	Rate of Energy (J/s)	Initial Temperature (44000 days) (^{o}C)	Final Temperature (44200 days) (^{o}C)	Decline (^{o}C)
7181	YAĞCI	-5	418200	38.857	30.491	8.366
7918	Injection	4		54.059	26.875	27.184
7923	Injection	4		52.046	26.446	25.6
7928	Injection	4		50.22	26.043	24.177
7933	Injection	4		48.519	25.662	22.857
8275	ED-3	-1.25	104550	54.55	39.533	15.017
8280	ED-3	-1.25	104550	52.62	37.343	15.277
8285	ED-3	-1.25	104550	50.845	35.621	15.224
8290	ED-3	-1.25	104550	49.147	34.194	14.953
10853	DERMAN	-5	418200	50.285	45.01	5.275
11159	ENTUR	-5	418200	53.739	40.373	13.366

Table 4.13 Hydraulic head decline in nodes used in scenario 3

Node No.	Well Name	Rate of mass (kg/s)	Rate of Energy (J/s)	Initial Hydraulic Head (44000 days) (m)	Final Hydraulic Head (44200 days) (m)	Rise (m)
7181	YAĞCI	-5	418200	108.327	108.546	0.219
7918	Injection	4		388.169	388.71	0.541
7923	Injection	4		338.211	338.764	0.553
7928	Injection	4		288.25	288.801	0.551
7933	Injection	4		238.285	238.824	0.539
8275	ED-3	-1.25	104550	388.123	388.552	0.429
8280	ED-3	-1.25	104550	338.224	338.593	0.369
8285	ED-3	-1.25	104550	288.203	288.627	0.424
8290	ED-3	-1.25	104550	238.239	238.656	0.417
10853	DERMAN	-5	418200	104.218	103.651	-0.567
11159	ENTUR	-5	418200	104.515	103.965	-0.55

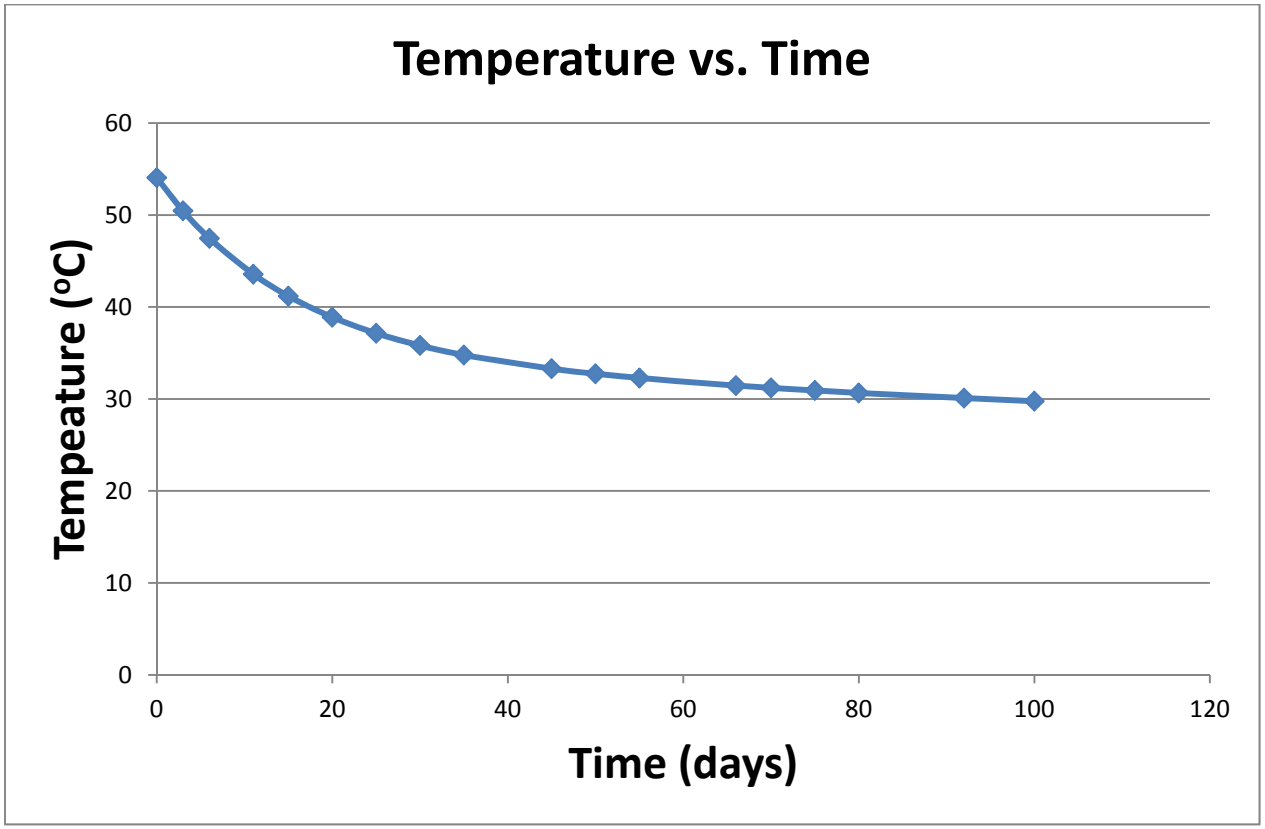

Figure 4.22 Graph of variation in temperature of node 7918 located at a depth of 380 meters in the injection well with time

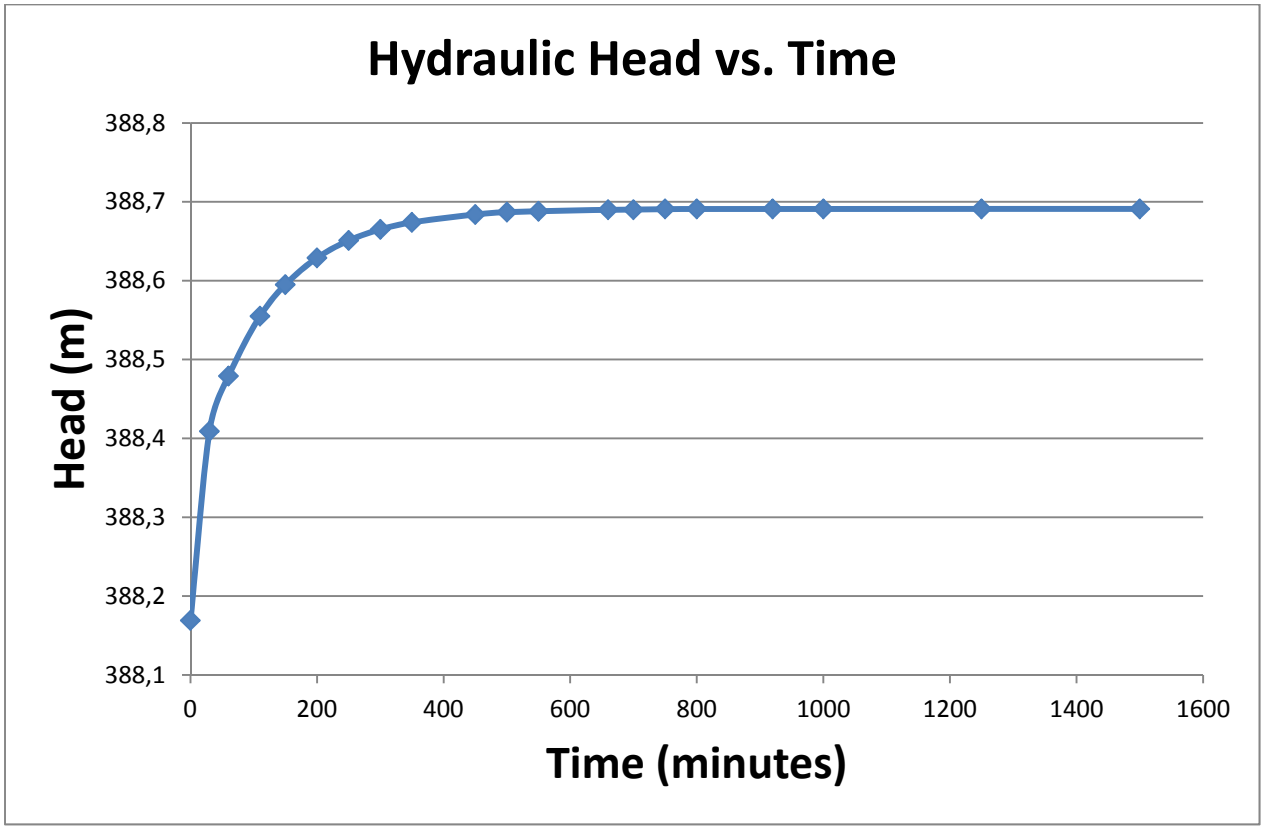

Figure 4.23 Graph of variation in hydraulic head of node 7918 located at a depth of 380 meters in the injection well with time

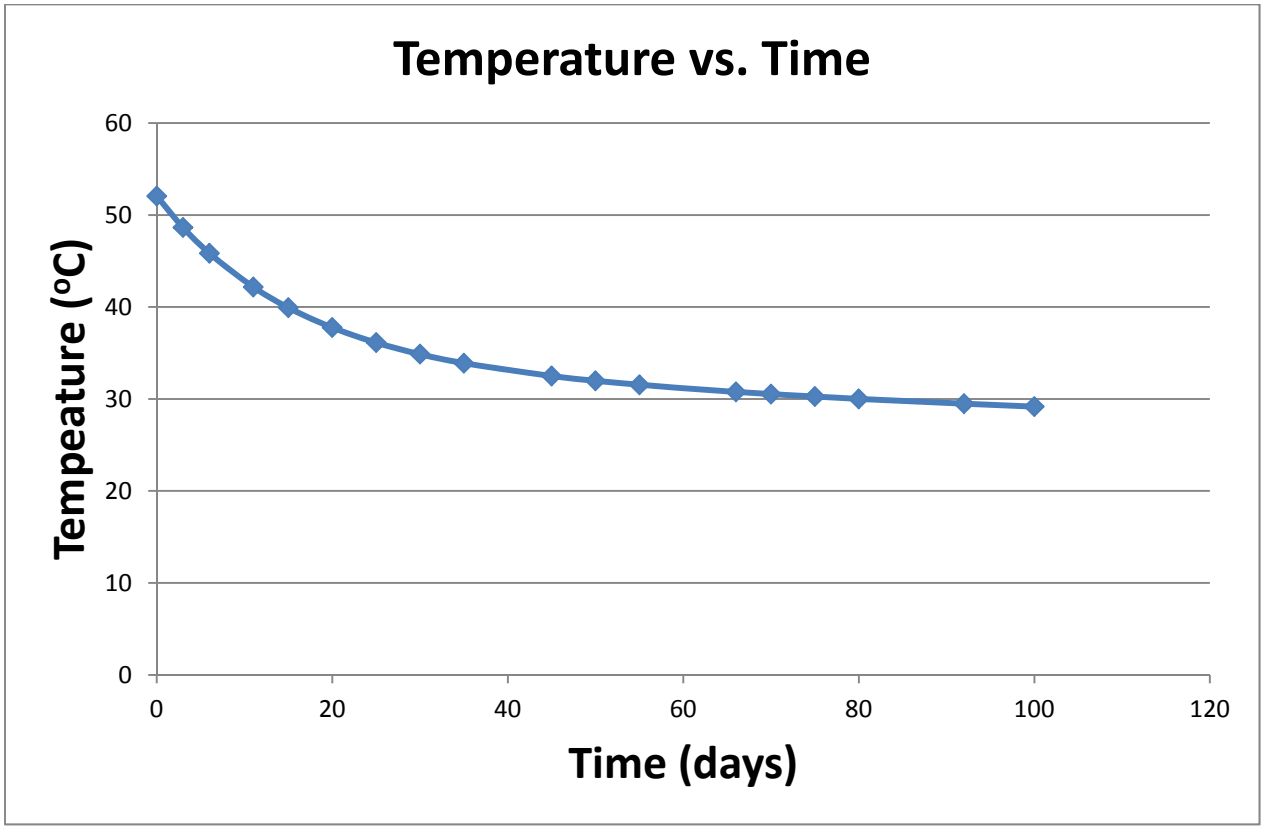

Figure 4.24 Graph of variation in temperature of node 7923 located at a depth of 330 meters in the injection well with time

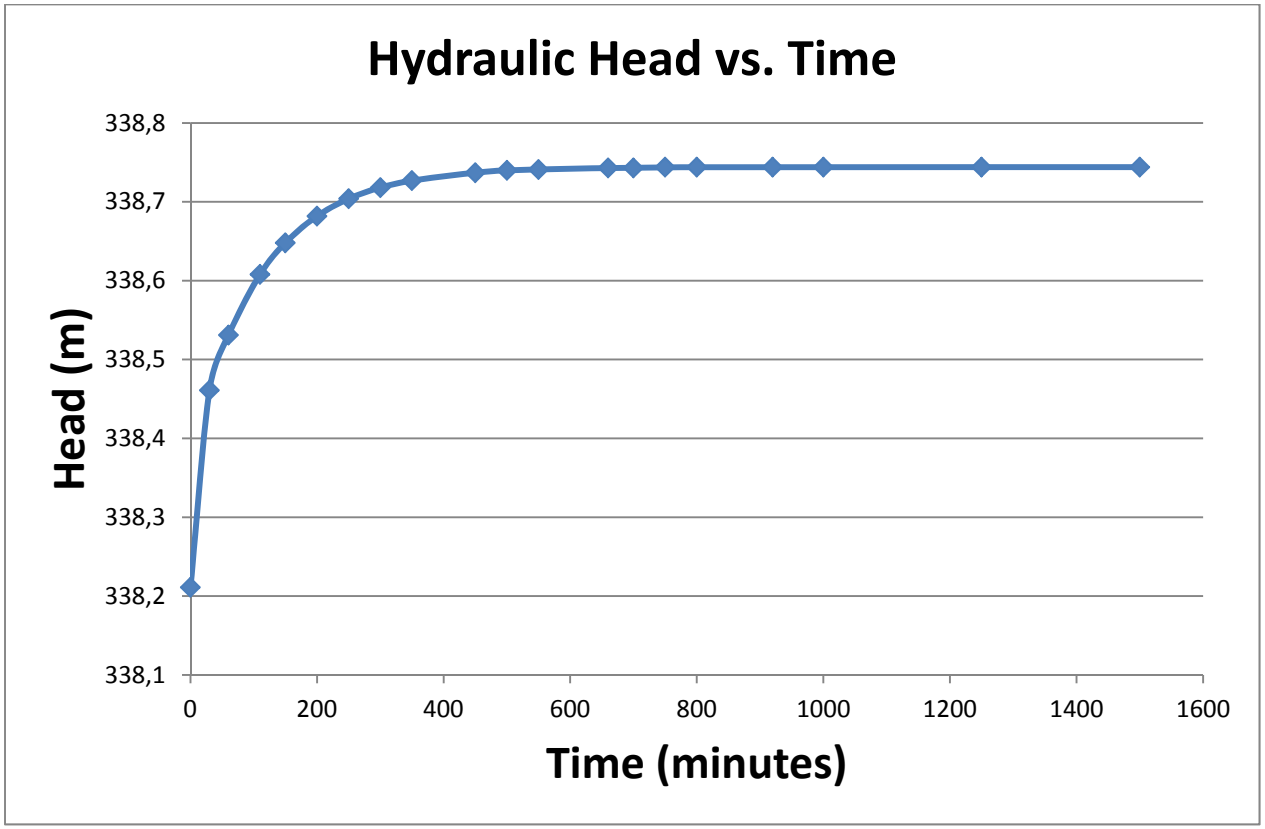

Figure 4.25 Graph of variation in hydraulic head of node 7923 located at a depth of 330 meters in the injection well with time

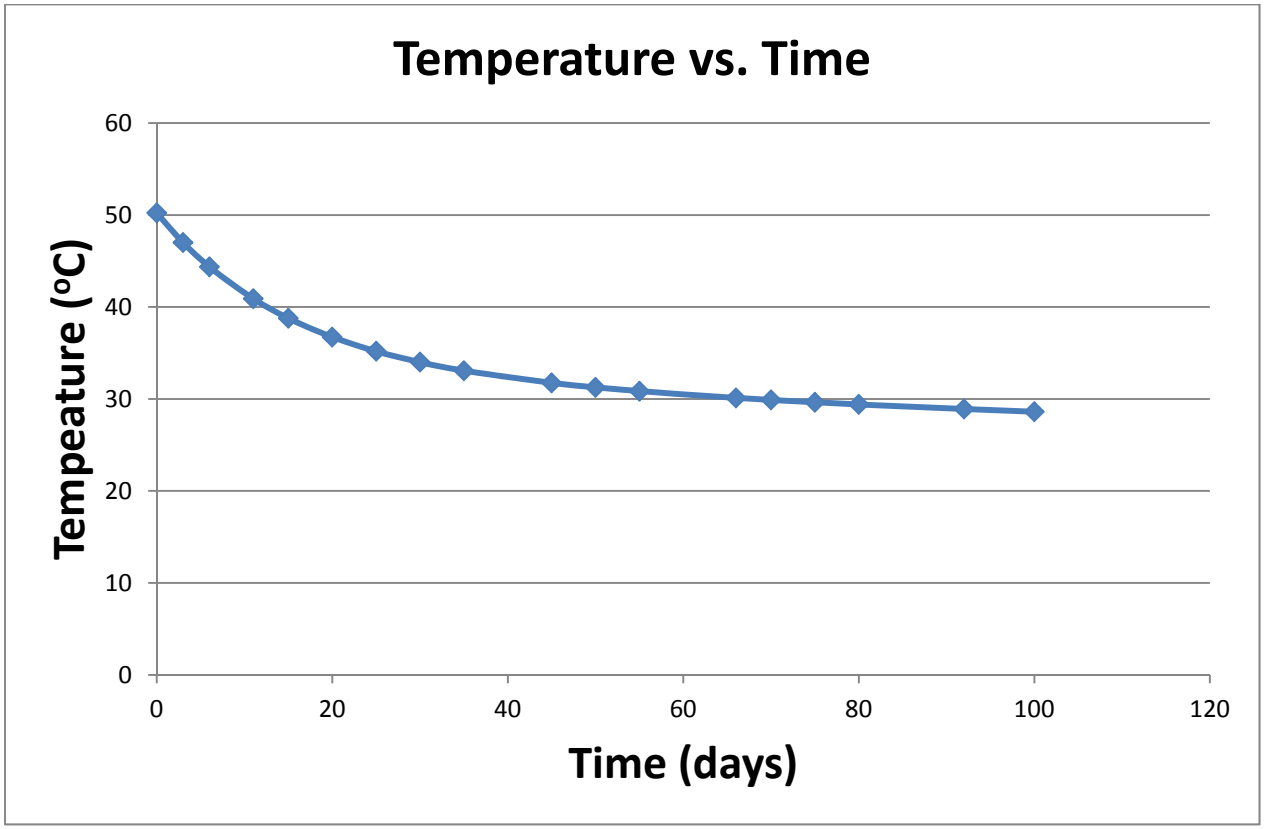

Figure 4.26 Graph of variation in temperature of node 7928 located at a depth of 280 meters in the injection well with time

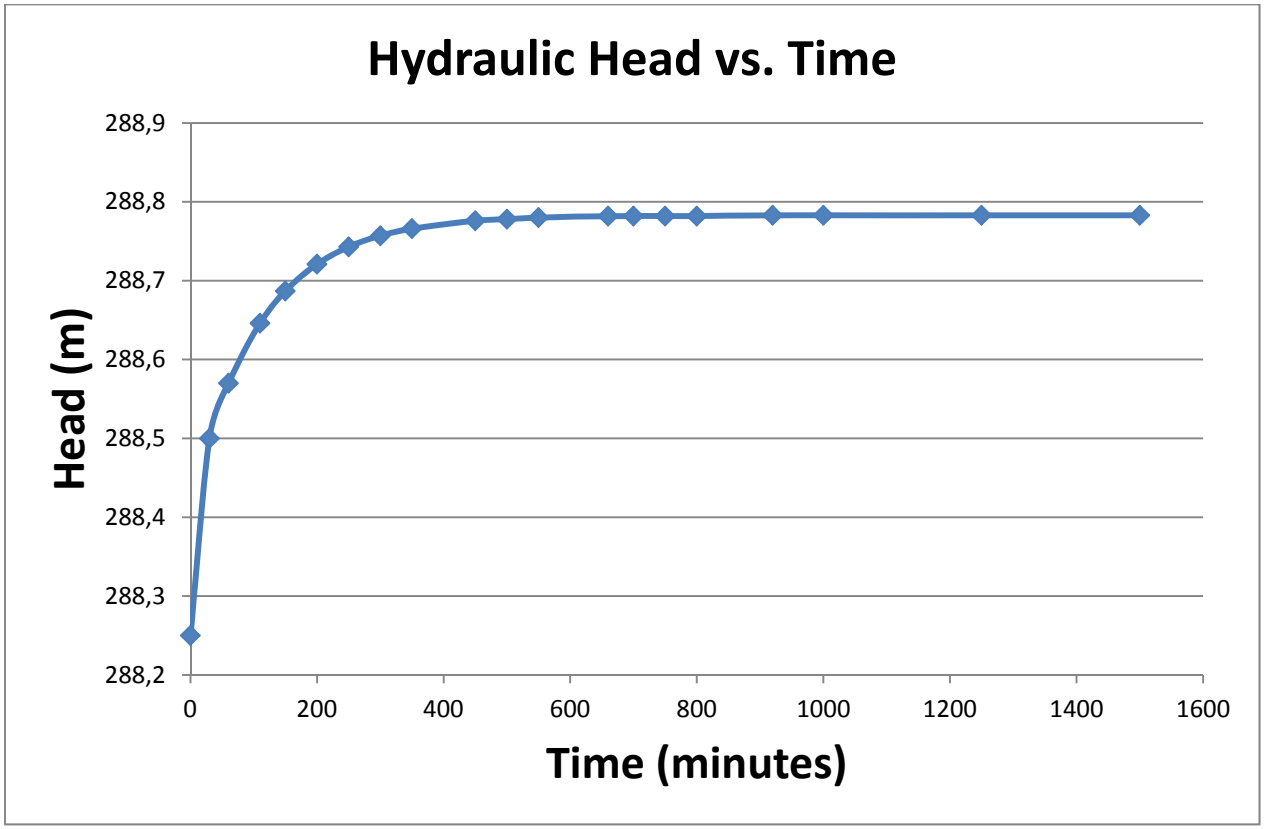

Figure 4.27 Graph of variation in hydraulic head of node 7928 located at a depth of 280 meters in the injection well with time

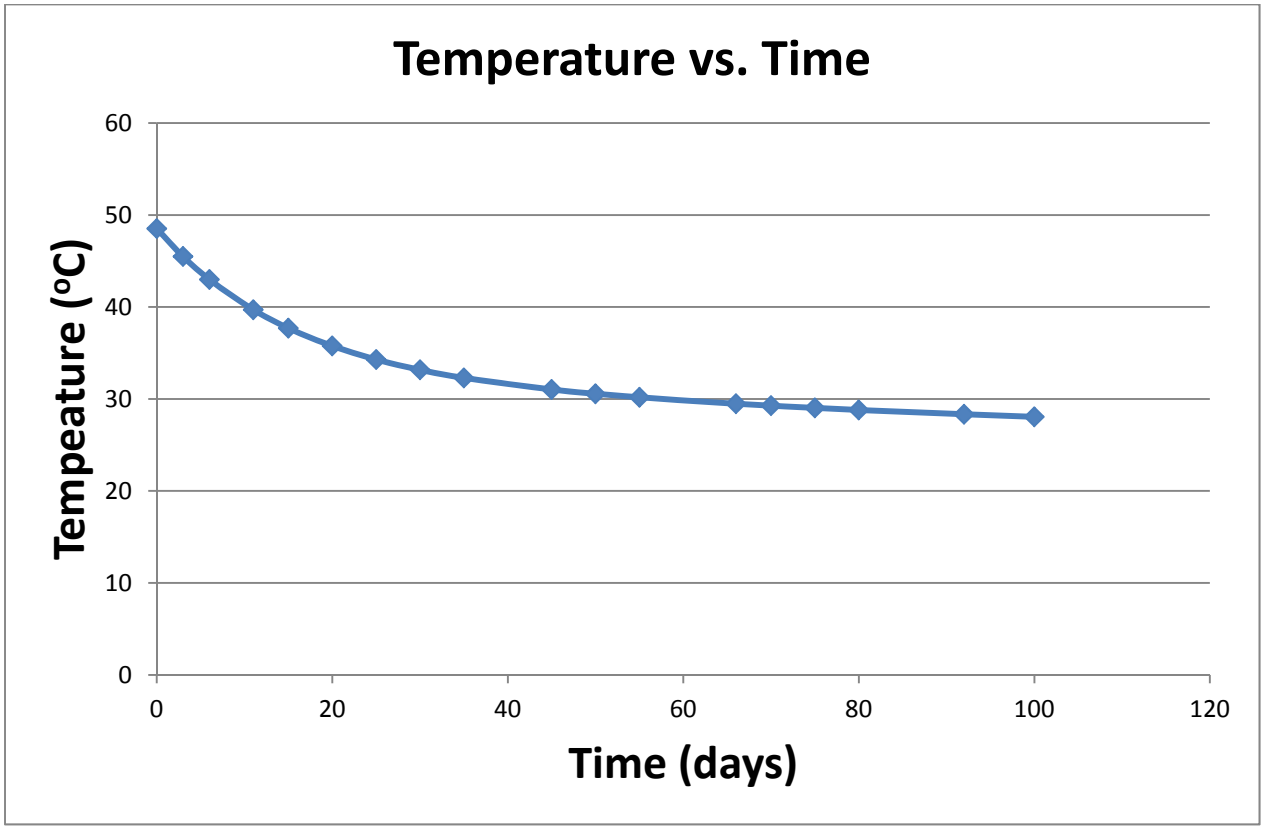

Figure 4.28 Graph of variation in temperature of node 7933 located at a depth of 230 meters in the injection well with time

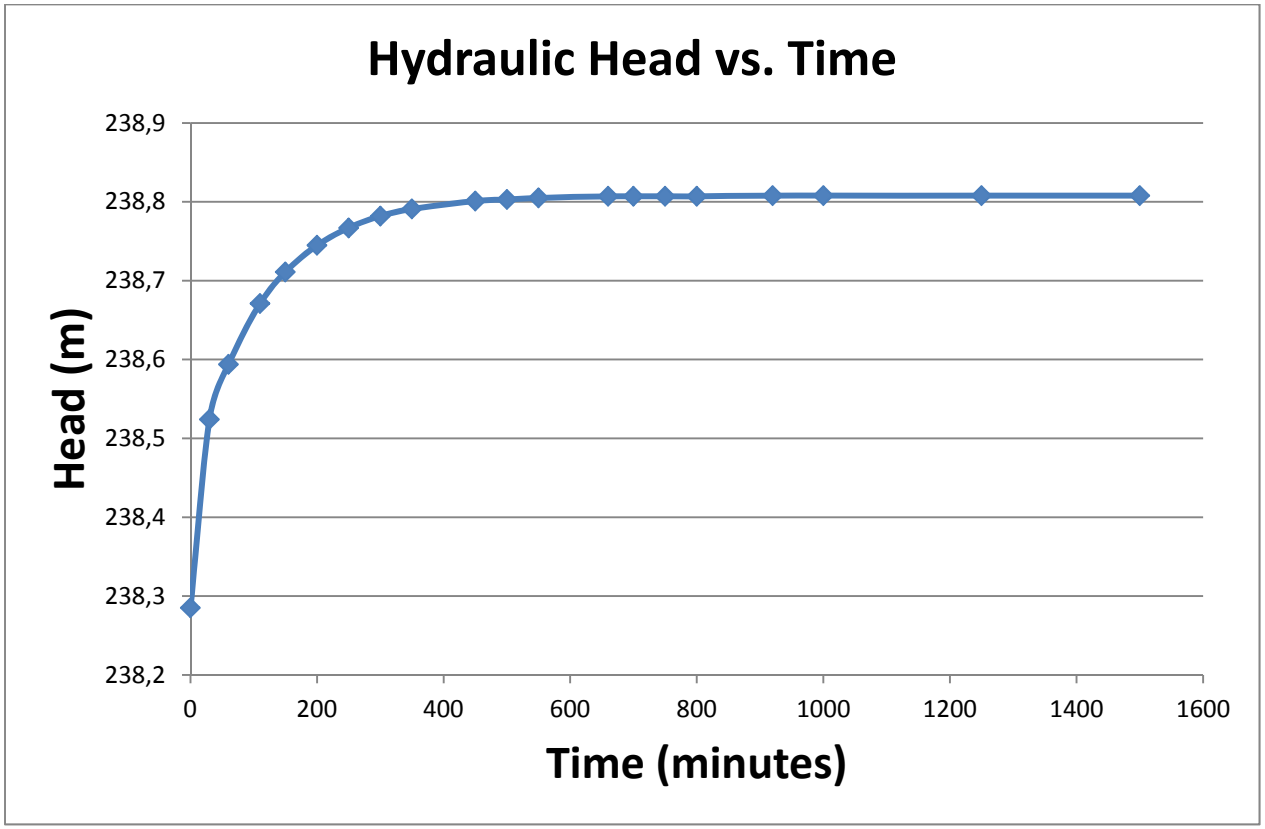

Figure 4.29 Graph of variation in hydraulic head of node 7933 located at a depth of 230 meters in the injection well with time

Table 4.14 Temperature decline of major nodes used in scenarios

Well Node No.	Temperature Decline in Scenario 1 (^{o}C)	Temperature Decline in Scenario 2 (^{o}C)	Temperature Decline in Scenario 3 (^{o}C)
7181	8.204	8.243	8.366
8275	12.269	16.782	15.017
8280	12.258	16.871	15.277
8285	12.244	17.3	15.224
8290	12.222	17.317	14.953
10853	4.63	4.695	5.275
11159	12.045	19.823	13.366

Table 4.15 Hydraulic head decline of major nodes used in scenarios

Well Node No.	Hydraulic Head Decline in Scenario 1 (m)	Hydraulic Head Decline in Scenario 2 (m)	Hydraulic Head Decline in Scenario 3 (m)
7181	0.376	0.864	-0.219
8275	0.385	0.803	-0.429
8280	0.448	0.87	-0.369
8285	0.39	0.814	-0.424
8290	0.387	0.815	-0.417
10853	0.348	0.657	0.567
11159	0.25	0.649	0.55

Table 4.16 % decline in temperature for major nodes used in scenarios

Well Node No.	% Temperature Decline in Scenario 1	% Temperature Decline in Scenario 2	% Temperature Decline in Scenario 3
7181	21.11	21.21	21.53
8275	22.49	30.76	27.53
8280	23.30	32.06	29.03
8285	24.08	34.02	29.94
8290	24.87	35.24	30.43
10853	9.21	9.34	10.49
11159	22.41	36.89	24.87

Table 4.17 % decline in hydraulic head for major nodes used in scenarios

Well Node No.	% Hydraulic Head Decline in Scenario 1	% Hydraulic Head Decline in Scenario 2	% Hydraulic Head Rise in Scenario 3
7181	0.35	0.80	0.20
8275	0.10	0.21	0.11
8280	0.13	0.26	0.11
8285	0.14	0.28	0.15
8290	0.16	0.34	0.18
10853	0.33	0.63	-0.54
11159	0.24	0.62	-0.53

CHAPTER 5

RESULTS AND DISCUSSION

This study was made in order to investigate the geothermal potential, sustainability, and reinjection possibility of the Edremit Geothermal Field. For this reason, a two dimensional cross sectional model made up of a hot unconfined aquifer and a cold confined aquifer separated by a semi pervious layer was constructed. The reason for the construction of this numerical model was to see the variation of temperature and pressure with depth. Also the majority of pumping wells' located at the central area and lack of data supported the selection of this type of numerical model. Several boundary conditions regarding temperature and pressure were given to the system.

After setting up the model, it was calibrated by adjusting the parameters mentioned in Table 3.2 before. The highest permeability was given to the fault zone while the the lowest permeability was given to the thin relatively impermeable layer. The observed temperature and pressure values from the nearby wells and the simulated values after the calibration indicated a high match. Thus, a good calibration was achieved.

The other indicator of the good match was the profile drawn before in Figure 3.8. The trend of the simulated profile of well ED-3 and observed profile obtained from the well log (mentioned in Figure 3.9 before) is quite similar although the simulated values are a little shifted.

The third evidence of the good match was after the simulation of the calibrated results for another 3500 days. The results showed no significant change in pressure and temperature results which proves a fairly good calibration.

After the end of model calibration, some future predictions about the production were performed. For this, three alternative scenarios were made (Table 4.1 as mentioned before). It was observed in all these scenarios that the pressure or hydraulic head changes happen to be faster and reach steady state conditions earlier than the temperature values.

At first water was pumped from several wells with the same rates, separately. In the second scenario water was drawn from the same wells used in scenario 2 but this time they all worked together. In the final scenario, 80% of the pumped water in scenario 2 was reinjected to the system while the pumping wells were still running.

The results of these scenarios showed that there is not a significant difference between the temperature decline. However, the decline in second scenario was slightly higher in most of the nodes, as expected because of the higher loss of the energy from the system.

In the third scenario, the temperature decline was the highest in the injection nodes since water of 20^{o}C was injected to the system from those nodes. The hydraulic head of the cross section decreases from North to South (from north boundary to south boundary) in the cross section. Thus, this injected water flows from north to south in the cross section. Therefore, nodes to the south of the injection well with the same elevation were affected secondly. Hence, ED-3 well were highly affected from this temperature decline. Derman and Entur wells are less affected since they are located far away from the injection well. Being in the opposite direction of water flow, well Yağcı is less affected.

The hydraulic head decline in the second scenario was more than the hydraulic head decline in the first scenario. This is the result of mass rates in these scenarios since pretty much water is pumped in the second scenario compared to the first one.

The hydraulic head rose in the third scenario in the wells closer to the injection well. The maximum rise happened in the injected nodes, as expected. The nodes at the right side of it were highly affected (ED-3). The wells at the left side of it were less affected (Yağcı) because of the flow direction as mentioned below. The wells away from the injection nodes were the least affected (Derman and Entur).

During simulation studies some hypothetical pumping and injection rates are used to get general response of the system. In order to apply the numerical model to the field, actual pumping and injection rates would be better used to make future predictions.

In the numerical modeling the two layer aquifer system is simulated by assuming that these layers are hydraulically connected. This assumption would be tested in a future study by applying a new research.

Careful inspection of the tables related with future declines show that the pressures/heads decline rapidly in a short period of time and reach to a steady state. It is also clear that these declines are very small, which indicate that the reservoir has enough potential to produce so much amount of hot water. On the other hand, similar tables for temperature declines are rather critical because it is understood that so much amount of energy withdrawal would cause temperature declines in the order of 10 to 30 % in the wells. Therefore, a future study would be focused on the optimization of the energy and pumping rates in the reservoir to provide continual support for the district heating in the area.

CHAPTER 6

CONCLUSIONS AND RECOMMENDATIONS

The following conclusions are withdrawn from this research:

1. A numerical simulation study performed to model the Edremit geothermal system is based on the conceptual model of the area. Successful calibration study shows that the conceptual model of the geothermal system is thus supported by the present research.

2. The scenarios applied in the simulations to examine the response of the the system show that the pressures decline in small percent rapidly and reach to a steady state in a short time and this depicts that the reservoir is capable of producing this amount of hot water.

3. In terms of temperature, present production scenarios indicate declines in temperatures reaching to 30 % in the wells. Similar to the pressure decline, they reach to steady values and this requires that production rates need to be revised. On the other hand, the reservoir is found to be productive for future productions since the declines in the steady period are almost negligible for the pressures and the temperatures.

4. A hypothetical well is opened in the north of the production wells to reinject used reservoir fluid back into the system to recover pressure declines. Reinjection

simulations show that the pressures are recovered in the injection and the surrounding wells. However, it causes temperature decrease in the wells located to the south of the production wells.

The following items are recommended from this thesis:

1. A successful numerical modeling of the Edremit geothermal system has been accomplished in this research. However, it is focused in a smaller section of the geothermal field due to lack of data. It would be better to consider the whole field in a 3D modeling study in the future.

2. This model has been used to simulate the geothermal system assuming that the wells are continuously operating for 24 hours a day. However, it would be more realistic if the actual production rates of the field are used in the simulation studies.

3. The simulation studies assume that there exists a hydraulic relation between the cold and hot aquifer layers although this is not yet clearly identified in the field. Therefore a future study may be planned to investigate this problem by means of such a numerical model.

REFERENCES

Altınlı, E., 1973. Bilecik Jurasiği. *Proceedings, Cumhuriyetin 50. Yılı yerbilimleri kongresi,* Ankara, 103

Avşar, 2011, Geochemical evaluation and conceptual modeling of Edremit geothermal field, Ph. D. Thesis, *Middle East Technical University*, Ankara, p. 158.

Barka, A., 1992. The North Anatolian Fault Zone, *Ann. Tectonicae,* 6, 164-195.

Bingöl, E., 1969. Kazdağ masifinin merkezi ve güneydoğu kesiminin jeolojisi. *MTA Journal*, 72, 110-124.

Bingöl, E., Akyürek, B., Korkmazer, B., 1973. Biga yarımadasının jeolojisi ve Karakaya formasyonunun bazı özellikleri. *Proceedings, Cumhuriyetin 50. Yılı yerbilimleri kongresi,* Ankara p. 70-76.

Bozkurt, E. and Mittwede, S.K., 2001. Introduction to the geology of Turkey-a synthesis. *International Geology Review*, 43, 578-591.

Bozkurt, E. and Rojay, B., 2005. Episodic two-stage Neogene extension and shortterm intervening compression in Western Turkey: field evidence from the Kiraz Basin and Bozdağ Horst. *Geodinamica Acta*. 18, 299-316.

Candan, O., Dora,O.Ö., Oberhänsli, R., Koralay, E., Çetinkaplan, M., Akal, C., Satır, M., Chen, F., Kaya, O., 2011. Menderes Masifi'nin Pan-Afrikan temelin stratigrafisi ve Gondvana'nın geç Neoproterozoyik/Kambriyen evrimi ile ilişkisi, *MTA Journal*. 142, 25-68.

Candan, O., Koralay, O.E., Akal,C., Kaya, O., Oberhänsli, R., Dora,O.Ö., Konak, N., Chen, F., 2011, Supra-Pan-African unconformity between core and cover series of the Menderes Massif/Turkey and its geological implications, *Precambrian Research*, 184, 1-23.

Candan, O., Oberhänsli, R., Dora,O.Ö., Çetinkaplan, M., Koralay, E., Rimmelé, G., Chen, F., Akal,C., 2011, Menderes Masifi'nin Pan-Afrikan temel ve Paleozoyik- Erken Tersiyer örtü serilerinin polimetamorfik evrimi, *MTA Journal*, 142, 123-165.

Coşkun, C., Oktay, Z., Dinçer, I., 2009, New energy and exergy parameters for geothermal district heating systems, *Applied Thermal Engineering*, 29, 2235-2242.

Demirel, Z., Yildirim, T., Burçak¸ M., 2004. Preliminary study on the occurrence of geothermal systems in the tectonic compressional regions: an example from the Derman geothermal field, *Journal of Asian Earth Sciences*, 22, 495-501.

Dewey, J.F., 1988, Extensional collapse of orogens. *Tectonics,* 7, 1123-1139.

Dewey, J.F., Şengör, A.M.C., 1979. Aegean and surrounding regions: complex multiplate and continuum tectonics in a convergent zone. *Geological Society of America Bulletin*, Part I 90, 84–92.

Dora, O.Ö., 2011, Menderes Masifindeki jeolojik araştırmaların tarihsel gelişimi, *MTA Journal,* 142, 1-23.

DSİ, 1977. Edremit ve Armutova (Gömeç) ovaları hidrojeokimyasal etüt raporu, *Gn. Directorate of State Hydraulic Works, Rep.No. 86940*, unpublished.

Duru, M., Pehlivan, Ş., Şentürk, Y., Yavaş, F., Kar, H., 2004. New results on the lithostratigraphy of the Kazdağ Massif in northwest Turkey. *Turkish Journal of Earth Sciences,* 13, 177-186.

Ercan, T., Günay, E., Türkecan, A., 1984. Edremit – Korucu yöresinin (Balıkesir) Tersiyer stratigrafisi magmatik kayaçların petrolojisi ve kökensel yorumu. *Bulletin of Türkiye Jeoloji Kurumu*, 27, 21-30.

Ercan, T., Satır, M., Steinitz, G., Dora, A., Sarıfakıoğlu, E., Adis, C., Walter, H.J., Yıldırım, T., 1985. Biga Yarimadasi ile Gökçeada, Bozcaada ve Tavşan adalarındaki (KB Anadolu) Tersiyer volkanizmasının özellikleri, *MTA Journal*, 117, 55-86.

Erdoğan, B., Akay, E., Hasözbek, A., 2011, Menderes Masifi'ndeki (Batı Anadolu) gnaysik granitlerin yerleşim özellikleri ve masifin tektonik evrimindeki yeri; yeni arazi bulguları ve yaş tayinleri, *MTA Journal*, 142, 167-193.

Genç, C., Altunkaynak, Ş., 2007. Eybek graniti (Biga yarımadası, KB Anadolu) üzerine: Yeni jeokimya verileri ışığında yeni bir değerlendirme. *Journal of the Earth Sciences Application and Research Centre of Hacettepe University*, 28 (2), 75-98.

Göncüoğlu, M.C., 2011, Kütahya-Bolkardağ kuşağının jeolojisi, *MTA Journal*, 142, 227-282.

Göncüoglu M.C., Turhan N., Şentürk K., Özcan A. and Uysal S., 2000. A geotraverse across NW Turkey: tectonic units of the Central Sakarya region and their tectonic evolution. In: E. Bozkurt, J. Winchester and J.A. Piper (Eds.), Tectonics and magmatism in Turkey and the surrounding area. *Geol. Soc. London Spec. Publ.*, 173: 139-161.

Kissel,C. and Laj,C., 1988. The Tertiary geodynamical evolution of the Aegean arc: a paleomagnetic reconstruction. *Tectonophysics*, 146, 183-201.

Koç, Ş., Erdoğan, S., Kadıoğlu, Y.K., 1994. Havran (Balıkesir) güneydoğusunda yer alan volkanitlerin epitermal cevherleşme potansiyeli. *MTA Journal*, 116, 65-80.

Koçyiğit, A., Yusufoğlu, H. and Bozkurt, E., 1999. Evidence from the Gediz graben for episodic two-stage extension in western Turkey. *Journal of the Geological Society of London*. 156, 605−616.

Koralay, O.E., Candan, O., Akal, C., Dora, O.Ö., Chen, F., Satır, M., Oberhänsli, R., 2011, Menderes Masifi'ndeki Pan-Afrikan ve Triyas yaşlı metagranitoyidlerin jeolojisi ve jeokronolojisi, Batı Anadolu, Türkiye, *MTA Journal*, 142, 69-121.

Krushensky, R.D., 1976. Neogene Calc-alkaline extrusive and intrusive rocks of the Karalar-Yeşiller area, Northvvest Anatolia. *Bulletin of Volcanology*, 40, 336-360.

Le pichon, X. and Angelier, J., 1979. The Hellenic arc and trench system; A key to the neotectonic evolution of the eastern Mediterranean. *Tectonophysics*. 60, 1-42.

Le pichon, X. and Angelier, J., 1981, The Aegean Sea, *Phiolosophical Transactions of the Royal Society of London,* A300, 357-372.

McKenzie, D.P., 1978. Some remarks on the development of sedimentary basins. *Earth and Planetary Science Letters*. 40, 25−32.

Meulenkamp, J.L., Wortel, W.J.R., Van Wamel, W.A., Spakman, W., and Hoogerduyn Strating, E., 1988. On the Hellenic subduction zone and geodynamic evolution of Cretein the late middle Miocene, *Tectonophysics,* 146, 203-215.

MTA, 2001. Balıkesir-Edremit-Derman jeotermal alanı ED-1, ED-2, ED-3 sondajları kuyu bitirme raporu, *Gn. Directorate of Mineral Research and Exploration, Rep.No. 10512,* unpublished.

MTA, 2007. 1:100 000 ölçekli Türkiye jeoloji haritaları No: 97 Balıkesir İ18 paftası, *Gn. Directorate of Mineral Research and Exploration,* Ankara.

Okay, A.,İ., 2011, Tavşanlı zonu: Anatolid-Torid Bloku'nun dalma-batmaya uğramış kuzey ucu, *MTA Journal,* 142, 195-226.

Okay, A., İ., İşintek, İ., Altıner, D., Altıner, S.,Ö., Okay, N., 2012, An olistostrome–mélange belt formed along a suture: Bornova Flysch zone, western Turkey, *Tectonophysics*, 2012, 282-295.

Okay, A.İ., Satır, M., 2000,. Coeval plutonism and metamorphism in a latest Oligocene metamorphic core complex in northwest Turkey, *Geo. Mag.* , 137, 495-516.

Okay, A.İ., Siyako,M., and Bürkan,K.A., 1991. Geology and tectonic evolution of the Biga Peninsula, northwest Turkey. *Bulletin of the Technical University of İstanbul, Special Issue on Tectonics,* 44, 191-256.

Robertson, A.H.F., Ustaömer, T., 2012, Testing alternative tectono-stratigraphic interpretations of the Late Palaeozoic−Early Mesozoic Karakaya Complex in NW Turkey: Support for an accretionary origin related to northward subduction of Palaeotethys, *Turkish Journal of Earth Sciences*, 21, 961-1007.

Sarp, S., Burçak, M., Yıldırım, T., Yıldırım, N., 1998. Biga yarımadasının jeolojisi ve jeotermal enerji olanakları ile Balıkesir-Havran-Derman kaplıca sahasının detay jeotermal etüdü ve gradyan sondajları, *Gn. Directorate of Mineral Research and Exploration*, *Rep.No. 10537,* unpublished.

Seyitoğlu, G., Scott, B.C., 1991. Late Cenozoic crustal extension and basin formation in west Turkey. *Geological Magazine*. 128, 155–166.

Seyitoğlu, G., Scott, B.C., 1992. The age of Büyük Menderes Graben and its tectonic implications. *Geological Magazine*. 129, 239-242.

Seyitoğlu, G., Scott, B.C., and Rundle, C.C., 1992. Timing of Cenozoic extensional tectonics in west Turkey. *Journal of Geological Society, London*, 149, 533-553.

Şengör, A.M.C, 1979. The North Anatolian Transform Fault: its age, offset and tectonic significance, *Journal of Geological Society, London,* 13, 268–282.

Şengör, A.M.C, 1980. Mesozoic-Cenozoic Evolution of Anatolia and surrounding regions. Abstract., *Bureau de Recherces Géologique et Minières Bulletin (France),* 115, 117.

Şengör, A.M.C, 1987. Cross faults and differential streching of hanging walls in regions of law-angle normal faulting: examples from western Turkey. In: Coward, M.P., Dewey, J.F., and Hancock, P.L., *Continental Extensional Tectonics*. Geological Society, London, Special Publications, 28, 575–589.

Şengör, A.M.C., Görür, N., Şaroğlu, F., 1985. Strike-slip faulting and related basin formation in zones of tectonic escape: Turkey as a case study: in: Biddle, K., Christie-Blick, N., (eds.), *Strike-slip Deformation, Basin Formation and Sedimentation,* Society of Economic Paleontologists and Mineralogists, Special Publication. 37, 227–264.

Şengör, A.M.C., Yılmaz, Y., 1981. Tethyan Evolution of Turkey: a Plate Tectonic Approach". *Tectonophysics* 75, 181-241.

T.C. Edremit Kaymakamlığı, 2012. , <http://balikesir edremit.gov.tr, last visited on 17 July 2012.

T.C. Meteoroloji Genel Müdürlüğü, 2012, http://www.mgm.gov.tr, last visited on 17 July 2012.

Ural, T., 1978. Finite difference modelling of Edremit valley aquifers, M.S. thesis, *Middle East Technical University*, Ankara, p. 65.

Voss, C.I., 1984. SUTRA: A Finite-Element Simulation Model for Saturated-Unsaturated Fluid-Density-Dependent Groundwater Flow with Energy Transport or Chemically Reactive Single Species Solute Transport, U.S. Geological Survey Water Resources Investigations Report 84-4369.